

Austere Field Light Attack Aircraft

Final Report

EAE 4255 – Aircraft Design II

Instructor: Dr. Elham Tolouei

Group 1

Members

Name	ID
Abdelmoussaour Boukhatem	20171141415
Al Shaima Saif	20171141078
Fawaz Jalal	20171141273
Mohammad Ahmad Almunir	20171141407
Mohammed Nurul	20171141196
Omar El Sardouk	20171141405
Omar Samy Taha	20171141388



Abstract

The purpose of the report was to design a light attack aircraft which was capable of finding, tracking, and attacking targets either on its own or with support from the ground. Military personnel use these aircraft to experience enhanced targeting capabilities and offer enhanced security to citizens. This aircraft can be operated on missions including near-air support, light strikes, security, tracking, armed identification, and major pilot training. In terms of range, durability, and sensors, the design outperforms conventional propeller aircraft. Five competitor's aircraft were chosen to compete and compare the results of the chosen parameters.

The aircrafts were Beechcraft AT-6, Wolverine Beechcraft T-6C Texan 2, North American P-51 Mustang, Douglas A-1 Skyraider, Embraer EMB 314 Super Tucano. All aircrafts chosen has similar characteristics. Furthermore, the takeoff weight for design and ferry mission was calculated. These takeoff weights were calculated to satisfy the requirements of AIAA and was based on a single engine propeller aircraft. Additionally, the drag polar and matching of all sizing requirements were found, as well as the performance analysis for steady unaccelerated and accelerated flight. The flight envelope and carpet plot were also plotted and explained.

Additionally, for the wing configuration, various wing designs were considered, and other required parameters were determined for the wing and control surfaces such as ailerons and flaps in attempt to provide suitable takeoff and landing for the austere field light attack aircraft. The integration of the fuel tank was also discussed along with the selection of materials for the interior of the wing, and a fuel system schematic was illustrated. Furthermore, the empennage was designed with the consideration of adding dorsal and ventral fins for spin recovery and stability. The selection of materials for each component of the empennage was listed and explained. Moreover, the fuselage was designed by determining the geometric fuselage parameters. The fuselage materials were selected and explained.

The PT6A-67F engine was selected for the Austere field light attack aircraft and the main characteristics were tabulated. The engine performance was justified along with the fuel and propeller systems. Following that, the location of the propulsion system, as well as the estimation of the propeller diameter with the number of blades were found. A trade analysis was conducted on various propeller types. Furthermore, various types of landings gears were compared from the competitors and elaborated. The sizing and type of arrangement for the landing gear was found and positioned showing the center of gravity for the designed aircraft.





Various types of wheel systems and shock absorbers were considered, and the material selection for the landing gear was explained to provide the best suitable condition for the aircraft. Furthermore, the cockpit was designed to satisfy all the essential factors. The type of seat selected for the aircraft was an ejection type, which was used to save the pilot in an event of an emergency. The specifications of the MK-J5D seat selected was listed. The avionics system and head-up display was also discussed. Regarding the weapons carriage, the Mk-81 & Mk-82 bombs, GBU-59 Enhanced Paveway II Laser-Guided Bombs, T64 H.V.A.R rockets and AN/M3 cannons, were the weapons considered for the austere field light attack aircraft.

The stability and control analysis was conducted, and the total weight breakdown was listed, and the total location of the center of gravity was obtained with respect to the components and their respective weights, and explained. The longitudinal stability and control parameters were acquired and explained as well as for the directional and lateral stability and control. The respective graphs for longitudinal and directional stabilities were generated and explained. The roll stability of the aircraft was explained following certain conditions and the rolling moment produced on the aircraft upon the event of sideslip was justified.

The 3D model of the austere field light attack aircraft was made using Solidworks and the final renderings and blueprint was illustrated. Each of the component was carefully designed following the dimensions provided from the configurations discussed previously. Following that, the auxiliary systems for the Austere field light attack aircraft were explained and the schematic diagrams were illustrated; this includes, hydraulic systems, pneumatic and environmental control system, and electric systems. Furthermore, the manufacturing process of the austere field light attack aircraft was discussed; this includes the design stage, production stage and assembly stage. Moreover, cost and market analysis were conducted for the aircraft.

The yearly fuel usage cost assumptions were sorted. The crew cost was calculated and the cost per flight hour was tabulated and compared with the competitor aircrafts. Additionally, the flyway costs for all competitors including the austere field light attack aircraft were listed and a graph was plotted based on it. Following that, the development support and Military operating costs was tabulated and compared with the competitors. Flight test operations were also discussed, and the flight test operations cost was sorted and compared likewise. Additionally, regarding the market analysis, a regional analysis, market research, and market segmentation were explained. Finally, the cost break-even point was obtained.





Nomenclature

Symbol	Definition	Symbol	Definition
AR	Aspect ratio	<i>L</i>	Lift force, lb
b	Wingspan, ft	<i>l_f</i>	Fuselage length, ft
c	Chord Length, ft	<i>M</i>	Mach number
\bar{c}	Mean Aerodynamic Chord, ft	<i>m</i>	Mass, slug
<i>C_D</i>	Drag coefficient	<i>n</i>	Load factor
<i>C_L</i>	Lift coefficient	P	Power, ft.lb/s
<i>C_{Lα}</i>	Airfoil Lift Curve Slope	<i>q</i>	Dynamic pressure, lb/ft ²
<i>C_{lβ}</i>	Static Roll Stability coefficient	R	Range, ft
<i>c_p</i>	Specific fuel consumption, lb/hp.hr	<i>R_{C0}</i>	Rate of climb at sea level, ft/min
<i>C_{m0}</i>	Pitching moment coefficient	<i>R_{Ch}</i>	Rate of climb at altitude, ft/min
<i>C_{nβ}</i>	Static Directional Stability coefficient	S	Wing Reference area, ft ²
<i>D</i>	Drag force, lb	<i>S_{wet}</i>	Aircraft wetted area, ft ²
<i>D_P</i>	Propeller Diameter, ft	V	Velocity, ft/s
<i>d_f</i>	Fuselage diameter, ft	<i>V_H</i>	Tail Volume Ratio
E	Endurance, s	W	Weight, lb
e	Oswald efficiency	<i>W_E</i>	Empty Weight, lb
<i>f</i>	Equivalent Parasite Area, ft ²	<i>W_F</i>	Mission Fuel Weight, lb
<i>g</i>	Acceleration due to gravity, ft/s ²		
h	Altitude, ft		
<i>h_{abs}</i>	Absolute ceiling, ft		
K	Interference Factor		
<i>K_N</i>	Empirical factor,		
<i>K_{Rl}</i>	A factor dependent on Reynold's Number		
<i>I_P</i>	Power Index		





Ratios

Ratio	Definition	Ratio	Definition
$\frac{C_p}{\eta_p}$	Brake specific fuel consumption (BSFC), lb/hp.hr	$\frac{L}{D}$	Lift-to-drag ratio
$\frac{EC}{L/D}$	Loiter-segment mission weight fraction, lb.s/hp.hr	$\frac{W}{S}$	Wing loading, lb/ft ²
		$\frac{W}{P}$	Power loading, lb/hp

Greek Symbols

Symbol	Definition	Symbol	Definition
α	Angle of attack, degrees	η_{Pr}	Propeller Efficiency
i	Angle of incidence, degree	η_h	Ratio of Dynamic Pressure at HT
γ	Climb angle, degree	β	Sideslip angle, degree or radian
ρ	Density, slug/ft ³	$\dot{\psi}$	Turn rate, degree/s
σ	Density ratio	Γ	Wing Dihedral Angle, degree
θ_{fc}	Fuselage cone angle, degree	Λ	Wing Sweep Angle, degree
α_0	Lift at zero angle of attack, degrees	i	Angle of incidence, degree
δ	Pressure ratio		

Subscripts

Subscript	Definition	Subscript	Definition
A	Available	HT	Horizontal tail
abs	Absolute	L	Landing
ac	Aerodynamic Center	ltr	Loiter
cg	Center of Gravity	mg	Main gear
cl	climb	max	Maximum
cont.	Continues	min	Minimum
cr	critical	ng	Nose gear
crew	crew	PL	payload
cruise	cruise	res	Reserve





D_0	Zero -lift Drag	req	required
D_i	Induced Drag	$stall$	Stall
E	Empty	TO	Take-off
F	Fuel	tfo	Trapped fuel and oil
fc	Cone length	VT	Vertical Tail
fn	Nose length	w	wing
ff	fuel fraction	wet	wetted
fus	Fuselage	wf	Wing-fuselage

List of Acronyms

Acronym	Definition	Acronym	Definition
AEO	All Engines Operating	$MTOW$	Maximum Take-off Weight
BFL	Balanced field length	MWE	Maximum Weight Empty
CG	Climb Gradient	$MZFW$	Maximum Zero Fuel Weight
ECU	Engine control unit	$NACA$	National Advisory Committee for Aeronautics
FAA	Federal Aviation Administration	OEI	One Engine in Operation
FAR	The Federal Aviation Regulations	OWE	Operational Weight Empty
FCU	Fuel control unit	RC	Rate of Climb
FOD	Foreign object damaged	SFC	Specific Fuel Consumption
GW	Gross weight	STO	Take-off field length
$IFSD$	Inflight shut down	$STOG$	Take-off distance run
MLW	Maximum Landing Weight	TOP	Take-off Parameter





Table of Contents

Abstract.....	ii
Nomenclature	iv
Ratios.....	v
Greek Symbols	v
Subscripts	v
List of Acronyms.....	vi
Table of Contents.....	vii
List of Figures.....	xi
List of Tables.....	xiii
List of Appendices.....	xiv
Chapter 1 Introduction.....	1
1.1. Literature Review	2
1.2. Advantages of Light Attack Aircraft	2
1.3. Drawbacks and Challenges.....	2
1.4. Competitors Aircrafts	2
1.4.1. AT-6 Wolverine.....	3
1.4.2. Embraer EMB 314 Super Tucano.....	3
1.4.3. Beechcraft T-6 Texan II.....	4
1.4.4. North American P-51 Mustang.....	4
1.4.5. Douglas A-1 Skyraider	5
1.5. Health, Safety and Environment	5
1.6. Federal Aviation Administration Requirements & Regulations	6
Chapter 2 Aircraft Features	7
2.1. Aircraft Specification.....	7
2.2. General Characteristics	7
2.3. Performance Specifications	8
2.4. Dimensions and Blueprints.....	9
Chapter 3 Design of a Propeller-Driven Austere Field Light Attack Aircraft	13
3.1. Mission Profile	13
3.2. Design Mission and Ferry Mission Take-off Weight Estimation	15
3.3. Sensitivity Analysis	16
3.4. Drag Polar for Design and Ferry mission	17
3.5. Wing Loading	20
3.6. Performance Analysis for Design and Ferry Mission	22
3.6.1. Aircraft in Steady, Unaccelerated Flight for Design and Ferry Mission.....	22
3.6.2. Power Required and Power Available	23
3.6.3. Rate of Climb.....	24





3.6.4. Absolute and Service Ceiling	25
3.6.5. Range and Endurance	25
3.7. Aircraft in Steady, Accelerated Flight	27
3.7.1. Lift Off Distance.....	27
3.7.2. Landing Distance	27
3.8. Flight Envelope.....	28
3.9. Carpet Plot	30
Chapter 4 Wing Configuration	32
4.1. Airfoil Selection	32
4.2. Design Lift Coefficient	33
4.3. Wing Designs	33
4.4. Wing parameters calculations	34
4.4.1. Verifying the maximum lift coefficient (CL_{max} , W)	36
4.4.2. Increasing lift using high lift devices.....	37
4.4.3. Single Slotted Flap.....	37
4.5. Fuel Tank Integration	41
4.5.1. Fuel Volume	41
4.5.2. Required Volume.....	41
4.6. Wing Material Selection	43
Chapter 5 Empennage Configuration	44
5.1. Tail arrangement for spin recovery.....	45
5.2. Benefits of using ventral and dorsal fin for spin recovery and stability.....	45
5.3. Typical methods for hinge moment reduction	46
5.4. Empennage Configuration Sizing and Calculations	46
5.5. Empennage Configuration Material Selection	48
Chapter 6 Fuselage Configuration	49
6.1. Austere field Light Attack Geometric Fuselage Parameters	49
6.2. Fuselage Fineness Ratio	49
6.3. Fuselage Cone.....	50
6.4. Austere Field Light Attack Fuselage Configuration	50
6.5. Fuselage material selection	51
Chapter 7 Propulsion System.....	53
7.1. Engine Selection	53
7.1.1. Compressor Technology	54
7.1.2. Engine Layout.....	54
7.1.3. Engine Outline.....	55
7.1.4. Engine Performance.....	56
7.1.5. Fuel System	57





7.1.6. Propeller System	57
7.2. Propulsion System Location	58
7.3. Propeller Diameter Estimation.....	58
7.4. Engine Control System	58
7.4.1. Gear box	59
7.4.2. Indicating System	59
7.5. Trade Analysis	60
Chapter 8 Landing Gear Configuration	62
8.1. Landing Gear Sizing	62
8.1.1. Landing gear arrangement type	62
8.1.2. Landing gear strut deposition and tires location	62
8.1.3. Maximum static load per strut	64
8.1.4. Number and size of tires	64
8.2. Wheel Arrangement.....	64
8.3. Shock Absorbers.....	65
8.4. Landing gear material selection	65
Chapter 9 Cockpit Configuration.....	66
9.1. Seat selection	66
9.2. Avionics System	69
9.2.1. Head-up display (HUD).....	70
Chapter 10 Weapons Carriage	71
10.1. Weapons and Missiles Selected for Austere Field Light Attack Aircraft	71
10.1.1. Missiles Selected for Austere Field Light Attack Aircraft.....	71
10.1.2. Guns Selected for Austere Field Light Attack Aircraft	73
Chapter 11 Stability and Control Analysis	74
11.1. Weight Estimation	74
11.2. Center of Gravity	75
11.3. Longitudinal Stability and Control	75
11.3.1. Contribution of aircraft components on Static Stability	76
11.4. Directional Stability and Control	81
11.4.1. Directional Control Requirements	83
11.5. Lateral Stability and Control.....	84
11.5.1. Roll Stability	85
Chapter 12 Model Development.....	86
12.1. Wing	86
12.2. Empennage	86
12.3. Fuselage.....	88
12.4. Propulsion System	88





12.5. Landing Gear	89
12.6. Cockpit Layout	90
12.7. Assembly and Final Renderings of Austere Field Light Attack Aircraft	92
12.8. Auxiliary Systems.....	92
12.8.1. Pneumatic and Environmental control system schematic	93
12.8.2. Electrical system	94
Chapter 13 Manufacturing Process of Austere Field Light Attack Aircraft	97
13.1. Design Stage	97
13.2. Production Stage.....	97
13.3. Assembly stage	98
Chapter 14 Cost and Market Analysis	99
14.1. Cost Analysis	99
14.2. Yearly Fuel Usage Cost	99
14.3. Crew Cost	100
14.4. Flyway cost.....	101
14.4.1. Development support.....	102
14.4.2. Military Operating Cost	102
14.4.3. Flight test operations.....	104
14.5. Market Analysis.....	105
14.5.1. Regional Analysis	105
14.5.2. Market research	105
14.5.3. Market segmentation	106
14.6. Production Break-Even Point	106
Chapter 15 Conclusion	108
Work Distribution.....	111
Gantt Chart for Aircraft Design 1	112
Gantt Chart for Aircraft Design 2	113
References	114
Appendix A	119
Appendix B	130
Appendix C	137
Appendix D	139





List of Figures

Figure 1.1: Beechcraft AT-6 Wolverine (Perry, 2021).....	3
Figure 1.2: Embraer EMB 314 Super Tucano (Overall, 2021).....	4
Figure 1.3: Beechcraft T-6C Texan 2 (T-6 Texan II Info, Forecast, Budget/Costs, 2021)	4
Figure 1.4: North American P-51 Mustang (World War II: North American P-51 Mustang, 2021).....	4
Figure 1.5: Douglas A-1 Skyraider (Douglas A-1 Skyraider - Wikipedia, 2021).....	5
Figure 1.6: Emissions from different modes of transport (Climate change, 2019).....	5
Figure 1.7: Aviation emissions growth in EU, since 2013 (Transport and Environment, 2020)	6
Figure 2.1: Beechcraft AT-6 Wolverine (AT-6 Wolverine, 2020)	9
Figure 2.2: Beechcraft T-6C Texan 2 (Beechcraft T-6 Texan II, 2020).....	10
Figure 2.3: North American P-51 Mustang (North American P-51 Mustang, 2020)	11
Figure 2.4: Douglas A-1 Skyraider (Douglas A-1 Skyraider, 2020)	11
Figure 2.5: Embraer EMB-314 Super Tucano (Embraer EMB 314 Super Tucano, 2020)	12
Figure 3.1: Design Mission.....	13
Figure 3.2: Ferry Mission	14
Figure 3.3: Drag polar Plot for Method 1 and 2	19
Figure 3.4: CL^2 against CD graph	19
Figure 3.5: Matching all sizing requirements	20
Figure 3.6: Power Available and Required against Velocity	23
Figure 3.7: Hodograph Diagram.....	24
Figure 3.8: Absolute and Service Ceiling	25
Figure 3.9: V-N Diagram.....	29
Figure 3.10: Carpet Plot.....	31
Figure 4.1: 4 Main Forces Acting on the Airfoil (Wing Design, 2020).....	32
Figure 4.2: Tail volume coefficient method (Roskam, 1985).....	36
Figure 4.3: Single Slotted Flap Geometry (Roskam, 1985).....	38
Figure 4.4: Ribs, spars, and stringers sizing and control surfaces dimensions (all dimensions are in ft)	40
Figure 4.5: The Aircraft Fuel Tank.....	42
Figure 4.6: Fuel system schematic	42
Figure 5.1: Conventional Empennage Design	44
Figure 5.2: Stages for spin recovery (Cutler, 2020).....	45
Figure 5.3: Dorsal and Ventral Fin Configurations (Roskam, 2003)	46
Figure 6.1: Top view of Austere Field Light Attack Aircraft Fuselage Configuration (all dimensions are in feet)	50
Figure 6.2: Side view of Austere Field Light Attack Aircraft Fuselage Configuration (all dimensions are in feet)	51
Figure 6.3: Fuselage monocoque structure (What is the difference between a monocoque and semi-monocoque fuselage type? 2021).....	51
Figure 7.1: PT6A-67F Engine	53
Figure 7.2: Power section (PT6A-67F SERIES TRAINING MANUAL, 2007).....	55
Figure 7.3: Engine stations (PT6A-67F SERIES TRAINING MANUAL, 2007).....	55
Figure 7.4: Gas generator section (PT6A-67F SERIES TRAINING MANUAL, 2007).....	56
Figure 7.5: Compressor (PT6A-67F SERIES TRAINING MANUAL, 2007).....	56
Figure 7.6: Fuel system and its components (PT6A-67F SERIES TRAINING MANUAL, 2007).....	57
Figure 7.7: Propeller system (PT6A-67F SERIES TRAINING MANUAL, 2007).....	57
Figure 7.8: Schematic diagram gear box control system (PT6A-67F SERIES TRAINING MANUAL, 2007)....	59
Figure 7.9: Engine Indicating System (PT6A-67F SERIES TRAINING MANUAL, 2007)	59
Figure 8.1: Longitudinal tip-over criterion and tire location	63
Figure 8.2: Lateral tip-over criterion	63
Figure 9.1: Ejection seat mechanism (EJECTION SEAT, MODEL MK-J5D, 2020).....	67
Figure 9.2: MK-J5D ground safety lock location view (EJECTION SEAT, MODEL MK-J5D, 2020)	68





Figure 9.3: Cockpit 4000 Nex Gen Systems (Cockpit 4000 NexGen, 2021)	69
Figure 9.4: Cockpit 4000 Nex Gen Display Screen and Digital Sparrowhawk Head up Display (Cockpit 4000 NexGen, 2021)	70
Figure 10.1: Mk-81 250LB GP Bomb	71
Figure 10.2: Mk-82 500LB GP Bomb	71
Figure 10.3: GBU-12 Paveway II	72
Figure 10.4: T64 H.V.A.R rocket	72
Figure 10.5: AN/M3 cannon	73
Figure 11.1: Effect of x_{cg} and x_{np} position on the longitudinal static stability (Nelson, 2010)	76
Figure 11.2: Moment Coefficient Versus Angle of Attack Graph for the Designed Light Attack Aircraft.....	81
Figure 11.3: Directional Stability	83
Figure 11.4: Adverse Yaw	83
Figure 11.5: Cross-wing landing without rudder deflection	84
Figure 11.6: Cross-wing landing with rudder deflection	84
Figure 11.7: Dihedral angle for lateral stability	84
Figure 12.1: Wing Model	86
Figure 12.2: Vertical Tail Model	87
Figure 12.3: Horizontal Tail Model	87
Figure 12.4: Fuselage Model	88
Figure 12.5: Engine Model	89
Figure 12.6: Propeller System Model	89
Figure 12.7: Landing Gear Model	90
Figure 12.8: Seat Dimension	90
Figure 12.9: Simple Seat Model	91
Figure 12.10: Rendered Ejection Seat Model	91
Figure 12.11: Final Renderings	92
Figure 12.12: Schematic diagram of large systems placement within the aircraft.....	93
Figure 12.13: Environmental system schematic (Richardson, 2000).....	93
Figure 12.14: Simplified schematic for the electrical system (FlightLiteracy, 2021).....	94
Figure 12.15: Austere Field Light Attack Aircraft Electrical System Path	95
Figure 13.1: Top view of the austere light attack aircraft	97
Figure 13.2: Front view of the austere light attack aircraft.....	97
Figure 14.1: Operating Cost Chart	99
Figure 14.2: Direct Operating Cost for Austere Field Light Attack Aircraft.....	100
Figure 14.3: Flyway Cost	101
Figure 14.4: 17 parts of the world selected to conduct regional analysis (Anon., 2020).....	105
Figure 14.5: Cost Break-Even Point Graph	107





List of Tables

Table 2.1: General Characteristics	7
Table 2.2: Performance Specifications	8
Table 3.1: Estimating take-off weight at different austere field light attack aircraft designs	15
Table 3.2: Design & Ferry Mission Assumptions	15
Table 3.3: Sensitivity Analysis Comparison for Design and Ferry Mission.....	16
Table 3.4: Drag Polar for design and ferry mission.....	17
Table 3.5: Design parameter at selected design point P	21
Table 3.6: Performance analysis constant parameters	22
Table 3.7: Lift off parameters for design and ferry mission	27
Table 3.8: Landing parameters for design and ferry mission	28
Table 4.1: General Characteristics of various wing types	33
Table 4.2: General Wing Parameters	34
Table 4.3: Assumption of Wing Design Parameters.....	34
Table 4.4: Required incremental section maximum lift coefficient, and effect of size of flap	37
Table 4.5: Single Slotted Flap Constants (Roskam, 1985)	38
Table 4.6: Summary of estimated parameters for single slotted flaps	38
Table 4.7: Final results of the Flap Geometry for Landing and Takeoff	39
Table 4.8: Wing Material Selection	43
Table 5.1: Functions of Dorsal and Ventral Fins (Roskam, 2003)	46
Table 5.2: Empennage configuration sizing and assumptions	47
Table 5.3: Empennage Configuration Material Selection.....	48
Table 6.1: The Optimum Fineness Ratio	49
Table 7.1: Main characteristics of PT6A engines (TYPE-CERTIFICATE DATA SHEET, 2019)	53
Table 7.2: Types of Propellers (Badger, 1993).....	60
Table 8.1: Landing gear types	62
Table 9.1: MK-J5D seat specifications (EJECTION SEAT, MODEL MK-J5D, 2020).....	68
Table 9.2: Specifications of cockpit 4000 Nex Gen (Cockpit 4000 NexGen, 2021)	69
Table 11.1: Weight Data for Austere Field Light Attack Aircraft	74
Table 11.2: Weight and Center of Gravity Location for Major Components of the Austere Field Light Attack Aircraft	75
Table 11.3: Longitudinal Stability Parameters for Wing Section	77
Table 11.4: Longitudinal Stability Parameters for Horizontal Tail and Fuselage Section.....	78
Table 11.5: Longitudinal Stability Parameters for Wing-Fuselage Section and the Total Aircraft	79
Table 14.1: Yearly Fuel Usage Cost Assumptions	99
Table 14.2: Cost per Flight Hour	100
Table 14.3: Development support cost	102
Table 14.4: Military operating costs per hour (Economic Values for Investment and Regulatory Decisions, 2021.)	103
Table 14.5: Military operating costs per hour for various light attack aircrafts.....	103
Table 14.6: Flight test operations cost	104
Table 14.7: Assumption to calculate the Variable Cost.....	106





List of Appendices

Appendix A.1: Suggested Fuel-Fractions for Several Mission Phases (Roskam, 2003)	119
Appendix A.2: Suggested Values for L/D, C _j , C _p , η_p and for C _p For Several Mission Phases (Roskam, 2003)	119
Appendix A.3: Regression Line Constants A and B (Roskam, 2003)	120
Appendix A.4: Typical Values for Maximum Lift Coefficient (Roskam, 2003)	120
Appendix A.5: Wing Loading from Historical Trends (Roskam, 2003)	121
Appendix A.6: Effect of Equivalent Skin Friction on Parasite and Wetted Areas (Roskam, 2003)	121
Appendix A.7: Correlation Coefficients for Parasite Area Versus Wetted Area (Roskam, 2003)	122
Appendix A.8: First Estimates for ΔC_D and 'e' With Flaps and Gear Down (Roskam, 2003)	122
Appendix A.9: Regression Line Coefficients for Take-off Weight Versus Wetted Area (Roskam, 2003)	122
Appendix A.10: Definition of Airplane Ceilings (Roskam, 2003)	123
Appendix A.11: Correlation of Airplane Speed with Power Index for Retractable Gear, Cantilevered Wing (Roskam, 2003)	123
Appendix A.12: Wing Fuselage Interference Factor (Roskam, 2003)	124
Appendix A.13: Lifting Surface Correction Factor (Roskam, 2003)	124
Appendix A.14: Turbulent Mean Skin-Friction Coefficient (Roskam, 2003)	125
Appendix A.15: Airfoil Thickness Location Parameter (Roskam, 2003)	125
Appendix A.16: Definition of Wing Wetted Area (Roskam, 2003)	125
Appendix A.17: Definition of Thickness Ratio for a Wing (Roskam, 2003)	125
Appendix A.18: Leading Edge Suction Parameter (Roskam, 2003)	126
Appendix A.19: Definition of Wing Twist Angle (Roskam, 2003)	126
Appendix A.20: Definition of Fuselage Parameters and Angle of Attack (Roskam, 2003)	127
Appendix B.1: Definition of Flapped Wing Area (Roskam, 2003)	130
Appendix B.2: Wing Geometric Data for Single Propeller Aircraft (Roskam, 2003)	130
Appendix B.3: Lift coefficient versus angle of attack (Roskam, 2003)	131
Appendix B.4: Effect of Flap Chord Ration and Flap Type on K (Roskam, 2003)	131
Appendix B.5: Effect of Thickness Ratio and Flap Chord Ratio on C _(l,δ_f) (Roskam, 2003)	132
Appendix B.6: Flap Deflection Graph (Roskam, 2003)	132
Appendix B.7: Effect of Thickness Ratio and Reynold's Number on Section Maximum Lift Coefficient (Roskam, 2003)	133
Appendix B.8: Military Trainers: Vertical Tail Volume, Rudder and Aileron Data (Roskam, 2003)	134
Appendix B.9: Military Trainers: Horizontal Tail Volume and Elevator Data (Roskam, 2003)	134
Appendix B.10: Planform Design Parameters for Horizontal Tails (Roskam, 2003)	135
Appendix B.11: Planform Design Parameters for Vertical Tails (Roskam, 2003)	135
Appendix B.12: Empennage Configurations Calculations and Assumptions	136
Appendix C.1: Currently Used Geometric Fuselage Parameters (Roskam, 2003)	137
Appendix C.2: Single Engine Propeller Driven Aircraft (Roskam, 2003)	137
Appendix C.3: Typical Landing Gear Wheel Data (n _s =2) (Roskam, 2003)	138
Appendix D.1: Effect of Fuselage or Nacelle segment location on upwash gradient (Roskam, 2003)	139
Appendix D.2: Layout for Computing Fuselage and Nacelle Contribution to Airplane Aerodynamic Center Location (Roskam, 2003)	139
Appendix D.3: Effect of Mach Number on Wing Zero-Lift Pitching Moment Coefficient (Roskam, 2003)	140
Appendix D.4: Factor Accounting for Wig-Fuselage Interference with Directional Stability (Roskam, 2003).140	
Appendix D.5: Effect of fuselage Reynold's Number on Wing-Fuselage Directional Stability (Roskam, 2003)	141





Chapter 1 Introduction

The United States Air Force is developing a new light counter-insurgency, ground attack, and surveillance aircraft program. The aircraft should be capable of locating, detecting, and striking targets on its own or in support of ground forces. The aims and objectives of this analysis is to design an affordable austere field light attack aircraft that satisfies all the AIAA requirements. Furthermore, choosing optimal preliminary configuration layout for all the major components. Moreover, Stability and control analysis is conducted to ensure the aircraft is statically stable in all motion's axis.

The first chapter provides an introduction and literature review to the Austere Field Light Attack Aircraft. Chapter 2 discusses the general and performance characteristics, aircraft specifications and blueprints of the competitive aircrafts. Following that, Chapter 3 provides the estimation of take-off weight for 2 mission profiles, and sensitivity studies are conducted, respectively. Wing loading at different sizing requirements and Performance Analysis are conducted; furthermore, V-n diagram and Carpet plot are illustrated in this chapter. Chapter 4 talks about the wing configuration including airfoil selection and fuel tank integration.

In Chapter 5, Empennage Configuration and material selection is justified, and the conventional tail design is selected with the addition of dorsal and ventral fins. Chapter 6 talks about the fuselage configuration. Following that, Chapter 7 justifies the Propulsion System including, engine performance, fuel system, propeller system and location. After that, Chapter 8 explains various types of landing gear and requirements. The wheel arrangements are also discussed in this chapter. In Chapter 9, Cockpit Configuration is discussed. Furthermore, Seat selection, Avionics system, Head-up display are justified in this chapter.

Chapter 10 elaborates the weapons carriage of the aircraft with various types. Furthermore, methods for missile launch from the aircraft and selection of missiles are discussed in this chapter. In Chapter 11, Stability and Control Analysis are discussed. The weight estimation of the Austere Field Light Attack Aircraft is dissected in this chapter. Chapter 12 talks about the Model Development. Following that, Chapter 13 talks about the Manufacturing Process of Austere Field Light Attack Aircraft. Chapter 14 discusses the Cost and Market analysis. Finally, Chapter 15 provides an overall Conclusion to the Austere Field Light Attack Aircraft.





1.1. Literature Review

The Air Force is pondering a return to the kind of light, prop-driven fighters and attack aircraft that carried out vital close air support and counterinsurgency missions. The attack aircraft is a small, two-seat turboprop airplane designed for operation in relatively permissive environments. The plane should be able, by itself or in support of ground forces, to locate, track and attack targets.

1.2. Advantages of Light Attack Aircraft

There are some key advantages of the LAAs during the construction and deployment of all modern arms systems. An off-the-shelf aircraft can be turned into a LAA that offers a range of options to conserve the production capital of aircraft, aircrew and technical training, and product's quality. The two-seat, single turboprop-powered aircraft includes state-of-the-art radios, data link and multiple sensors (Light-Attack Aircraft | Joint Air Power Competence Centre, 2020).

The cockpit and engine of the aircraft are armor-protected on modern fighter aircraft. Multiple weapon stations, including a wide spectrum of weapons and ammunition, as well as a capable self-defense system complete the LAA. Furthermore, the purchase of LAA would not only pay dividends by prolonging the lifetime of the aircraft, but also by saving resources during actual operations. (Light-Attack Aircraft | Joint Air Power Competence Centre, 2020).

1.3. Drawbacks and Challenges

Due to the wide altitude gap, the markedly slower reaction speed is a significant drawback. Airfield specifications for the LAA are not as demanding as compared to any light attack aircraft. Even a smaller airstrip, combined with simple airplanes maintenance and minimal logistical effort, could transform the necessary runway length and gravity into a high-quality forward operation base (Light-Attack Aircraft | Joint Air Power Competence Centre, 2020).

1.4. Competitors Aircrafts

In this report various competitor aircraft designs will be analyzed, these include Beechcraft AT-6 Wolverine, Beechcraft T-6C Texan 2, North American P-51 Mustang, Douglas A-1 Skyraider, and Embraer EMB 314 Super Tucano. The goal of this analysis is to design an affordable austere field light attack aircraft that can serve close to the front lines and provide sufficient air support to ground forces.





1.4.1. AT-6 Wolverine

The AT-6 Wolverine aircraft is developed by Beechcraft, a Textron Aviation brand. It is tailored to meet the light attack requirements of the armed forces worldwide. With its flexible weapons and external fuel tank configurations, the AT-6 Wolverine light attack/armed reconnaissance aircraft offers warfighters an ideal solution to engage targets in low-intensity combat missions. This type of aircraft is capable land in full take-off weight. It is the first lasers-guided rocket aircraft to launch laser-guided rockets and is the first aircraft to operate a fixed wing (Beechcraft AT-6 Wolverine – a next-generation light attack aircraft, 2021).

The multi-mission aircraft is designed to meet the demanding requirements of warfighters while accommodating 95% of the aircrew population. A full suite of synchronized ground-based training capabilities, as well as an established global logistics infrastructure, further enable AT-6 to outperform its contenders.



Figure 1.1: Beechcraft AT-6 Wolverine (Perry, 2021)

1.4.2. Embraer EMB 314 Super Tucano

The EMB-314 Super Tucano is a Brazilian attack aircraft that has also been used by Colombia, the United Kingdom, Egypt, and the United States. The 314 is a very different plane, which stands out for its size, despite looking very similar to the trainer aircraft that came before it. Owing to the need to fit a more powerful engine, the Super Tucano is longer and taller than its predecessor. This allows for more power and faster speeds. As a result, it is better suited to the tasks for which it is developed (Embraer EMB-314 Super Tucano, 2021).

Embraer Super Tucano is currently being used in many countries as a light attack and recognition aircraft. The Super Tucano won the US Light Air Support contract for Hawker Beechcraft AT-6 Texan II in 2011. Nevertheless, Embraer is able to continue the studies due to recent combat uses of aircraft in Peru and Venezuela.





Figure 1.2: Embraer EMB 314 Super Tucano (Overall, 2021)

1.4.3. Beechcraft T-6 Texan II

It is a turboprop plane with one engine. The aircraft is a low-wing monoplane with tandem seats. The turboprop engine in the aluminum tractor, 97 inch (8.1 ft; 2.5 m), four-blade, constant speed, variable pitch, non-renewable, feathering propeller set and has a retractable tricycle landing gear and is driving by Pratt & Whitney Canada PT6A-68.



Figure 1.3: Beechcraft T-6C Texan II (T-6 Texan II | Info, Forecast, Budget/Costs, 2021)

1.4.4. North American P-51 Mustang

The P-51 Mustang North America Aviation is an American long-range, single-seat fighter and bomber used, among other wars, during the Second World War, and the Korean War. The design team of the Mustang is led by James Kindelberger in April 1940. More than 15,000 of these aircraft are built. It is withdrawn from military active service in 1984 (North American P-51 Mustang - Wikipedia, 2021).



Figure 1.4: North American P-51 Mustang (World War II: North American P-51 Mustang, 2021)





1.4.5. Douglas A-1 Skyraider

This is an American single-seat attack aircraft operating from the end of the 1940s to the beginning of the 1980s. In jet-age it became a propeller-driven anachronism, and is surrendered to the name of "Spad," after the French First World War fighter. The Skyraider had a surprisingly effective and long career. It is run by the U.S. Navy, the United States Marine Corps (USMC) and the US Air Force (U.S. Air Force) as well as by the British Royal Navy, the French Air Force, the RVNAF, etc. It is in the USA service until the beginning of the 1970s.



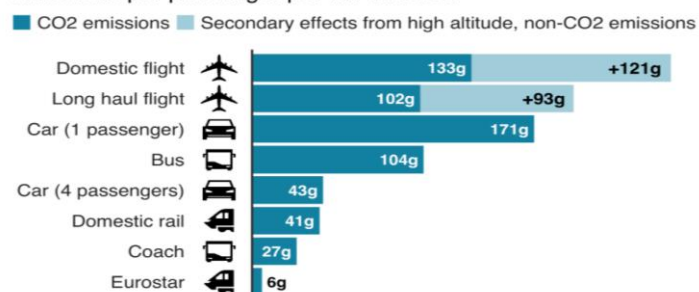
Figure 1.5: Douglas A-1 Skyraider (Douglas A-1 Skyraider - Wikipedia, 2021)

1.5. Health, Safety and Environment

The austere field aircraft affect many aspects, including safety, health, economics and climate, in many different ways. These impacts should be taken into account when designing an aircraft and should strive as much as possible to minimize them. The construction of a fighter aircraft or during flight involves many serious dangers. To be aware of the dangers, several protection directives may be used. Furthermore, aircrafts previously built have an important impact on human health, leading to health risks, such as pollution from the engine.

Emissions from different modes of transport

Emissions per passenger per km travelled



Note: Car refers to average diesel car

Source: BEIS/Defra Greenhouse Gas Conversion Factors 2019

BBC

Figure 1.6: Emissions from different modes of transport (Climate change, 2019)

The aircraft causes many risks on the runway, it cannot stop easily and effectively, even though it is at low velocities, just like any normal vehicle. People should also keep distance specifically if they turn on the engine





and the propellers are rotating. Ground workers and engineers should take the greatest precautions in the performance of aircraft tasks (SAMANCTA, 2020).

The airline industry is aiming to improve the aircraft's performance and aim to minimize noise and pollution as much as possible (Information on the environmental impact of aviation, 2020). Around 2 to 3 % of the overall global CO₂ emissions and the Non-CO₂ emissions in are caused by the aviation industry as showed in figure (1.7) (Aviation Environmental Impacts, 2020).

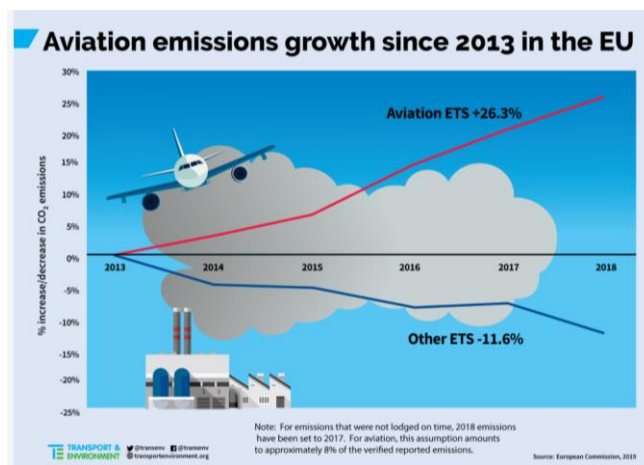


Figure 1.7: Aviation emissions growth in EU, since 2013 (Transport and Environment, 2020)

1.6. Federal Aviation Administration Requirements & Regulations

The FAA has some significant tasks, such as U.S. Private Space Transportation Control, civil aviation law for protection promotion, promoting and improving civil aviation infrastructure, Global airspace and civil aviation infrastructure research and development., creation and implementation of a civil and military aviation control and navigation device and, creation and application of aircraft noise reduction programs and other environmental implications of civil aviation. In terms of the military aircraft the FAA has significant considerations. (Surplus Military Aircraft, 2020).

FAA regulations on all aviation operations, such as the construction and maintenance of aircraft, airline flights, pilot training, etc. In areas such as structural loads, airframe operations, reliability, stability, control and safety mechanisms, design of seats, air-pressure and fire suppression systems, escape capsules, flight management procedures, flight control coordination and urgent air landing and other restrictions FAR 23 has various aviation regulations. FAR 23 has a wide range of applications. There are also specific aspects to the performance of the flight including stable altitude, climbing pace, starting speed and weight of each pilot and passenger. (Federal Aviation Regulations, 2020).





Chapter 2 Aircraft Features

2.1. Aircraft Specification

In attempt to design an Austere Field Light Attack Aircraft, various sorts of competitor aircrafts are tabulated and compared to satisfy the AIAA requirements. With these measurements and parameters taken into consideration, the optimal light attack aircraft is designed.

2.2. General Characteristics

Table (2.1) displays the general characteristics and features for the competing light attack aircrafts which helps in the design of the original aircraft.

Table 2.1: General Characteristics

DATA	Beechcraft AT-6 Wolverine	Beechcraft T-6C Texan 2	North American P-51 Mustang	Douglas A-1 Skyraider	Embraer EMB 314 Super Tucano
CREW	2	1	1	1	2
NUMBERS BUILT	630+	850+	15,000+	3,180	200+
UNIT COST	\$35.1 million	US\$4.272 million (2003)	US\$50,985 in 1945 (equivalent to \$590,000 in 2019)	414,000 US\$	\$9–18 million \$430–500/hour (operational cost 2010)
LENGTH	10.16 m (33 ft 4 in)	10.16 m (33 ft 4 in)	9.83 m (32 ft 3 in)	11.84 m (38 ft 10 in)	11.38 m (37 ft 4 in)
AIRFOIL	-	-	NAA/NACA 45-100 / NAA/NACA 45-100	root: NACA 2417; tip: NACA 4413	root: NACA 63A415 tip: NACA 63A212
WINGSPAN	10.4 m (34 ft 3 in)	10.2 m (33 ft 5 in)	11.28 m (37 ft 0 in)	15.2464 m (50 ft 0.25 in)	11.14 m (36 ft 7 in)
HEIGHT	3.25 m (10 ft 8 in)	3.25 m (10 ft 8 in)	4.08 m (3 ft 4.5 in)	4.7816 m (15 ft 8.25 in)	3.97 m (13 ft 0 in)
WING AREA	16.60 m ² (179 ft ²)	16.28 m ² (175.3 ft ²)	21.83 m ² (235 ft ²)	37.192 m ² (400.33 ft ²)	19.4 m ² (209 ft ²)
EMPTY WEIGHT	2,671 kg (5,890 lb)	2,336 kg (5,150 lb)	3,465 kg (7,635 lb)	5,429 kg (11,968 lb)	3,200 kg (7,055 lb)
MAX TAKE-OFF WEIGHT	4,536 kg (10,000 lb)	3,765 kg (8,300 lb)	5,488 kg (12,100 lb)	8,213 kg (18,106 lb)	5,400 kg (11,905 lb)
FUEL CAPACITY	544kg (maximum internal fuel) Total Fuel w/2 External Tanks 2,054 lb (932 kg) Total Max. Usable Fuel w/4 Tanks 2,908 lb (1,319 kg)	1,200 lb (544 kg) (Total Internal Fuel) 2,054 lb (932 kg) (Total Fuel w/2 External Tanks) 2,908 lb (1,319 kg) (Total Max. Usable Fuel w/4 Tanks)	269 US gal (224 imp gal; 1,020 l)	380 US gal (320 imp gal; 1,400 l) internal tanks	184 gallon (697 litre)
POWER PLANT	1,177kW (1,600shp)	820 kW (1,100 shp)	1 × Packard (Rolls Royce) V-1650-7 Merlin 12-cylinder liquid cooled engine 1,490 hp	1 × Wright R-3350-26WA Duplex-Cyclone 18-cylinder air-cooled radial piston engine, 2,700 hp (2,000 kW)	1 × Pratt & Whitney Canada PT6A-68C turboprop engine, 1,196 kW (1,604 hp)
TYPES OF MISSILES	Mk 81, Mk 82, GBU-12, GBU-38, GBU-58, GBU-49, GBU-59, APKWS 2.75" laser-guided, ALON 2.75" laser-guided, GATR 2.75" laser-guided, AGM-114	Mk 82, GBU-12, GBU-38, GBU-58, GBU-49, GBU-59	T64 H.V.A.R rockets (P-51D-25, P-51K-10 on)	-	LM-70/19 (SBAT-70) (Pod), AIM-9L Sidewinder, MAA-1A Piranha, Python 3, Python 4, AGM-65 Maverick, Roketsan Cirit, Mark 81, Mark 82, M-117, BINC-300,





	Hellfire laser-guided,				
NO. OF MISSILES	-	-	6 or 10	-	11
GUNS	HMP-400 .50 caliber,	-	AN/M2 Browning machine guns	AN/M3 cannon	FN Herstal M3P and its pod (1 on each wing), GIAT M20A1
NO. OF GUNS	2	-	6	4	3
PAYOUT WEIGHT	1,361 kg (3000 lb)	1,000 kg (2,205 lb)	1,000 kg (2,212 lb)	3,600 kg (8,000 lb)	1,550 kg (3,300 lb)
CREW WEIGHT	2 Crew members (200 lb each)	1 Crew member (200 lb)	1 Crew member (200 lb)	1 Crew member (200 lb)	2 Crew members (200 lb each)

2.3. Performance Specifications

Modern aircraft are designed and built according to strict standards which are laid down by national and international authorities to conform with International Civil Aviation Organisation (ICAO).

Table (2.2) provides the performance parameters of the following light attack aircrafts.

Table 2.2: Performance Specifications

DATA	Beechcraft AT-6 Wolverine	Beechcraft T-6C Texan 2	North American P-51 Mustang	Douglas A-1 Skyraider	Embraer EMB 314 Super Tucano
ENGINE TYPE	PT6A-68D	PT6A-68A	Packard V-1650 Merlin	Wright R-3350 Duplex-Cyclone 4-bladed Aeroproducts constant-speed propeller	Pratt & Whitney Canada PT6
MAXIMUM SPEED	580 km/h	585 km/h	708 km/h	518 km/h	590 km/h
CRUISE SPEED	510 km/h	515 km/h	583 km/h	319 km/h	520 km/h
MAXIMUM MACH	0.67	0.67	0.80	0.45	0.80
SFC	0.54 lb/hp	0.54 lb/hp	0.54 lb/hp	0.48 lb/hp	0.58 lb/hp
RANGE	3,195km (1,725 nm) ((with four external fuel tanks) 2,895 km (1,563 nm) (with four external fuel tanks and MX-15D)	884nm (1,637 km (without external fuel tanks) 1,382 nm (2,559 km) (with two external fuel tanks)	1,650 mi (2,656 km, 1,434 nmi) with external tanks	1,316 mi (2,118 km, 1,144 nmi)	1,330 km (830 mi, 720 nmi)
ABSOLUTE/SERVICE CEILING	10,700 m (35,105 ft)	9,400 m (31,000 ft)	12,800 m (41,900 ft)	8,700 m (28,500 ft)	10,668 m (35,000 ft)
RATE OF CLIMB	3,245 ft/min	3848 ft/min	3,200 ft/min	2,850 ft/min	3,230 ft/min
TAKE-OFF DISTANCE	384 m (1259.84 ft)	397 m (1,302.48 ft)	366 m (1,200 ft)	400 m (1312.84 ft)	350 m (1,148.28 ft)
LANDING DISTANCE	623 m (2043.96 ft)	687 m (2253.94 ft)	457 m (1,500 ft)	800 m (2624.67 ft)	550 m (1,804.44 ft)
SERVICE LIFE	18,130 hours	18,720 hours	16,700 hours	15,100 hours	12 Years 5 months
MAXIMUM LANDING WEIGHT	10,000 lb	8,300 lb	13,000 lb	12,600 lb	8,400 lb
TRAPPED FUEL WEIGHT	50 lb	41.5 lb	60.5 lb	90.53b	59.5248 lb





2.4. Dimensions and Blueprints

The following competing light attack aircraft shown in the figures below displays the model in isometric, top, front & side views. Furthermore, these competitor aircrafts are carefully analyzed and compared to create the resulting Austere field light attack aircraft in chapter (12).

These blueprints help in designing the model using Solidworks. Additionally, sketches are made on these blueprints and certain parameters for each configuration are assumed. Finally, an average estimate of the parameters is taken from these competitor aircraft blueprints.

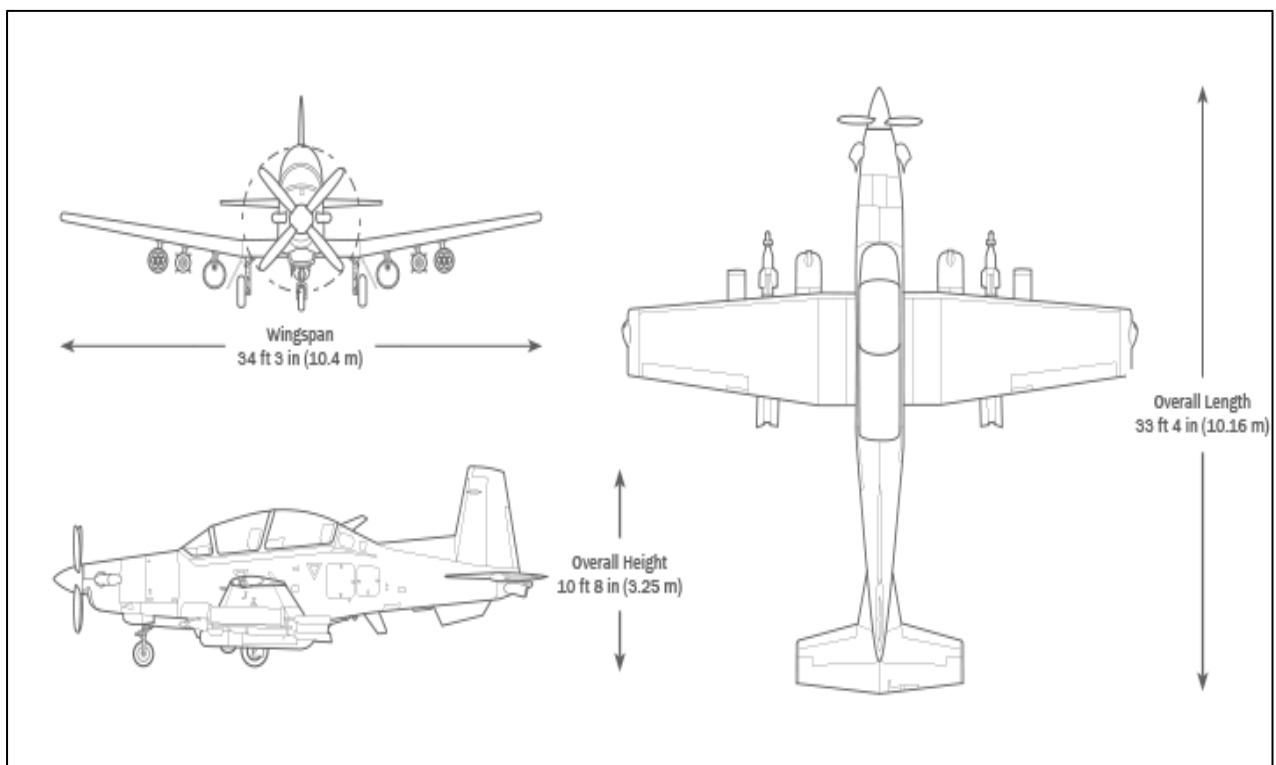


Figure 2.1: Beechcraft AT-6 Wolverine (AT-6 Wolverine, 2020)

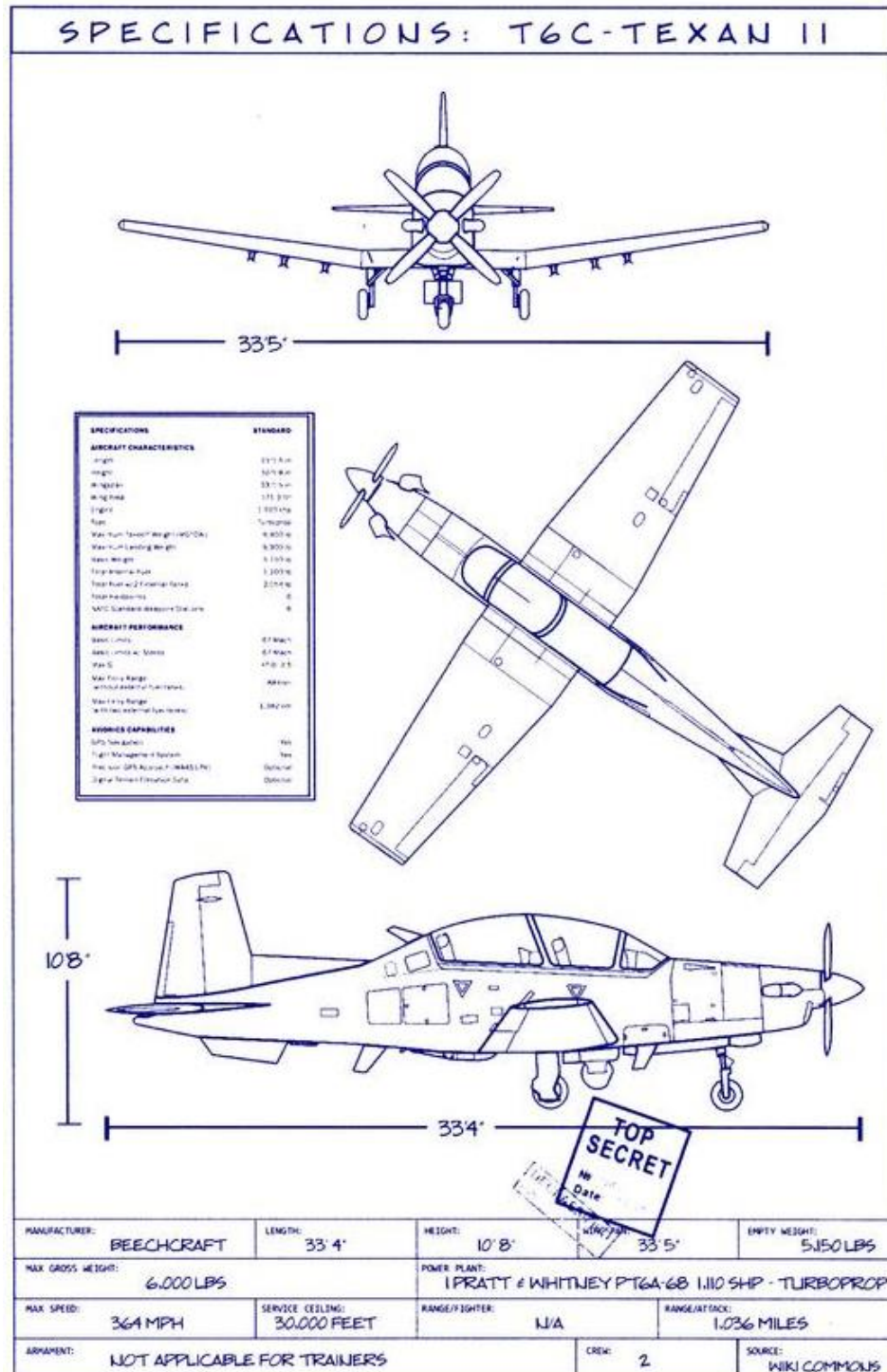


Figure 2.2: Beechcraft T-6C Texan 2 (Beechcraft T-6 Texan II, 2020)

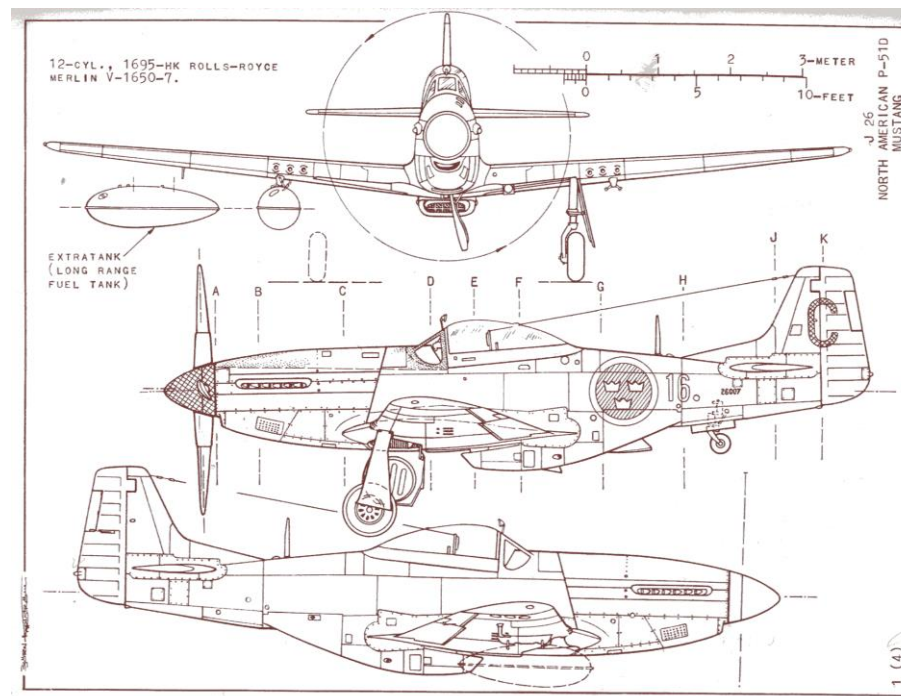


Figure 2.3: North American P-51 Mustang (North American P-51 Mustang, 2020)

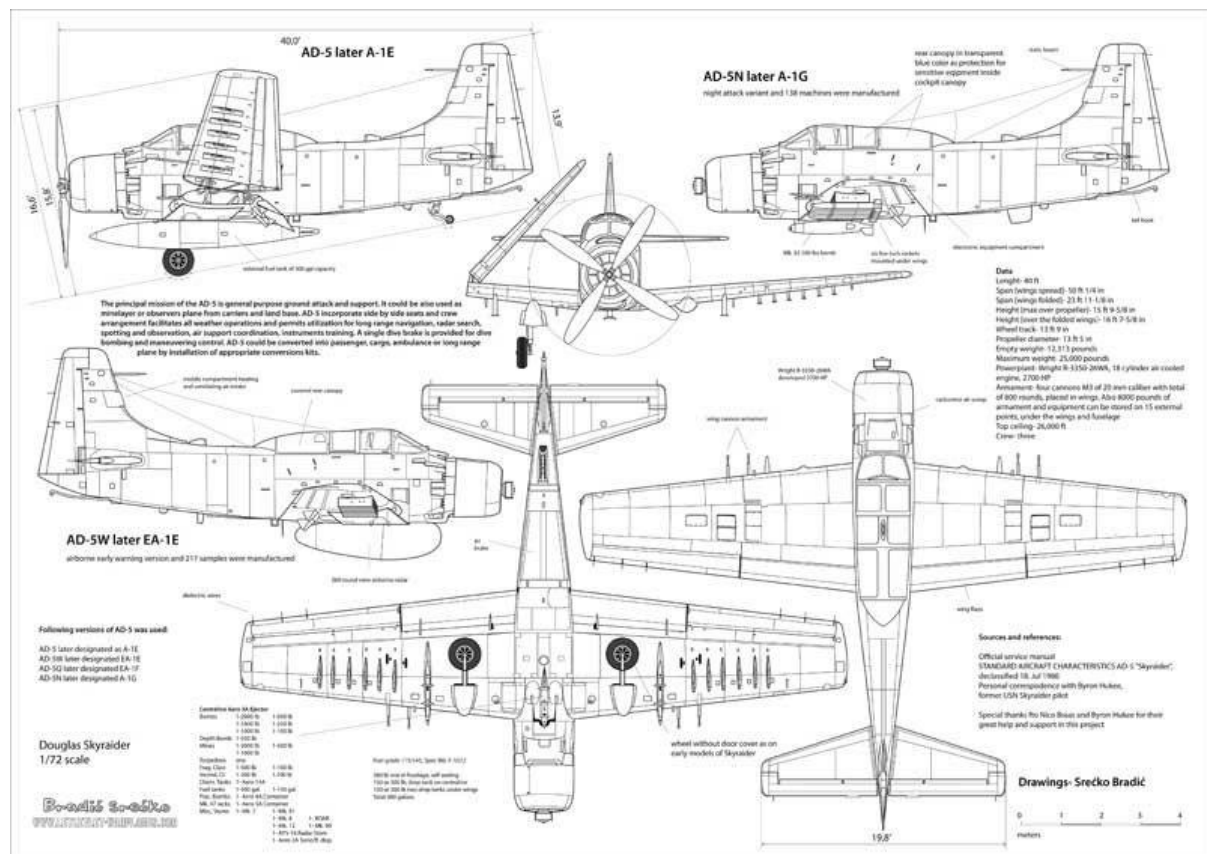


Figure 2.4: Douglas A-1 Skyraider (Douglas A-1 Skyraider, 2020)

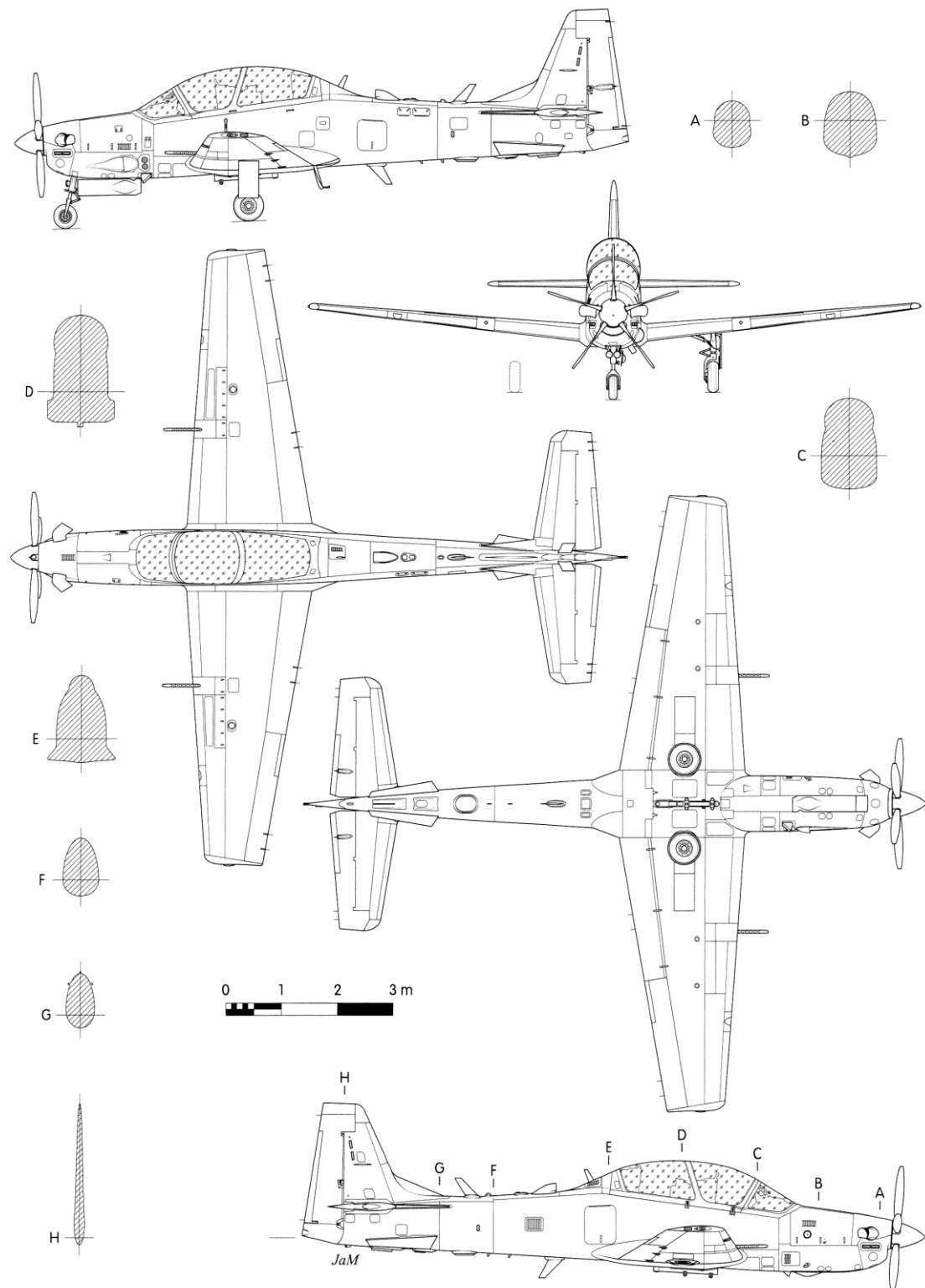


Figure 2.5: Embraer EMB-314 Super Tucano (Embraer EMB 314 Super Tucano, 2020)



Chapter 3 Design of a Propeller-Driven Austere Field Light Attack Aircraft

3.1. Mission Profile

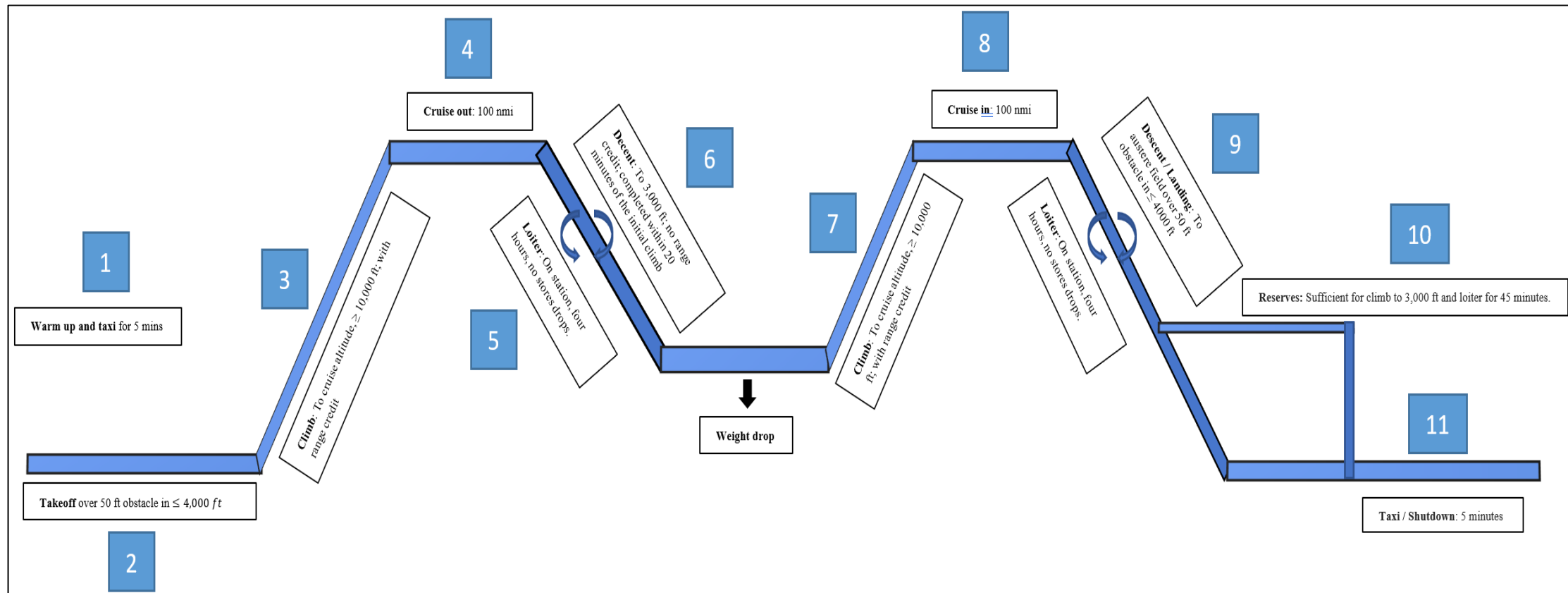


Figure 3.1: Design Mission



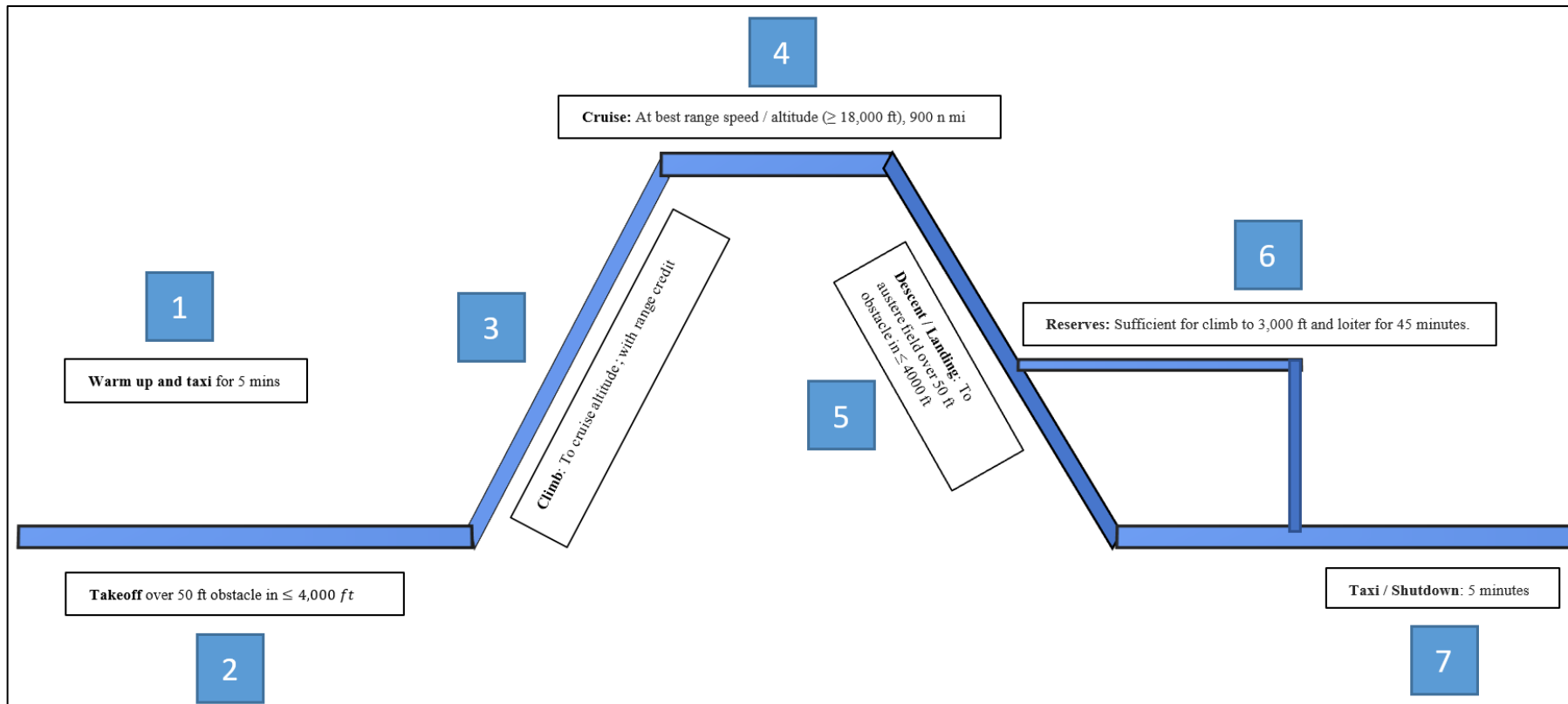


Figure 3.2: Ferry Mission





3.2. Design Mission and Ferry Mission Take-off Weight Estimation

Table (3.1) illustrates different design configurations for austere field light attack aircraft. However, the single engine propeller driven type is the most optimal design for AIAA requirements. Thus, the other designs are not considered due to high take-off weight.

Table 3.1: Estimating take-off weight at different austere field light attack aircraft designs

Design Trials	Take-off Weight	Match the AIAA requirements
Military jet	35,500 lb	No
Twin-propeller Engine	33,000 lb	No
Military Trainer jet	27,000 lb	No
Single Engine Propeller	11,500 lb	Yes

However, by assuming single engine propeller the design mission takeoff weight is evaluated as 11,500 lb and from the ferry mission the takeoff weight is found as 8,000lb after several iterations.

Table 3.2: Design & Ferry Mission Assumptions

Assumptions for Fuel-Weight Ratio	
Engine Start up, Warm-up: 0.995	
Taxi: 0.997 & Take-off: 0.998	
Climb: 0.992 & Decent: 0.993	
Landing, taxi, and shutdown: 0.993	
Design Mission	
Cruise Phase	
Design Mission	Ferry Mission
Range: 100 nautical miles = 607,612 ft	Range: 900 nautical miles = 5.469×10^6 ft
$C_p = 0.5 \text{ lbs/hp/hr} = 2.525 \times 10^{-7} \text{ 1/ft}$	$C_p = 0.5 \text{ lbs/hp/hr} = 2.525 \times 10^{-7} \text{ 1/ft}$
L/D = 8 & $\eta_p = 0.80$	$\eta_p = 0.80$ & L/D = 9 (Best range speed)
Loiter Phase	
Endurance: 4hrs = 14400 s	
Velocity assumed: 350ft/s	
$C_p = 0.6 \text{ lbs/hp/hr} = 3.03 \times 10^{-7} \text{ 1/ft}$	
L/D = 11 & $\eta_p = 0.7$	
Reserve Phase	
Sufficient for climb to 3,000 ft and loiter for 45 minutes	
Endurance: 2700s	
Velocity assumed: 300ft/s	
$C_p = 0.7 \text{ lbs/hp/hr} = 3.54 \times 10^{-7} \text{ 1/ft}$	
L/D = 12 & $\eta_p = 0.70$	

Table (3.2) represents all the assumptions made for take-off weight estimation for both design and ferry mission. It can be depicted that the specific fuel consumption for cruise phase was assumed to be 0.5/lbs/hp/hr for both missions. According to appendix (A.2) this was the lowest possible value in the range for single engine propeller,





this was assumed because during cruise condition around 70% - 80 % of the available thrust was used, thus this validates the assumption made (Transition to Jet-Powered Airplanes, n.d.).

Furthermore, the specific fuel consumption value was increased for loiter and reserve phase due to increased thrust during these stages. As per AIAA requirements, the cruise range was specified to be 100 and 900 nautical miles for design and ferry mission, respectively. For the loiter and reserve phase the velocity was assumed to be 350 ft/s and 300 ft/s with respect to maximum speed from the historical trend and competitor's aircrafts in table (2.2). This assumption was made because the loitering procedure happens within a small region area, circling waiting for landing clearance. In contrast to, the velocity of reserve phase was assumed lower than loitering because it incorporates climbing to a certain altitude thus low velocity was required.

Similarly, lift to drag ratio for both loiter and reserve phase were selected as 11 and 12 respectively, from appendix (A.2). It can be observed that the lift to drag ratio for both phases were higher than cruise phase. This was because during cruise phase the light attack aircraft operates at certain service ceiling altitude hence, the density was lower, and this results in reducing aerodynamic performance (Koh, Mazlan, Rajendran and Ismail, 2017). On the other hand, in loiter and reserve phases control surfaces were deployed to support the aerodynamic performance. Thus, this validates the assumptions made for aerodynamic efficiency for these phases.

3.3. Sensitivity Analysis

After preliminary sizing, it is essential to conduct sensitivity analysis on the parameters listed in table (3.3).

Table 3.3: Sensitivity Analysis Comparison for Design and Ferry Mission

Sensitivity Analysis Data $\frac{\partial W_{TO}}{\partial y}$	Design Mission	Ferry Mission
$y = W_{PL}$	2.95	3.065
$y = W_E$	2.19	2.11
$y = R$	5.1 (lbs/mile)	3.51 (lbs/mile)
$y = E$	1,211.26 (lbs/hr)	N/A
$y = V$	13.85 (lbs/ft/s)	N/A
$y = c_p$	$1,171.35 \frac{lbs}{hp.hr}$ (Range) $8,075.71 \frac{lbs}{hp.hr}$ (Endurance)	$7,267.13 \frac{lbs}{hp.hr}$ (Range) N/A
$y = \eta_p$	-732.02 lbs (Range) -6,920.74 lbs (Endurance)	-4,540.68 lbs (Range) N/A
$y = L/D$	-73.20 lbs (Range) -440.43 lbs (Endurance)	-403.49 lbs (Range) N/A

This provides a quick estimate of the impact of optimization selection on the design. Essentially, if some new mission capability must be obtained, the sensitivity studies help determine which areas of technological change





must be pursued. Accordingly, takeoff weight is improved to obtain optimum results from sensitivity analysis and enhance the aircraft performance.

3.4. Drag Polar for Design and Ferry mission

Drag polar was the relationship between the lift and drag on the aircraft expressed as per the drag coefficient's dependence on the lift coefficient.

Table 3.4: Drag Polar for design and ferry mission

Parameters	Design Mission	Ferry Mission
Wetted Area	1,510.92 ft ²	1,253.5 ft ²
Reference Area	225 ft ²	200 ft ²
Zero-lift Drag Coefficient	0.030	0.031
Propeller Efficiency	0.8	0.8
Low speed, clean	$C_D = 0.030 + 0.0534C_L^2$	$C_D = 0.031 + 0.0534C_L^2$
Take-off, gear up	$C_D = 0.045 + 0.0568C_L^2$	$C_D = 0.046 + 0.0568C_L^2$
Take-off, gear down	$C_D = 0.062 + 0.0568C_L^2$	$C_D = 0.063 + 0.0568C_L^2$
Landing, gear up	$C_D = 0.090 + 0.0606C_L^2$	$C_D = 0.091 + 0.0606C_L^2$
Landing, gear down	$C_D = 0.107 + 0.0606C_L^2$	$C_D = 0.108 + 0.0606C_L^2$

Table (3.4) shows method one on the drag polar estimation of the austere field light attack aircraft for both missions. After comparing a wide range of C_F and wing loading ($\frac{W}{S}$)_{TO} values, the most precise value for zero-lift drag coefficient were selected as 0.030 and 0.031 for both design and ferry mission, respectively. Accordingly, the wetted area and reference area were obtained as 1,510.92 ft² and 225 ft² for design mission, and for ferry mission it's 1,253.5 ft² and 200 ft² respectively. The additional zero-lift drag coefficients $\Delta C_{D,o}$ and values of Oswald efficiency due to flaps and gear were assumed from appendix (A.8).

$$S_{Wet,planforms} = 2s_{exp} \left(1 + \frac{0.25 \left(\frac{t}{c} \right)_r (1 + \tau\lambda)}{1 + \lambda} \right) \quad (1)$$

$$S_{Wet,Fuselage} = \pi D_f l_f \left(0.5 + 0.1351 \left(\frac{l_n}{l_f} \right) \right)^{2.3} \left(1.015 + \frac{0.3}{\lambda^{1.5}} \right) \quad (2)$$

Method two used the equations (1 & 2) for finding the wetted area, also SolidWorks was used to get the exact dimensions of the aircraft. Equation (1) was used to find the wetted area for the wing, vertical tail, and horizontal tail. The difference will be the reference area, thickness to chord ratio, taper ratio. Furthermore, the wetted area





for the wing was only for the exposed area, which means the surface which was in contact with air only. So, the area that's inside the fuselage was subtracted.

The wetted area for the wing, vertical tail, and horizontal tail were found as 425.5 ft^2 , 121.5 ft^2 and 168.2 ft^2 respectively. For the vertical tail, the dorsal and ventral fins where included. Equation (2) was for streamlined fuselage without a cylindrical mid-section. The wetted area for the fuselage was calculated and found as 614.6 ft^2 . The engine cowling was attached to the fuselage, so it was also included. The summation of the wetted areas will be $1,329.7 \text{ ft}^2$. However, in method 1 it was initially estimated as $1,500 \text{ ft}^2$. Since the difference was 11%, then the assumption for the drag polar remains the same.

In order to find the actual $C_{D,0}$, Equations (3,4 & 5) were used.

$$C_{D0,w} = \frac{R_{wf} R_{LS} C_{fw} \left(1 + L' \left(\frac{t}{c} \right) + 100 \left(\frac{t}{c} \right)^4 \right) S_{wet_wing}}{S} \quad (3)$$

$$C_{D0,fus} = R_{wf} C_{f,fus} \left(1 + \frac{60}{\left(\frac{l_f}{d_f} \right)^3} + 0.0025 \left(\frac{l_f}{d_f} \right) \right) \left(\frac{S_{wet,fus}}{S} \right) + C_{D,b,fus} \quad (4)$$

$$C_{D0,emp} = \frac{R_{wf} R_{LS} C_{fw} \left(1 + L' \left(\frac{t}{c} \right) + 100 \left(\frac{t}{c} \right)^4 \right) S_{wet,emp}}{S} \quad (5)$$

These equations were for subsonic aircrafts, the assumptions were based on the parameters of each configuration and with reference to appendix (A.12-A.20). For the empennage part it was done twice, one with horizontal tail parameters and one with the vertical tail parameters.

The $C_{D,0}$ for fuselage, wing, horizontal tail, and vertical tail were 0.0130, 0.0102, 0.0060, and 0.0040. 39.3% of the total $C_{D,0}$ was obtained by the fuselage, 30.9% from the wing, 18.1% from the horizontal tail and finally 12.1% from the vertical tail. The total $C_{D,0}$ will be the summation of these values, which was 0.0332. For the design mission, the difference of $C_{D,0}$ between the two methods was 9.6%. whereas. For ferry mission, the difference was 6.6%.



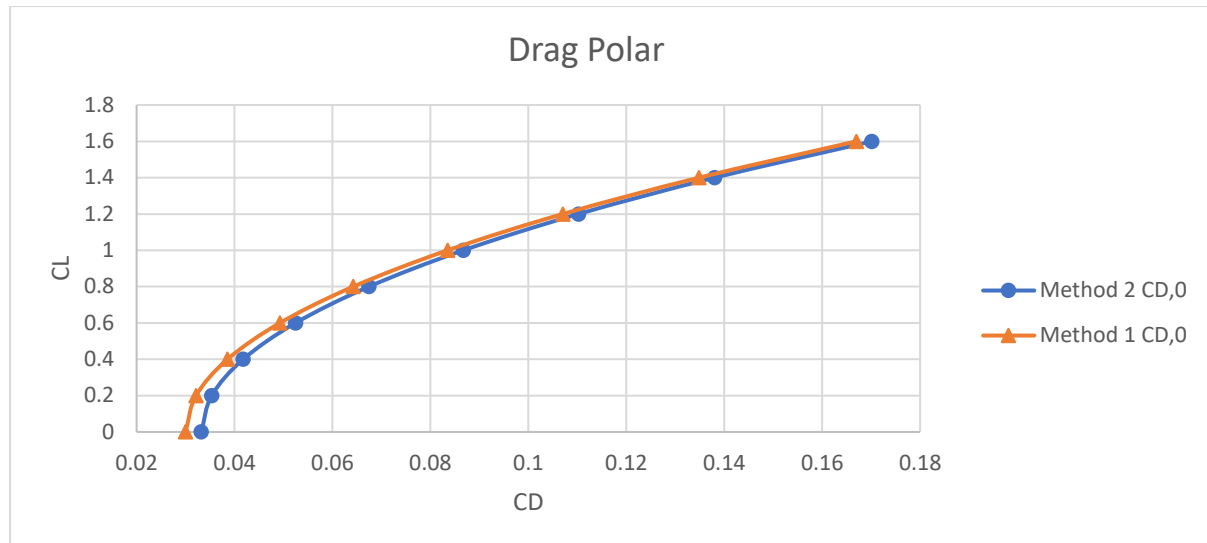


Figure 3.3: Drag polar Plot for Method 1 and 2

Figure (3.3) illustrates the drag polar plot for both methods, it can be depicted that as lift coefficient increases the drag coefficient concurrently increases due to the rise of angle of attack which leads to wake region behind the wing due to flow separation, thus, this results in reaching to the stall condition. When lift coefficient was equal to zero, the zero lift drag coefficient for method one was 0.03, whereas, in method two it was 0.0332. In sections (3.5 & 3.8), the clean maximum lift coefficient was obtained as 1.6. Therefore, the stall velocity was evaluated as 190.5 ft/s. For method one and two, at the maximum lift coefficient, the C_D was at 0.167 and 0.170, respectively. Therefore, the difference between the two methods was 1.76%.

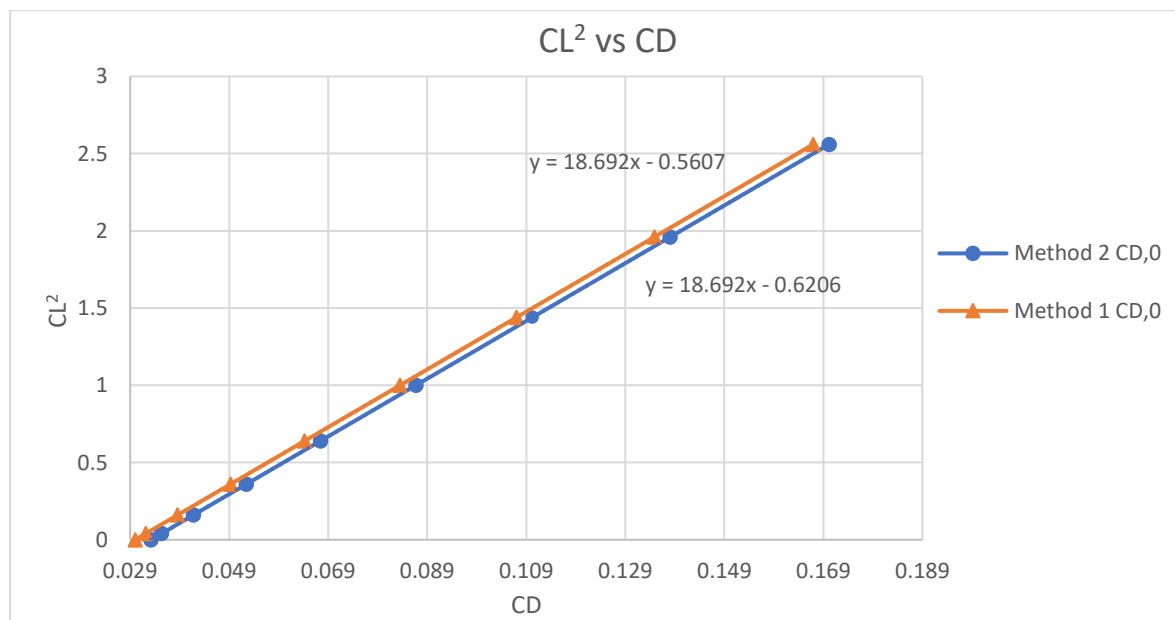


Figure 3.4: C_L^2 against CD graph





It can be seen from figure (3.4) that there was a direct proportional relationship between C_L^2 and C_D . The gradient was same for both methods and was 18.692, the only difference was the constant part which was due to the variation of zero lift drag coefficient. Using the gradient obtained, equation (6) was used to evaluate the span efficiency.

$$e = \left\{ \pi * AR * \frac{dC_D}{dC_L^2} \right\}^{-1} = \left\{ \pi * (7) * \frac{1}{18.692} \right\}^{-1} = 0.8499 \quad (6)$$

3.5. Wing Loading

Wing loading is the ratio of weight of aircraft to its wing area. Wing loading is a vulnerable measure factor for stalling speed requirements of an aircraft.

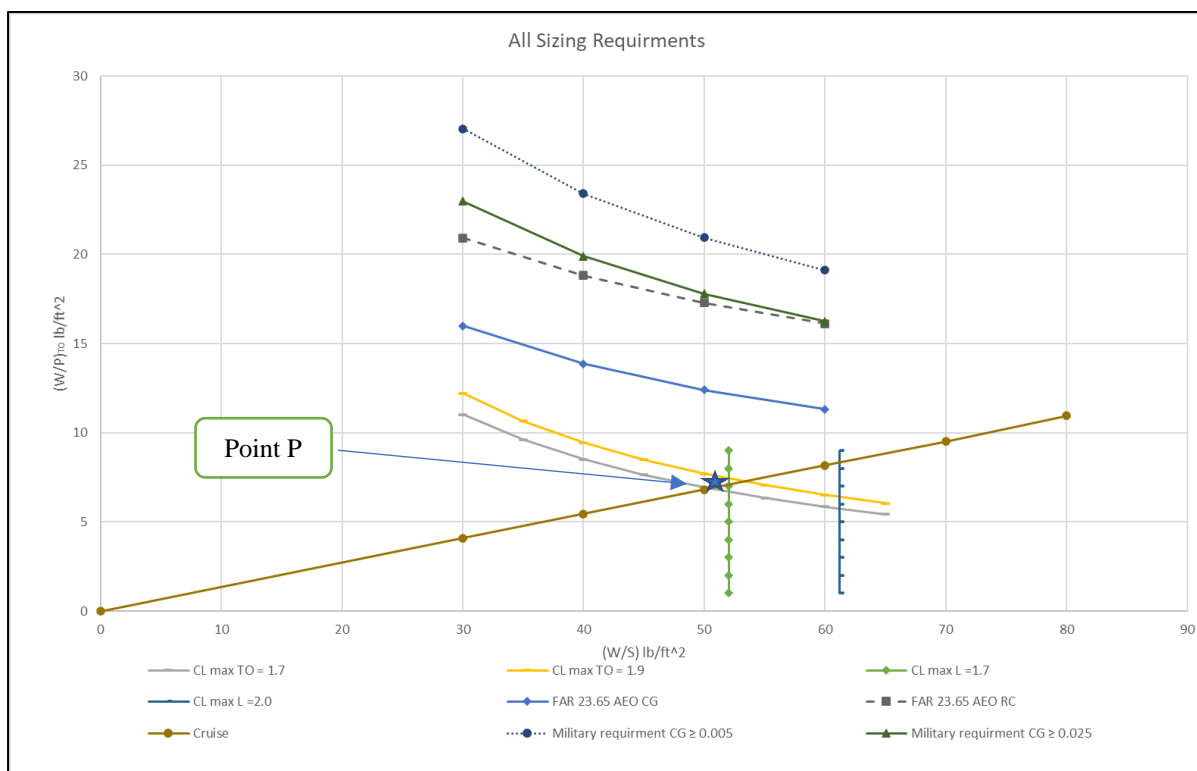


Figure 3.5: Matching all sizing requirements

Figure (3.5) illustrates the results obtained from various wing loadings at different phases such as: takeoff, climb, cruise, landing etc. It can be observed that at climb phases both conditions were considered FAR 23 and military requirements, this was done to have better understanding of design parameters and their limitations at this phase. Furthermore, wing loading for stall phase was not considered while plotting because, the values were not reasonable when compared to other conditions. The values for stall condition diverge away from other sizing requirements.





From figure (3.5), design point P was selected because it provides optimum performance required and it intersects with most of sizing requirements trends. The optimal point P was at wing loading of $51 \text{ lb}/\text{ft}^2$ and the value found for AT-6 Wolverine $56 \text{ lb}/\text{ft}^2$ (Beechcraft AT-6 Wolverine - Africair, Inc., 2020), for North American P-51 Mustang the wing loading was $44.7 \text{ lb}/\text{ft}^2$ (Schiff, 2007). With less power loading the aircraft will be able to take off and land at lower speed or carry more load and vice versa (Wing loading, 2011), also lower wing loading provides sustained turn performance.

However, the power loading obtained from the selected point was $6.8 \text{ lbs}/\text{hp}$, and it was $6.3 \text{ lbs}/\text{hp}$ for AT-6 Wolverine, for North American P-51 Mustang power loading was $6.6 \text{ lbs}/\text{hp}$, which provides short take off distance, high climb rate and high cruise speed (Cavagnaro, 2019). The selected design point P was reasonable and within the range provided in the historical trend and other competitor aircrafts.

Table 3.5: Design parameter at selected design point P

Design parameter	Value
Take-off weight	11,500 lb
Empty weight	4,831.7 lb
Fuel weight	3,210.8 lb
Payload Weight	1,800 lb
Crew Weight	400 lb
Trapped Fuel Weight	57.5 lb
Austere Field (μ_G)	0.25
Single propeller disk loading	$6 \text{ hp}/\text{ft}^2$
Take-off Maximum lift coefficient	$C_{L_{max,TO}} = 1.8$
Landing Maximum lift coefficient	$C_{L_{max,L}} = 2.0$
Clean Maximum lift coefficient	$C_{L_{max}} = 1.6$
Aspect ratio	7
Take-off wing loading	$51 \text{ lb}/\text{ft}^2$
Power loading at take-off	$6.8 \text{ lb}/\text{hp}$

Table (3.5) illustrates the design parameters obtained at the most optimal wing loading of $51 \text{ lb}/\text{ft}^2$. As per AIAA requirements, the crew weight was selected as 200 lb per pilot and the payload weight was 1,800 lb. Furthermore, the lift coefficients for different flight conditions were obtained from the ranges provided in appendix (A.4). The Aspect ratio was assumed as 7 and it was slightly higher with 16% than the competitor light attack aircrafts. The reason for the assumption was to increase lift and reduce induce drag, also to provide more stability, and damp the wing tip vortices (Wing aspect ratios, 2011). It can be observed that the landing maximum lift coefficient was the highest because while landing the aircraft was flying at minimum speed and in case of any emergency there will be a quick response to climb again to a certain altitude.





From the scope of military having a greater wingspan can be equipped with more missiles and weapons and new technologies which can be efficient in terms of missions. Moreover, Although, the maneuverability of the aircraft will be slightly reduced but, the advanced technology of control surfaces nowadays can compensate.

3.6. Performance Analysis for Design and Ferry Mission

The Austere field light attack aircraft is evaluated for level, steady unaccelerated/accelerated flight. Besides that, the necessary parameters for the desired aircraft are evaluated at sea level, including power required, minimum power required, maximum velocity, rate of climb, maximum rate of climb, maximum angle of climb, absolute and service ceiling at different altitudes, maximum range and endurance, lift-off, and landing distance.

Table 3.6: Performance analysis constant parameters

Austere Field Light Attack Aircraft Constant Parameters	
Wingspan (ft)	39.7
Length (ft)	35.7
Wing Area (ft ²)	225
Aspect Ratio	7
Cruise Mach Number	0.42
Maximum Mach Number	0.45
Cruise Altitude (ft)	10,000
C _{D,0} for design mission	0.030
C _{D,0} for ferry mission	0.031
Oswald Efficiency	0.85
Propeller Efficiency	0.80
μ _r (smooth surface)	0.02
μ _r (braking)	0.4
Take Off Weight, W _o for design mission (lb)	11,500
Take Off Weight, W _o for ferry mission (lb)	8,000
Empty Weight, W ₁ (lb)	4,831.7
Shaft Power (SHP)	1,700
SFC/h (lb/hp)	0.546
Density at sea level (slug/ft ³)	0.002377

3.6.1. Aircraft in Steady, Unaccelerated Flight for Design and Ferry Mission

The thrust required to overcome drag for the aircraft to move is referred to as thrust required. Equation (7) is used to calculate the thrust. Following that, for a propeller-driven aircraft, power required is calculated using Equation (8) (Anderson, 1999).

$$T_R = q_\infty S C_{D,0} + q_\infty S \frac{C_L^2}{\pi e A R} \quad (7)$$

$$P_A = T_R \cdot V_\infty \quad (8)$$





$$T_A = \frac{P_A}{V_\infty} = \frac{\eta_{PR} \cdot P}{V_\infty} \quad (9)$$

Thrust available is calculated using the propeller efficiency and shaft power available with respect to the velocity at sea-level using Equation (9). A range of velocity is taken from 0 ft/s to 600 ft/s to determine the conditions and how does some parameters change when increasing the velocity, such as thrust required and rate of climb. Since the weight of the airplane is known, C_L is generated for a variety of velocities. The flight is to be steady and unaccelerated, so the weight is assumed to be equal to the lift.

3.6.2. Power Required and Power Available

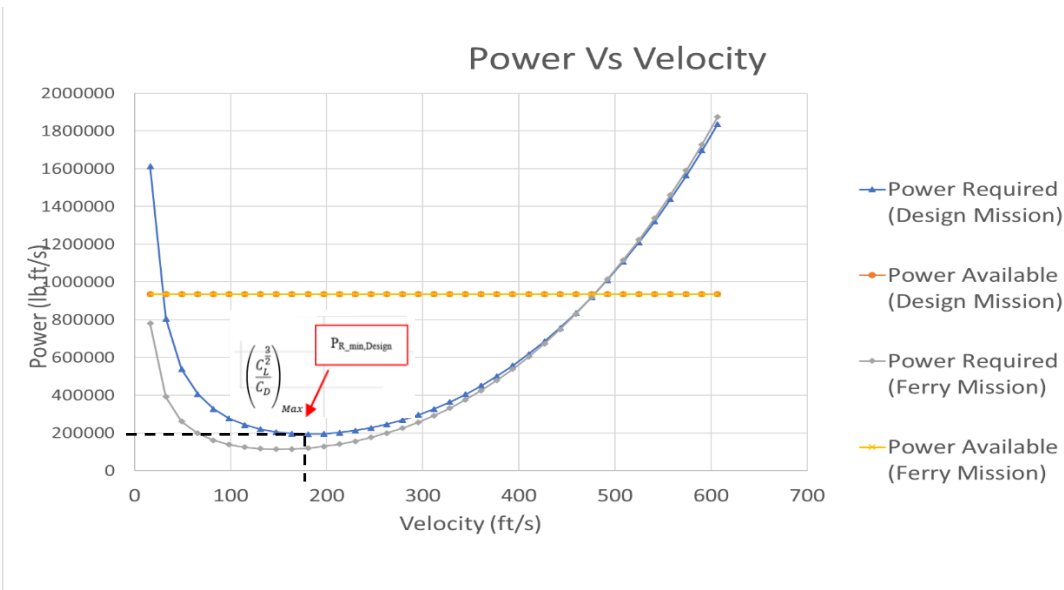


Figure 3.6: Power Available and Required against Velocity

Power available was a constant throughout various velocities, while the power required varies from altitude and velocity to another. The shaft power available is around 1,700 SHP (PT6A Engine Sales & Leasing Airforce Turbine Service (ATS), 2021). The two mission profiles were analyzed and compared as shown in figure (3.6). It was clearly shown that the minimum power required was slightly lower for ferry mission compared to design mission, due to the reduction of take-off weight. The maximum velocity of the aircraft can be obtained from the intersection of the two trends. The intersection occurs at almost 480 ft/s (284 kts) which was the same for both mission profiles.





3.6.3. Rate of Climb

The rate of climb is the aircraft's vertical speed; pilots use it to assess if the aircraft's altitude is rising or decreasing. The rate of climb at the sea level is calculated using equation (10). The rate of climb is determined by dividing the excess power by the aircraft's weight, using the excess power from the previous section (Anderson, 1999).

$$\frac{R}{C} = \frac{\text{Excess Power}}{W} \quad (10)$$

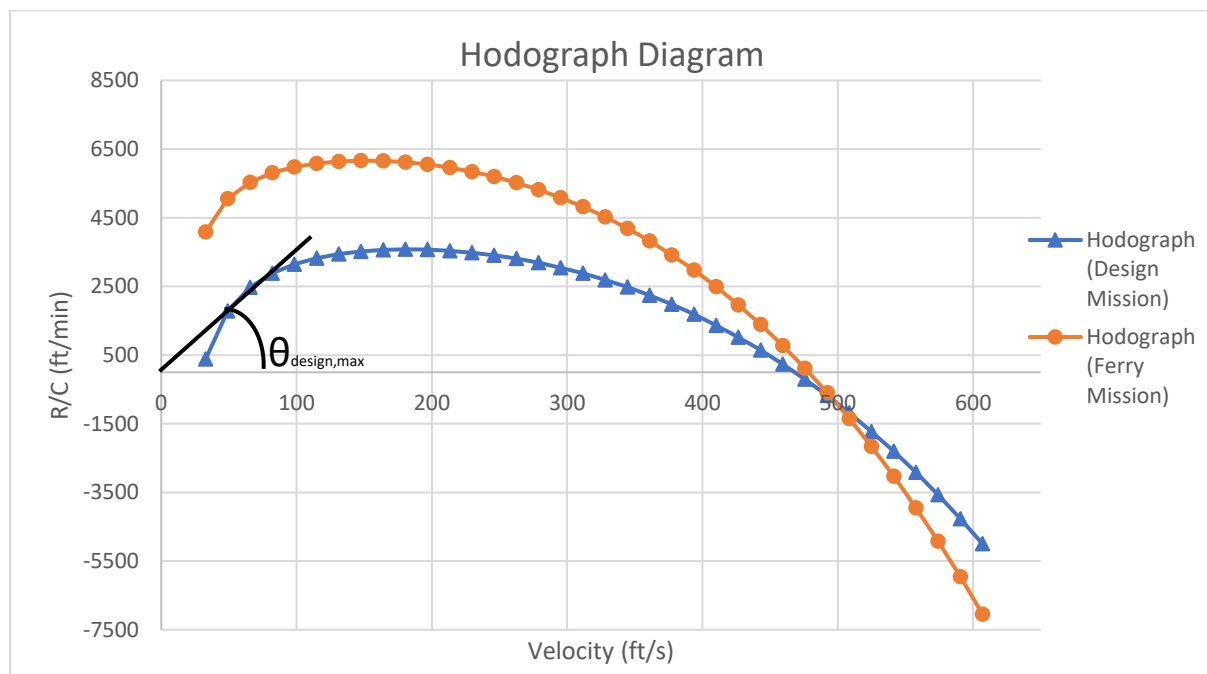


Figure 3.7: Hodograph Diagram

Since the ferry mission has lower takeoff weight, the maximum rate of climb and maximum climb angle was larger compared to the design mission. The Maximum rate of climb for design and ferry mission was 3,580 ft/min and 6,162 ft/min respectively. While the maximum climb angle was 32.16 deg and 64.26 deg, respectively. To keep in mind that the main factor that was changed between the two missions was the take-off weight.

The aircraft rate of climb calculated in Matching of all sizing requirements in figure (3.5) at a range of wing loading and at stall velocity was found to be $\geq 300\text{ft/min}$ for military climb sizing requirements. However, the result from the Performance analysis was found for the maximum velocity which means the maximum rate of climb, comparing to the competitor's aircrafts, the designed aircraft gave better results than the competitors which is shown in table (2.2).





3.6.4. Absolute and Service Ceiling

The Rate of climb section is done for six different altitudes using the same approach. This is preformed to determine the aircraft's absolute and service ceilings. At sea level, 3,300 ft, 16,400 ft, 23,000 ft, 30,000 ft, and 32,000 ft were reached.

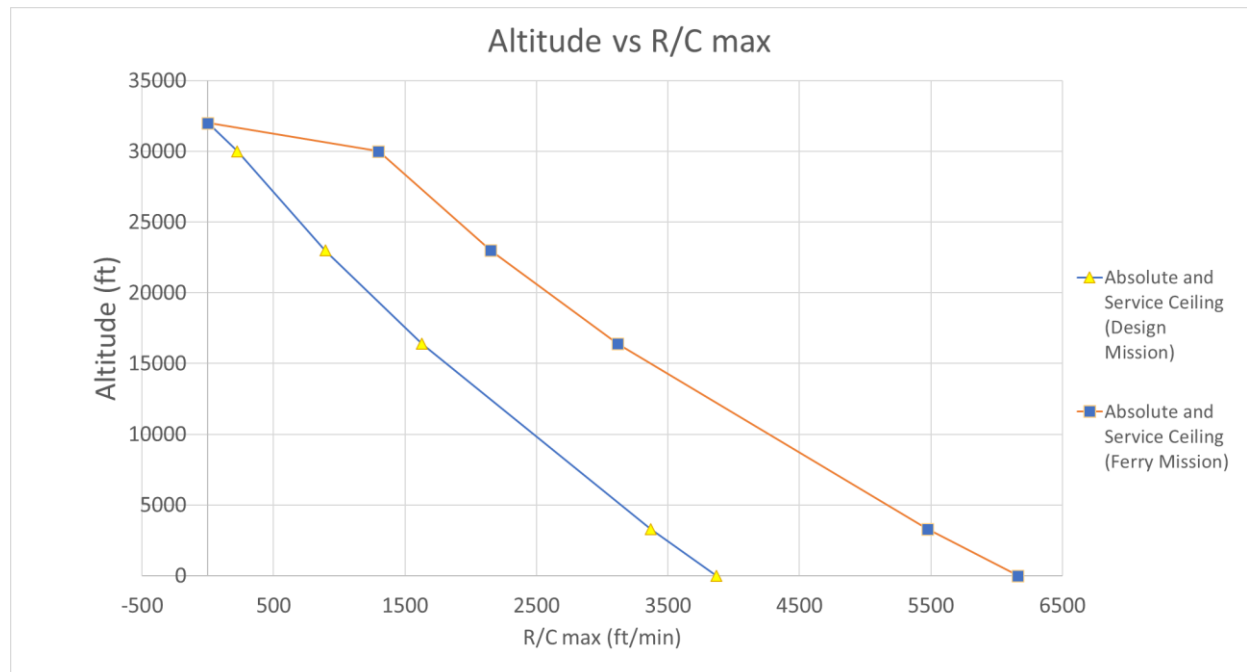


Figure 3.8: Absolute and Service Ceiling

The service ceiling is the altitude at which the aircraft is at its maximum operating altitude, while the absolute ceiling is higher than the service ceiling but is risky to fly at because of the thin air at that altitude and low density, which affects the engines' performance. Moreover, it will necessitate more shaft power and energy, resulting in high fuel consumption. The absolute ceiling is estimated to be 32,000 feet (10 km) (Aircraft engine performance - Wikipedia, 2021).

3.6.5. Range and Endurance

The range of an aircraft is the distance it travels from takeoff to landing, which is determined by the aircraft's fuel capacity as well as cross-country speed and weather conditions. In this study, the calculated range is at sea level. Equation (11) is used to calculate the range of the aircraft. Since, the aircraft is operating at steady, unaccelerated flight, lift and drag coefficients were calculated separately. (Anderson, 1999).

$$R = \frac{\eta_{pr}}{c} \cdot \frac{C_L}{C_D} \cdot \ln \frac{W_0}{W_1} \quad (11)$$





$$R = 1,062 \text{ Nm (for Design Mission)}$$

$$R = 1,164 \text{ Nm (for Ferry Mission)}$$

The maximum range occurs when (L/D) is maximum. The range calculated for the design mission is 1,062 nm at sea level conditions. On the other hand, the maximum range for the ferry mission is 1,164 nm. The increase of the range for the ferry mission is due to the reduction of the takeoff weight, which leads to less drag and less fuel consumption.

The actual range of the aircraft assumed initially in section (3.2) and table (3.2) is 100 nm only at the cruise phase from the design mission. For the ferry mission, the cruise phase assumed as 900 nm. However, the range found in the performance analysis is for the whole mission profiles not only at cruise phase. The time it takes for the aircraft to empty its fuel tanks is known as endurance. The equation (12) that is used to calculate endurance (Anderson, 1999).

$$E = \frac{\eta_{pr}}{c} \cdot \frac{C_L^{\frac{3}{2}}}{C_D} \cdot (2\rho_{\infty}S)^{\frac{1}{2}} \cdot (W_1^{-\frac{1}{2}} - W_0^{-\frac{1}{2}}) \quad (12)$$

$$E = 7.2 \text{ Hrs (for Design Mission)}$$

$$E = 10.5 \text{ Hrs (for Ferry Mission)}$$

Minimum power required occurs when the aircraft is at a condition such that $\frac{C_L^{\frac{3}{2}}}{C_D}$ is a maximum value. (Anderson, 1999). Which is shown in Figure (3.6). At this condition with this velocity, the aircraft will give the maximum endurance. So, the number of hours could possibly be high due to this condition. However, it is nearly impossible for the aircraft to maintain its flight at the minimum power required, so the endurance for the real flight will be less than the ones calculated.

In the wing loading section (3.5), the assumption for endurance in the design mission is only for the loiter and reserve missions, the endurance for these two missions is 4hours for the loiter and 45 minutes for the reserve. However, the total endurance for the design mission is found as 7.2 hours. On the other hand, the total endurance for ferry mission is calculated as 10.5 hours, and the assumption is made for ferry mission to have 45 minutes for reserve phase.





3.7. Aircraft in Steady, Accelerated Flight

Steady level flight when an aircraft flies at a steady speed over a level route parallel to the earth. If the aircraft has achieved this balance, all four flight forces are balanced. Therefore, the main applications that can be estimated in these conditions are aircraft performance and flight planning.

3.7.1. Lift Off Distance

The horizontal distance from the start of the aircraft departure until aircraft is airborne is called lift off distance. The aircraft experience a resistance force (R) while on the runway because of rolling frictions between tires and ground. However, the factor for rolling friction is 0.02 which is smooth (Anderson, 1999). The altitude selected for takeoff and landing is at 6,000ft as per AIAA requirements. The density is assumed as 0.00198 slug/ft³.

The lift off distance equation is:

$$S_{LO} = \frac{1.44W^2}{g \cdot \rho_\infty \cdot S \cdot C_{L,max} \{T - [D + \mu_r(W - L)]av\}} \quad (13)$$

Table 3.7: Lift off parameters for design and ferry mission

Parameters	Design Mission	Ferry Mission
Height of wing from ground (ft)	5.4	5.4
Lift off velocity (ft/s)	203.2	169.5
Average velocity (ft/s)	142.2	118.6
Drag (lb)	779.2	545.1
Lift (lb)	8,107	5,639
Lift Off Distance (ft)	1,503	961.4

The main changes that occurred between design and ferry missions is that the takeoff weight is reduced and $C_{D,0}$ increased for the ferry mission. This led to reduction in the distance required for the take off. The Assumption made in the wing loading section (3.5) for the Lift-off distance is < 4,000 ft at an altitude of 6,000 ft in standard atmosphere. So, the results obtained from the performance analysis is within the range assumed.

3.7.2. Landing Distance

The landing distance is from the airport runway horizontally to a specific location at the airport until the aircraft stops. At the landing, the aircraft will again experience a resistance force (R), which is due to the rolling friction





which comes from ground and tires. The rolling friction factor is assumed as 0.4. Below are the main factors the affects the landing distance of an aircraft.

- 1- The weight of the aircraft
- 2- Runway condition
- 3- Braking system.

$$S_L = \frac{(1.69)(W^2)}{g\rho_\infty S C_{L,max} \{ [D + \mu_r(W - L)] 0.7 V_T \}} \quad (14)$$

Table 3.8: Landing parameters for design and ferry mission

Parameters	Design Mission	Ferry Mission
Empty Weight (lb)	4,831.7	4,831.7
V_T (ft/s)	135.38	135.38
V_{avg} (ft/s)	94.7	94.7
C_{D,0}	0.03	0.031
Drag (lb)	412.5	414.59
Lift (lb)	3,995.3	3,995.3
Landing Distance (ft)	1,840.7	1,835.6

The small difference in landing distance is because of the change in drag specifically in the C_{D,0}. The weight that is used in this calculation for the aircraft is the empty weight, this is because most of the fuel will be used already while landing. The empty weight is the same for both missions. The assumption made for the landing distance in the wing loading section (3.5) is that the required distance is 4,000ft at an altitude of 6,000ft.

3.8. Flight Envelope

The flight envelope is a concept in aerodynamics that describes the operating boundaries of an aerial platform in terms of maximum speed and load factor for a given air density. The flight envelope refers to the safe operating range of an aircraft. The structural load limitations as a function of airspeed is the most essential and typical plot used for an airplane's aerodynamic characteristics. Normally, the flying envelope is specified during the design process. A speed versus load factor chart (or V-n diagram) provides a visual representation of an aircraft's performance limitations. It illustrates how much load factor may be accomplished safely at various airspeeds.



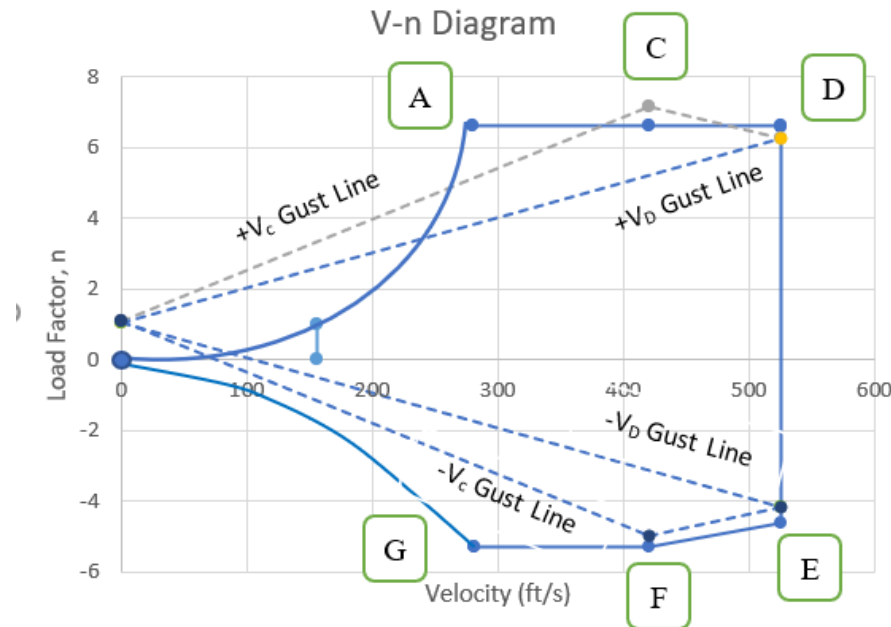


Figure 3.9: V-N Diagram

In figure (3.9) V-N diagram was plotted for Austere field light attack aircraft, the lines of maximum lift capability were the first points of importance on the V-N diagram. The stall speed for the aircraft was found using $C_{L,max}$ as 1.6, this value was obtained from section (3.5). Since the maximum load factor varies with the square of the airspeed, the maximum positive lift capability of this airplane was 6.6 at 280.2 ft/s as shown in point (A). The light attack airplane cannot fly above the line of maximum load factor. The maneuvering speed V_A was calculated from equation (15) as 280.2 ft/s, and the stall speed V_s evaluated as 156.15 ft/s from equation (16). The conditions were taken for cruise phase.

$$V_A \geq V_s \sqrt{n_{lim}} \quad (15)$$

$$V_s = \sqrt{\frac{\frac{2GW}{S}}{\rho C_{N_{max}}}} \quad (16)$$

The limit airspeed was a design reference point of the airplane, which was the dive speed of the aircraft, the light attack aircraft was limited to 525 ft/s. To avoid structural damage and ensure that the airplane's expected service life was achieved, the plane must be operated inside the envelope defined by velocity and load factor limits. The V-N diagram must be understood by the pilot as describing the safest mix of airspeeds and load factors. The dive speed V_D was determined from equation (17) as 525 ft/s, the cruise speed was 420 ft/s.

$$V_D \geq 1.25V_C \quad (17)$$





A maneuver or a gust of wind will momentarily push an aircraft out of its safe flight envelope, causing structural damage and risking flight safety. The gust usually starts from load factor of 1, it consists of linear lines slightly crossing the load factor limits at some conditions. However, the light attack aircraft's structure should be designed to be strong enough to withstand such conditions.

There are two points of great importance on the V-N diagram as shown in figure (3.9). The intersection of the negative limit load factor and line of maximum negative lift capability was represented by point (G). Any velocity greater than point (G) produces enough negative lift to damage the aircraft by excessive flight loads. The positive limit load factor and the line of highest positive lift capability meet at point (A). The minimum velocity at which the limit load factor can be reached aerodynamically was at this stage, this occurs at a velocity of 280.2 ft/s where the light attack aircraft was at maneuver stage.

Any velocity greater than point (A) produces enough positive lift to cause the airplane to be damaged by extreme flight loads. Since subsonic aerodynamics will expect a minimal available turn radius at this condition, the velocity at point (A) was commonly referred to as "maneuvering velocity". Since an airplane flying below this level cannot generate a damaging positive flight load, the maneuver speed was a useful reference point. When the airplane is below the maneuver speed, no combination of maneuver and gust will damage due to excess flight load (Operating Flight Strength (V-g / V-n Diagrams), 2021).

3.9. Carpet Plot

In a two-dimensional plot, a carpet plot depicts the interaction between two or more independent variables and one or more dependent variables. In general, Carpet Plots are built to identify an ideal design that meets all of the performance requirements while being lightweight and low expense.



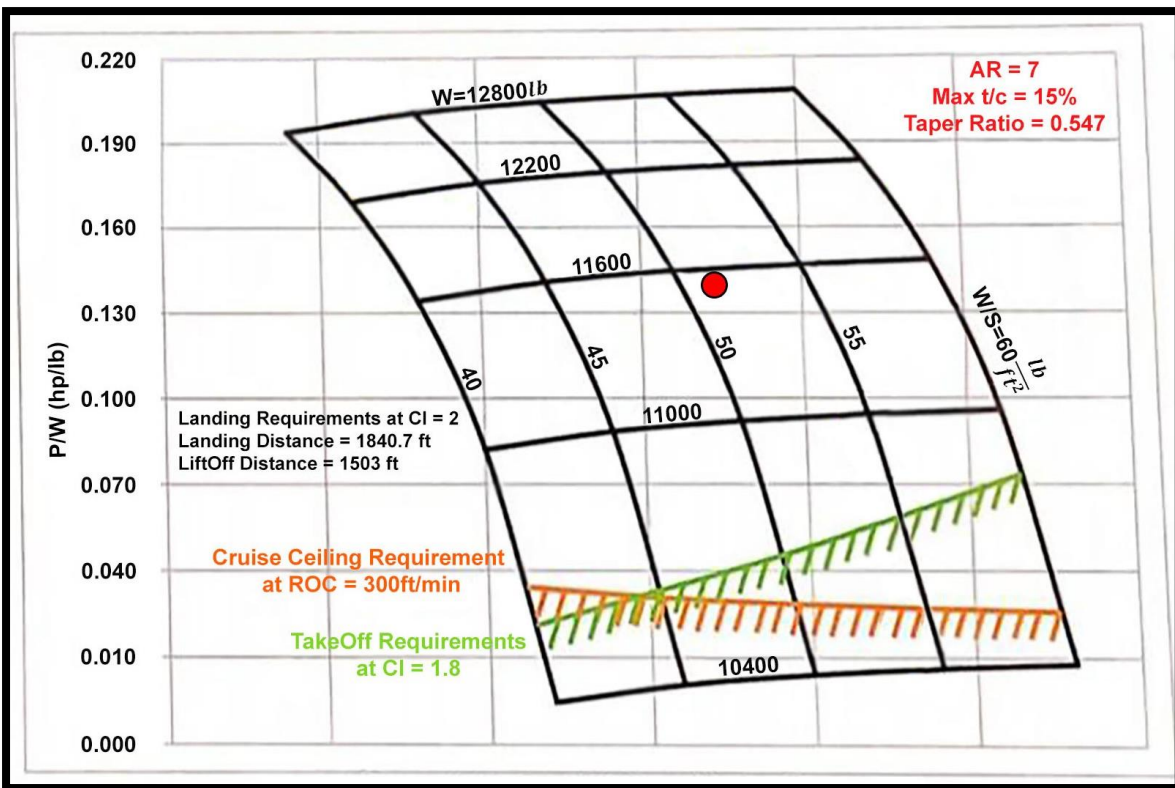


Figure 3.10: Carpet Plot

Figure (3.10) is showing the carpet plot for Austere field light attack aircraft, the takeoff weight values estimated were between 10,400 lb and 12,800 lb, which were within the range for light attack aircrafts. The calculations for wing loading were evaluated with different takeoff weights, then the process was repeated several times with different wind loadings, and the variation of power to weight ratio was obtained. The power loading range was taken from 40 lb/ft² to 60 lb/ft², and the power to weight ratio was varied from 0.005 to 0.21.

The optimum point selected for the designed light attack aircraft at 0.147 hp/lb power to weight ratio, wing loading of 51 lb/ft² and 11,500 lb takeoff weight, this point provides suitable power loading with low weight and cost. It can be observed that decreasing the takeoff weight results in significant reduction in power to weight ratio. Plotting carpet plot helps in studying several parameters at one time and selecting the optimum point that satisfies all the condition.





Chapter 4 Wing Configuration

Wing is one of the main elements of the aircraft that lifts and is fitted to the fuselage. The first step before a wing is designed is to pick an airfoil that meets the design requirements e.g. cruise velocity, take-off, aerodynamic efficiency, etc.

4.1. Airfoil Selection

The airfoil is the backbone of the airplane in many ways. The main force produced by the airfoil is called lift which depends on the direction of the speed. The Lift is based on the angle of attack; the higher the attack angle, the larger the lift is. The Stall angle is the highest lift that is achieved as the flow separation occurs at the top of the airfoil.

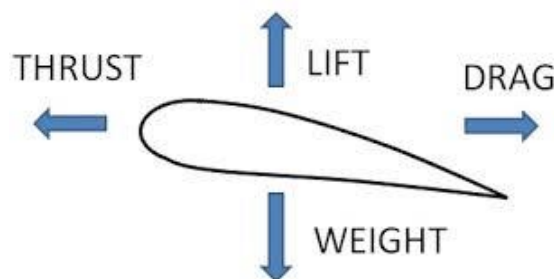


Figure 4.1: 4 Main Forces Acting on the Airfoil (Wing Design, 2020)

In fact, engineers may choose to use different types of root and tip airfoils with a selected tip airfoil, which stalls at greater angle of attack than the root. This produces a smoother flow over the roll control surfaces at various attack angles, under which the root is stalled. Two designs are tested and analyzed in the report. Each design has 2 different types of airfoils, one for the root and the other for the tip.

For Design one, the airfoils are NACA 2412 and NACA 4412. The Second design airfoils are NASA MS (1)-0317 and NASA MS (1)-0313. Design 1 is eliminated because it did not meet the requirements of the Lift needed for the aircraft and the values are shown in section (4.2.1).

The two airfoils have proven the good $C_{L,max}$ at the high angle of attack, as compared to the airfoil's designs. These airfoils make it possible for the pilot to maneuver with high alpha over a wide variety of attack angles in the case of flights and emergencies. Since the cambered airfoil has been chosen rather than symmetrically because it generates lift at zero angle of attack. The cambered airfoil must be optimized for a positive angle of attack. Since it generates less drag with the same amount of lift, plus it gives more lift before the stall angle is reached.





4.2. Design Lift Coefficient

The optimal one should be chosen from current airfoils based on the one that is similar to the one with the desired characteristics. The current airfoils should be used by the engineers to optimize their flight efficiency. In addition, a well-planned subsonic flight airfoil is operated by a design lift coefficient that has a drag coefficient that is greater than the skin friction drag. The plane should be designed to fly near the design lift coefficient to improve aerodynamic efficiency at the design mission.

$$W = L = q \cdot S \cdot C_L = q \cdot S \cdot C_l \quad (18)$$

$$C_l = \frac{1}{q} \cdot \left(\frac{W}{S} \right) \quad (19)$$

4.3. Wing Designs

For the Austere Field Light Attack aircraft three major wings have been compared and examined and are: rectangular, tapered, and elliptical. The wings detail as seen below in table (4.1).

Table 4.1: General Characteristics of various wing types

Rectangular	Tapered	Elliptical
Easiest and simplest wing to manufacture. It is not the most desired wing, aerodynamically.	Has lower induced drag, high performance, and low operating costs. Lower inertia along the axis reduces landing stresses on the main spar.	Provides the minimum induced drag compared to the other two wing designs. Stall characteristics are low. Difficult and expensive.





4.4. Wing parameters calculations

The selected wing type for the aircraft is finalized to be a tapered wing. Furthermore, some assumptions and calculations are chosen according to appendix (A) as well as competitor aircrafts which are shown in table (2.2) were applied to the wing; in order to have a compatible wing design that satisfies the aim of the research (Roskam, 1985).

Table 4.2: General Wing Parameters

Airfoil Thickness ratio	Lift	The thickness ratio affects the maximum lift and stall characteristics mainly by its effect on the leading edge.
	Drag	Increasing thickness will lead to increase in separation which will however lead to increase in drag
Aspect Ratio	Lift coefficient	Higher AR will lead to greater maximum CL
	Stall Angle	Lower AR will lead to delayed Stall angle
Tapered ratio	Structural	less area toward the tips, most of the lift is inboard, which further reduces bending loads at the root.
	Aerodynamic	Smaller tips means less impact of wingtip vortices, which leads to less drag
Twist	Geometric Twist	the change in angle of incidence of the airfoil measured with respect to the root airfoil.
	Aerodynamic Twist	the difference of angles between the zero-lift angle of the airfoil and zero-lift angle of the root airfoil.
Wing Incidence	General aviation aircrafts	2-degrees
	Transport Aircraft	1-degrees
	Military Aircrafts	0-degree
Dihedral Wings	Advantage	Helps with lateral stability
	Disadvantage	increase drag, and decrease roll rate.

Table 4.3: Assumption of Wing Design Parameters

Assumptions	
Aspect Ratio (AR)	7
Sweep Angle, c/4 (deg)	0
Sweep Angle, LE (deg)	2.4
Sweep Angle, TE (deg)	-7.15
Thickness Ratio, root	0.17
Thickness Ratio, tip	0.13
$\tau_w = \frac{\left(\frac{t}{c}\right)_t}{\left(\frac{t}{c}\right)_r}$	0.76
Taper Ratio	0.547
Dihedral Angle (deg)	6





$$S = \frac{W_{TO}}{\frac{W}{S}} = \frac{11,500}{51} = 225 \text{ ft}^2 \quad (20)$$

$$b = (AR * S)^{0.5} = 39.7 \text{ ft}$$

$$C_r = \frac{2S}{b(1 + \lambda)} = \frac{2 * 225}{b(1 + 0.547)} = 7.32 \text{ ft} \quad (21)$$

$$C_t = \lambda \cdot C_r = 4 \text{ ft} \quad (22)$$

$$\bar{c} = \frac{2}{3} \cdot C_r \cdot \left(\frac{1 + \lambda + \lambda^2}{1 + \lambda} \right) = 5.82 \text{ ft} \quad (23)$$

$$\bar{Y} = \left(\frac{b}{6} \right) \cdot \frac{1 + 2\lambda}{1 + \lambda} = 8.95 \text{ ft} \quad (24)$$

The designing phase was made to find the wing configuration and parameters such as wing area and wingspan etc. Following that, the tip and root chords were calculated from equation (21 & 22). Then, this was after assuming the taper ratio as 0.547 by taking the average of the competitors' aircraft. An assumption was made that sweep angle of the quarter chord is equal to zero since the aircraft does not exceed Mach 1.

Wing sweep was used primarily to reduce the adverse effects of transonic and supersonic flow (Raymer, 1889). The mean aerodynamic chord was found using two methods, by calculation as shown in equation (23 & 24) and manually using a rough sketch of the wing. Both methods gave similar results.

The thickness ratio of the wing depends on the airfoils selected. The dihedral angle was estimated from the light attack competitor aircrafts. No wing twist and wing incidence were applied to the aircraft since the competitor aircraft did not apply it because the more twist required to produce a good lift distribution at the design lift coefficient, the worse the wing will perform at other lift coefficients. (Raymer, 1889).

Following that, the estimation of the aileron chord and span wise ratios were assumed. The assumptions were made by following the appendix (A) as a reference for Military/trainer aircrafts. The ratios were taken from appendix (B.8).

- Aileron span location in/out = 0.56/0.99
- Aileron Chordwise location in/out = 0.21/0.31





4.4.1. Verifying the maximum lift coefficient ($CL_{max,W}$)

The following parameters for clean, takeoff, and landing maximum lift coefficients, taken from section (3.5) are 1.6, 1.8, and 2, respectively. The $CL_{max,W} = 1.05$ to $1.1 C_{l, clean}$ depends on the l_h/\bar{c} . the parameter can be estimated as shown in the figure (4.2). the ratio estimated for the aircraft is 3.5. Therefore, by means of interpolation, $CL_{max,W} = 1.08 C_{l, clean}$ is selected. Furthermore, the $CL_{max,W}$ is equal to 1.728. (Roskam, 1985).

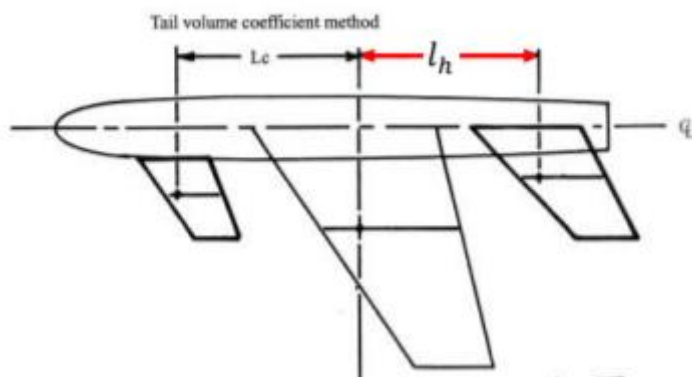


Figure 4.2: Tail volume coefficient method (Roskam, 1985)

$$CL_{max,W} = \frac{k_\lambda(Cl_{max,r} + Cl_{max,t})}{2} \quad (25)$$

In order to find the $CL_{max,W}$ an iteration is done for k_λ . This parameter depends on the taper ratio. So according to the aircraft taper ratio, the k_λ is found as 0.9328. To verify the wing planform, a rough estimation is made to validate the Cl_{max} . The following equation is used:

$$Cl_{max,r} + Cl_{max,t} = \frac{2 \cdot CL_{max,W}}{k_\lambda} \quad (26)$$

$$3.7 = 3.7$$

The $Cl_{max,r}$ and $Cl_{max,t}$ obtained from the airfoils selected are 2 and 1.7, respectively. This concludes that the left-hand side of the equation is equal to the right-hand side of the equation which further verifies that the wing planform met the required Cl_{max} which is 1.728.

Another design worked through the same calculations as said earlier in airfoil selection section. The design had two airfoils, NACA 2412 for the root and NACA 4412 for the tip. It is eliminated because when verifying in Equation (26), the left hand side is not equal to the right-hand side of the equation. So the lift coefficient obtained



from these two airfoils where not enough for the aircraft. The lift coefficient obtained is 2.6, whilst the required lift coefficient is 3.7.

4.4.2. Increasing lift using high lift devices

Aircraft designers attempt to increase the wing area and change the form of the airfoil by moving parts on the edge of the airfoil. The part is called a flap. The movement of the flaps to the rear increases the wing area, which increases the lift. On the other hand, the large rear area of the flap also increases the aircraft drag, which helps to slow the aircraft to land.

$$\Delta CL_{max,TO} = 1.08(Cl_{max,TO} - Cl_{max}) = 0.216 \quad (27)$$

$$\Delta CL_{max,L} = 1.08(Cl_{max,L} - Cl_{max}) = 0.432 \quad (28)$$

To verify the area and position of the flaps. Some assumption from and calculations is made as shown below:

$$\Delta C_{l,max} = \Delta C_{L,max} \left(\left(\frac{S}{S_{wf}} \right) \right) \quad (29)$$

$$k_A = (1 - 0.08 \cos^2(\Lambda_{c/4})) \cos^{\frac{3}{4}} \Lambda_{c/4} \quad (30)$$

The effect of sweep angle is calculated as the sweep correction factor, k_A is 0.92 since the sweep angle for quarter chord is assumed as zero. Assuming the ratio of area $\frac{S_{wf}}{S}$ from 0.3 to 0.5 to see which ratio will be needed for the aircraft. Then by substituting in Equation (29) to find the $\Delta C_{l,max}$.

Table 4.4: Required incremental section maximum lift coefficient, and effect of size of flap

	Landing	Take off
$\frac{S_{wf}}{S}$	0.3 – 0.5	0.3 – 0.5
$\Delta C_{l,max}$	1.56 – 0.93	0.782 - 0.469

4.4.3. Single Slotted Flap

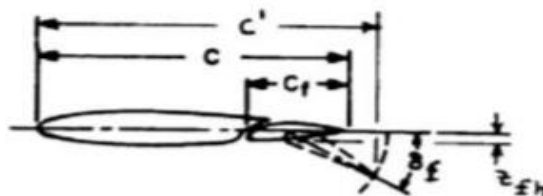
It is observed that simple single slotted flaps might be sufficient for this aircraft since the required flap increments are not very high. The following constants are for the single slotted flap geometry in table (4.5).




Table 4.5: Single Slotted Flap Constants (Roskam, 1985)

$Z_m = 0.1$	$\delta_{f,TO} = 15 \text{ deg}$	$\delta_{f,L} = 40 \text{ deg}$	$c_f/c = 0.25$
-------------	----------------------------------	---------------------------------	----------------

Figure (4.3) shows the single slotted flap with its constant dimensions and angles for take-off and landing.


Figure 4.3: Single Slotted Flap Geometry (Roskam, 1985)

$$C_{l,\delta_f} = C_{l\alpha} \left(\frac{c'}{c} \right) \quad (31)$$

$$\frac{c'}{c} = 1 + 2 \left(\frac{Z_{fh}}{c} \right) \tan(\delta_f) \quad (32)$$

$$\Delta Cl = \delta_f \alpha_{\delta_f} C_{l,\delta_f} \quad (33)$$

Table 4.6: Summary of estimated parameters for single slotted flaps

	Landing	Take Off
$\frac{c'}{c}$	1.012	1.004
C_{l,δ_f}	6.359	6.311
α_{δ_f}	0.41	0.5
ΔC_l	1.82	0.82

Equation (31,32 & 33) is used to find the ΔC_l . The constants in these equations are assumed from table (4.5) for the single slotted flap. K is a constant that depends on the flap deflection angle and it is equal to 0.93 which is found from the historical trend as shown in appendix (B.6).

$$\Delta C_{l,max} = \Delta C_l \cdot K \quad (34)$$

Incremental value of lift coefficient due to the flap is shown in table (4.7).




Table 4.7: Final results of the Flap Geometry for Landing and Takeoff

	Landing	Takeoff
ΔC_l	1.82	0.82
$\Delta C_{l,max}$ (Generated by flaps)	1.69	0.762
$\Delta C_{l,max}$ (Required) Range: 0.3 – 0.5	1.56 – 0.93	0.782 - 0.469

Comparing with required $\Delta C_{l,max}$ in table (4.7). The values show that the wing with the high lift device (Flaps) can easily generate the required lift coefficient for landing, while for takeoff the $\frac{S_{wf}}{S}$ ratio 0.3 is not verified with the required Lift coefficient. So, by means of interpolation, the value for the wing-flap ratio ($\frac{S_{wf}}{S}$) is estimated as 0.314. To find the flaps size in spanwise, the equation (35) is used.

$$\frac{S_{wf}}{S} = (\eta_0 - \eta_i) \left(\frac{(2 - (1 - \lambda)(\eta_0 + \eta_i))}{(1 + \lambda)} \right) \quad (35)$$

Where:

$$\frac{S_{wf}}{S} = 0.314,$$

$$\eta_i \text{ (at the fuselage side)} = 0.128,$$

$$\lambda = 0.547$$

Therefore,

$$\eta_0 = 0.404$$

The η_i and η_0 values represent the beginning of the flaps in spanwise. Which starts from the beginning of the wing until 40.4% of half the span.



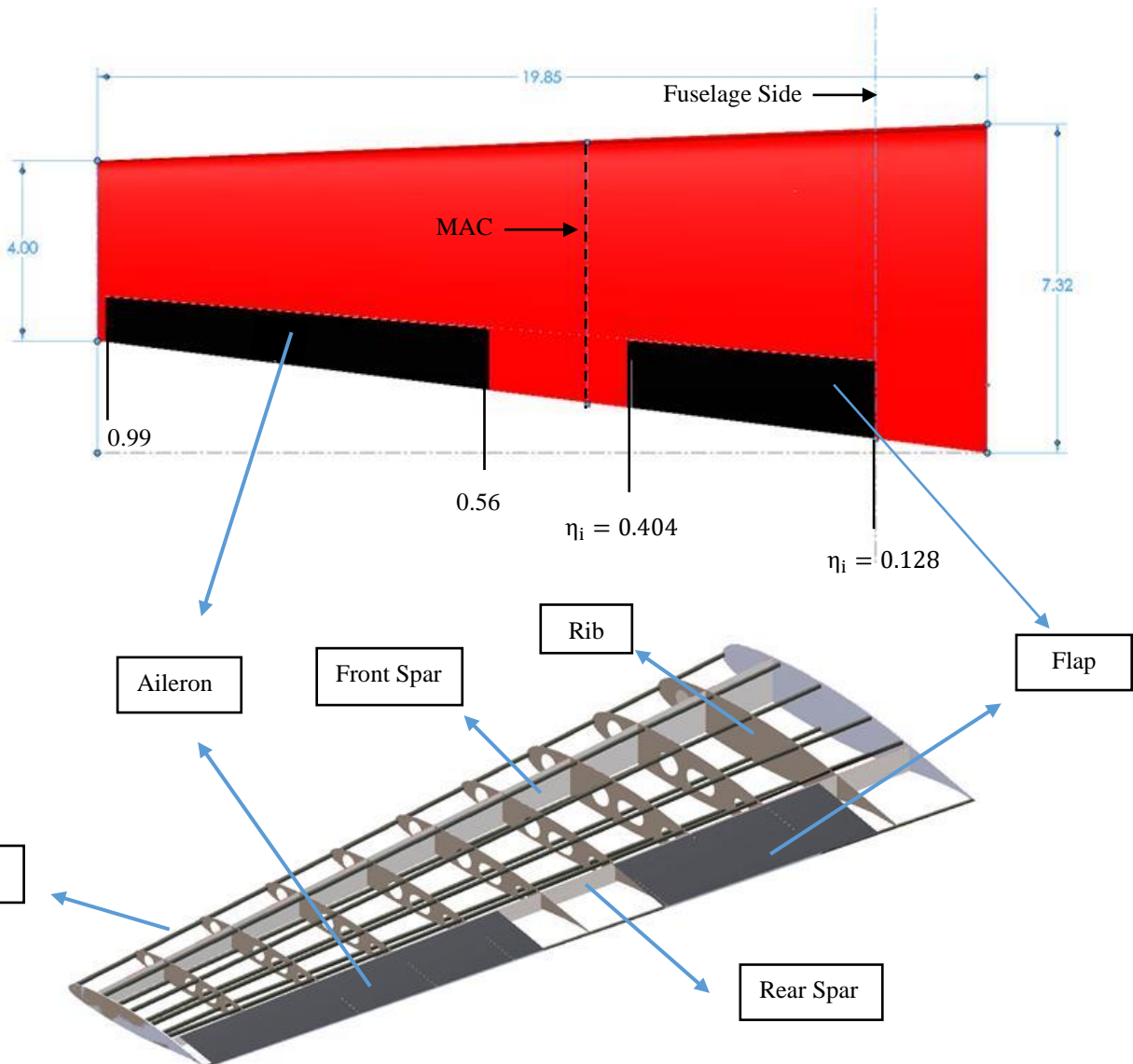


Figure 4.4: Ribs, spars, and stringers sizing and control surfaces dimensions (all dimensions are in ft)

Figure (4.4) mainly shows the mean aerodynamic chord which is 5.82ft and shows the dimensions of the control surfaces on the wing. On the other hand, shows the sizing of the ribs, spars, and stringers. The front spar is at 20% of the chord. The rear spar is at 74.5% of the chord which leaves 0.5% free space between the rear spar and the control surfaces. In the next section, the fuel tank will be added, and adjustments will be made.



4.5. Fuel Tank Integration

An aircraft fuel system permits the loading, storage, handling, and delivery of fuel to an aircraft engine. This is because of the relative dimension and complexity of the airplanes on which they are installed, fuel systems differ considerably from aircraft to aircraft. It is likely that the fuel system will consist of a series of fuel tanks that can be found in a wing or in a fuselage or in the empennage in some cases. Each tank may have an internal fuel pump and the associated valves and plumbing for engine feeding.

4.5.1. Fuel Volume

The available space inside the wing can be found using equation (36). This will help to determine the volume required for the fuel tanks, flaps, and ailerons.

$$V_{WF} = 0.54 \cdot \left(\frac{S^2}{b} \right) \cdot \left(\frac{t}{c} \right)_r \cdot \left(\frac{1 + \lambda \sqrt{\tau_w} + \lambda^2 \cdot \tau_w}{(1 + \lambda)^2} \right) = 83.36 \text{ ft}^3 \quad (36)$$

4.5.2. Required Volume

The required fuel volume can be found using the steps below, using the assumptions from the take-off weight estimation section (3.2). The fuel type chosen for the engine is the Kerosene, since this is the most used fuel type on this engine, due to its low viscosity and good properties. The density of the fuel is 1.55 slug/ft³ (6.66 lb/gal).

The type of the fuel tank is integral fuel tank which perfectly fits the wing.

$$W_F = W_{TO} (1 - M_{ff}) = 0.2792 W_{TO} \text{ (Takeoff weight estimation Section)}$$

$$W_F = W_{TO} (1 - M_{ff}) = 0.2792 * 11500 = 3210.8$$

$$M_F = \frac{W_F}{32.2} = 99.71 \text{ slug}$$

$$V_{FR} = \frac{M_F}{1.55} = 64.33 \text{ ft}^3 \text{ (482 gal)}$$





Figure 4.5: The Aircraft Fuel Tank

When an aircraft maneuvers, an integral wing tank needs to be disturbed to ensure that the fuel is not slipped off. The structural components of the wing ribs and box beamer serve as blurs and for that purpose others may be added. Valves are commonly used for baffle control. These valves allow the fuel to move into the tank's low internal sections, while avoiding moving outboard.

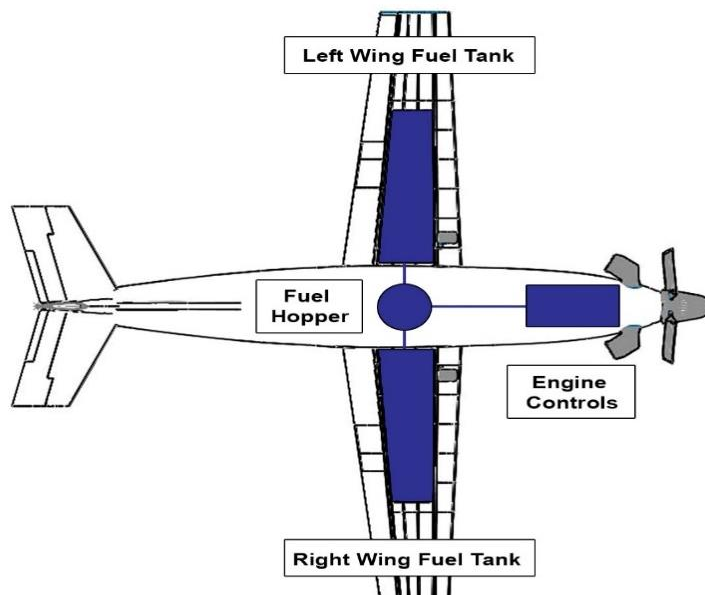


Figure 4.6: Fuel system schematic

Fuel system is used as required for safe storage and feeding of fuel to the engine. All fuel is located in two main fuel tanks on each side of the wing. The fuel is constantly stored at the same volumes in these two tanks to maintain the aircraft balance. When the fuel control unit in the engine requires fuel, the fuel hopper pumps the fuel into the engine. As found previously, the required fuel volume for the aircraft is 64.33ft^3 , which means that each tank will be able to hold 32.16 ft^3 .





4.6. Wing Material Selection

Table 4.8: Wing Material Selection

Wing Section	Material
Wing Spar	Composite Material
Wing Ribs	Titanium
Wing Flaps	Composite Material
Aileron	Carbon Epoxy Material
Wing Fuel Tank	Stainless Steel
Wing Skin	Composite Material

The main elements of a wing are the spars. They sustain all loads distributed and concentrated weights such fuselage, landing gear. Part of the load imposed during flying is on the skin that is attached to the wing. Ribs give the wing section its shape. The stresses are transferred to the ribs in the wing. In return, the ribs pass the stress to the wing spars.

The material selected for the wing spar is composite materials which is strong enough to maintain the stresses on the spars due to the fact that the aircraft is a light attack aircraft, which means that the aircraft might have a huge stress while in battle which will cause a lot of maneuvering. The material selected for the ribs of the wing is Titanium.

The ribs should be strong and yet should be light, so the reason titanium is used is because it has an excellent strength to weight ratio. Its heavier than aluminum but also stronger. The wing skin material selected is the composite material. Composites are great at handling tension compared to aluminum and yet lighter than aluminum (Composite vs Aluminum, 2021).

The flaps material of the aircraft is preferable to be the same as the wing skin material. So, the flaps material selected is composite material. The aileron material selected is the carbon epoxy, reason is that it's a high strength material and it is needed for an light attack aircraft due to the high stresses on the aileron during a battle and maneuvering. Finally, the Fuel tank material selected is the stainless steel, the reason is that it has a good corrosion resistance, so the fuel tank won't be able to rust (Structures, 2021).





Chapter 5 Empennage Configuration

As seen in figure (5.1), the empennage is a structure at the rear of an aircraft that provides stability and directional control during flight. It is also described as the tail or tail assembly. Empennages help to maintain equilibrium, control, and trim.

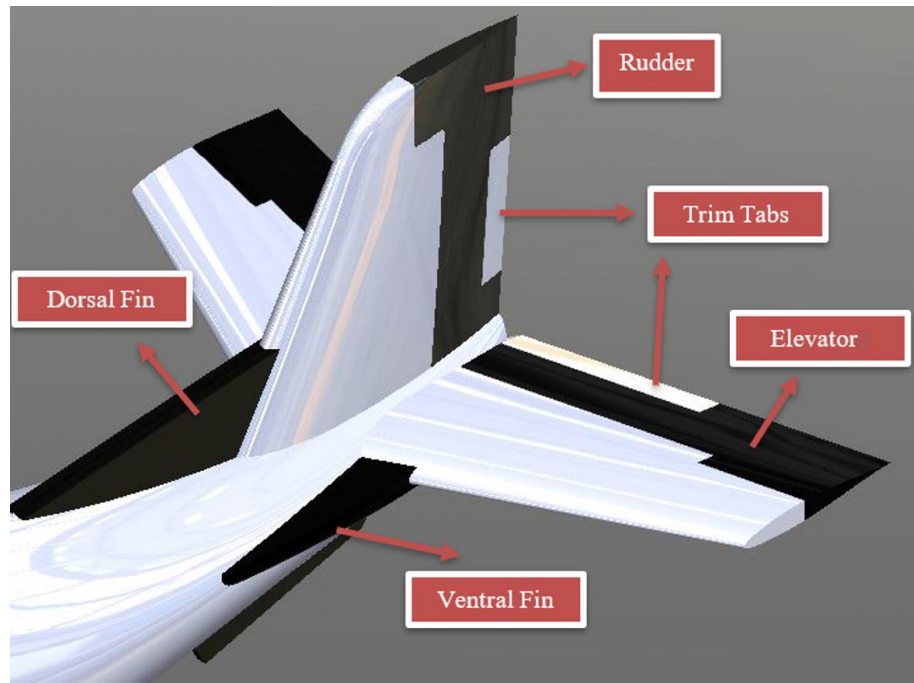


Figure 5.1: Conventional Empennage Design

Empennages produce a force that acts upon a lever arm. As a result, empennages are used to create a moment. The vertical tail generates a moment along the vertical axis for yawing motion whereas, the horizontal tail produces a moment along the lateral axis for pitching motion. Furthermore, Ailerons and spoilers on the wing create moment around the longitudinal axis for rolling motion. Moreover, there are other ways for creating moments such as: moving the center of gravity tail aft the aircraft and engine thrust control during vertical take-off and landing.

For Austere field light attack aircraft, conventional tail design illustrated in figure (5.1) best suits AIAA requirements. It has one vertical stabilizer and one horizontal stabilizer separated into two parts on the tapered tail portion of the fuselage, one on either side of the vertical stabilizer. The conventional configuration provides enough stability and control for the lightest structural weight. Furthermore, it has simple control actuation and fuselage attachment. In addition, pitch trim alignment with center of gravity adjustments becomes easier with this design (Torenbeek, 2013).





5.1. Tail arrangement for spin recovery

In a spin, an airplane is basically upright and rotating around a vertical axis. The spin is a mix of yaw and roll. There are two kinds of spin: steep and flat. Steep spin is influenced by roll and is easier to recuperate from a spin. Yaw affects flat spin, making it difficult to recover from a spin (Cutler, 2020).

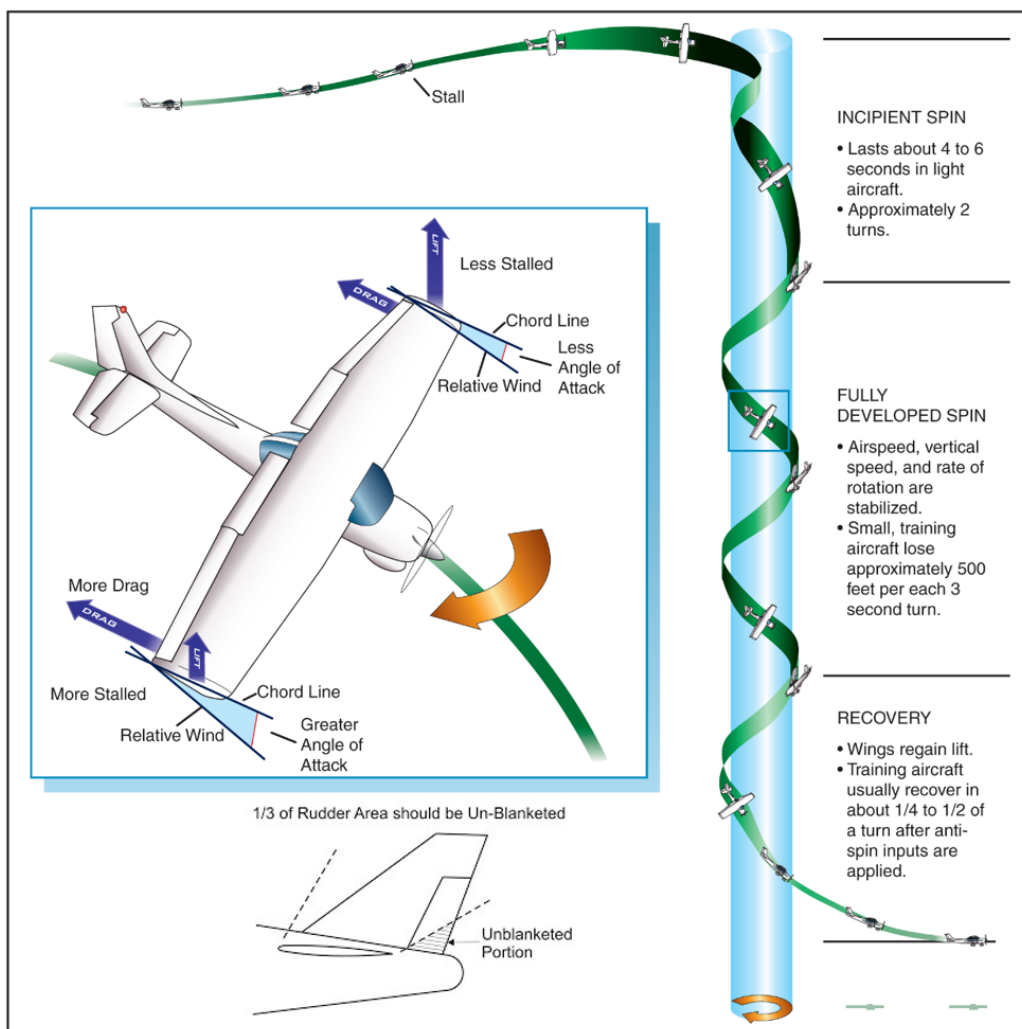


Figure 5.2: Stages for spin recovery (Cutler, 2020)

The vertical tail is critical in spin recovery. Additionally, sufficient rudder control is needed for spin recovery. Only the rudder region outside the horizontal tail wake (gray area) as seen in figure (5.2) maintains its effectiveness during spin recovery.

5.2. Benefits of using ventral and dorsal fin for spin recovery and stability

Dorsal Fin and Ventral fin as illustrated in figure (5.3) play a pivotal role in the spin recovery process and stability.



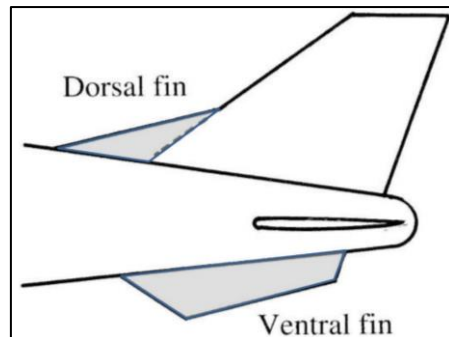


Figure 5.3: Dorsal and Ventral Fin Configurations (Roskam, 2003)

Table (5.1) illustrates the functions of these fins and their impact to the design.

Table 5.1: Functions of Dorsal and Ventral Fins (Roskam, 2003)

Types of Fins	Function
Dorsal Fin: A small filet at the forward base of the vertical stabilizer	<ul style="list-style-type: none"> ▪ It enhances tail effectiveness at lateral stability in high side-slip conditions by creating a vortex, such as engine failure or crosswind landing. ▪ It augments rudder control in spin
Ventral Fin: An external fin on the aircraft belly below the normal vertical stabilizer for extra directional stability.	<ul style="list-style-type: none"> ▪ It enhances stall and Dutch roll characteristics; it prevents high side-slip angle. ▪ It cannot be blanketed by the wake experienced by the wing.

Finally, dorsal, and ventral fins may enhance directional stability, especially at elevated angles of attack.

Fighting maneuvers, both for target acquisition and for prevaricate maneuvers.

5.3. Typical methods for hinge moment reduction

The Notched or Horn Aerodynamic balance is a part of the control surface that extends ahead of the hinge line at the tip, usually this configuration can be observed in elevators and rudders. Horn balance eliminates the tendency to float and it contributes in preventing the control surfaces from fluttering (Wainfan,2020). Shielded horn balance is a fixed surface that is placed ahead of the moveable balance surface. Shielded horn balances are popular on modern light airplane tail surfaces.

5.4. Empennage Configuration Sizing and Calculations

Table (5.2) represents the sizing and assumptions made to develop the empennage configuration.




Table 5.2: Empennage configuration sizing and assumptions

Empennage Configuration		
Design Parameters	Vertical Tail	Horizontal tail
Span (ft)	5.5	13.48
Area (ft ²)	25.4	54.9
Aspect Ratio	1.19	3.31
Mean Aerodynamic Chord (ft)	5.05	4.115
Root Chord (ft)	6.35	4.89
Tip Chord (ft)	3.49	3.23
Sweep Angle quarter chord (°)	25	18
Airfoil root	NACA 0015	NACA 23015
Airfoil tip	NACA 0015	NACA 63-212
Thickness ratio, root	0.15	0.15
Thickness ratio, tip	0.15	0.12
Taper Ratio	0.55	0.66
Dihedral angle (°)	0	0
Incidence angle (°)	0	0

The assumptions made for empennage sizing were selected from appendix (B.8-B.11) and the blueprints in section (2.4). Furthermore, for vertical tail configuration as symmetrical airfoil was selected NACA 0015 because it provides improved stability and control. On the other hand, two different airfoils were selected for the horizontal tail and the reason behind this choice was to enhance stall characteristics.

Moreover, mean aerodynamic chord, tip and root chord, area, and aspect ratio were found using the theoretical calculations in appendix (B.12). Other parameters like the taper ratio, dihedral, incidence, and sweep angle at quarter chord were assumed using trial and error method from blueprints in section (2.4) In addition, sweep angle at quarter chord was assumed to be for horizontal tail as 18° and for vertical tail as 25 ° because sweep angle contributes in delaying the critical Mach number. Thus, this deters the onset of wave drag (Anderson, 1999). Furthermore, it increases the moment arm for both vertical and horizontal tails.

Selection of taper ratio for both horizontal and vertical tail was based on performance of the empennage configuration, the selected values indicated in table (5.2) were reasonable because according to the study of effects of taper ratio on aircraft wing aerodynamic parameters (Güzelbey, Eraslan and Doğru, 2019), this study showed that lower taper ratio decreases induced drag and also contributes in lower structural weight. For medium speed aircraft, the range for taper ratio for Horizontal tail is 0.36-1, while for the vertical tail, 0.32-0.74. (E.G. Tulapurkara, 2021).





5.5. Empennage Configuration Material Selection

Table 5.3: Empennage Configuration Material Selection

Empennage Configuration	
Component	Material
Horizontal Stabilizer	Carbon laminate composite
Elevator	Carbon Sandwich Composite
Vertical Stabilizer	Carbon Laminate Composite
Rudder	Carbon Sandwich composite
Trim Tabs	Carbon Sandwich Composite .

Carbon laminate and carbon sandwiches were the materials used in the empennage section due to its lightweight and strong strength to weight ratio. Lightweight is needed in the control surfaces such as the rudder, elevator, and trim tabs, because of the deflection of these control surfaces so they will be easily deflected. However, they also need to be strong materials since the mission is a light attack aircraft so stresses on the control surfaces are huge in case of an attack (Sandwiches, 2021).





Chapter 6 Fuselage Configuration

The fuselage of the aircraft that holds the crew and weapons is the main body of an aircraft. The fuselage can also help monitor and stabilize surface's location in special links to elevating surfaces, critical for aircraft stability and maneuverability (Fuselage, 2020). There are several various types of structures used for most types of aircraft Struss structure, Geodesic construction, Monocoque shell and Semi-monocoque. For the Austere Field aircraft, Monocoque shell structural type is selected for the structure of the aircraft's fuselage.

6.1. Austere field Light Attack Geometric Fuselage Parameters

$$l_f = aW^c = 0.93 \times 11500^{0.39} = 35.7 \text{ ft} \quad (37)$$

By using the fuselage length Equation (37), the length is calculated, and it is 35.7 ft, and the diameter to length ratio is chosen to be 7 from the historical trend in appendix (C.1). Furthermore, the fuselage diameter is as 5.1 ft.

From appendix (C.1) $\frac{l_{fc}}{d_f} = 3$ and $\theta_{fc} = 6$ are selected to give the best fuselage parameters.

6.2. Fuselage Fineness Ratio

The ratio of fuselage fineness is the proportion of the length of a body to its maximum width. Short and wide forms of fuselage have low thinness, whereas long and conical forms have a high thinness ratio. By using the fuselage length and the fuselage maximum diameter, this ratio can be determined to be 7 by using equation (38).

$$\text{Fineness ratio} = \frac{\text{fuselage length}}{\text{maximum fuselage diameter}} = \frac{l_f}{d_f} = \frac{35.7}{5.1} = 7 \quad (38)$$

Table 6.1: The Optimum Fineness Ratio

The Optimum Fineness Ratio	
Subsonic aircraft ($\frac{l_f}{d_f}$)	6-8
Supersonic aircraft ($\frac{l_f}{d_f}$)	14
Fuselage cone ($\frac{l_{fc}}{d_f}$)	2.6-4
Fuselage nose ($\frac{l_{fn}}{d_f}$)	0.95-1.2

Since the austere field aircraft is a subsonic aircraft, the optimum fineness ratio is determined to be equal to 7 after finding the length and the maximum diameter of fuselage.





6.3. Fuselage Cone

The fuselage cone is a seamless shift from the whole cross section of the fuselage towards the end of the fuselage.

The cone of the fuselage is calculated from equation (39) and is 15.3 ft.

$$l_{fc} = d_f \times 3 = 5.1 \times 3 = 15.3 \text{ ft} \quad (39)$$

Therefore:

$$\frac{l_{fc}}{d_f} = \frac{15.3}{5.1} = 3 \quad (40)$$

The nose of the fuselage is estimated to be 9.9 ft based on the competitive light attack aircrafts. Therefore:

$$\frac{l_{fn}}{d_f} = \frac{9.9}{5.1} = 1.94 \quad (41)$$

And it is aerodynamically better to have $l_{fc} > l_{fn}$ and in this case $l_{fc} = 15.3 > l_{fn} = 9.9$.

6.4. Austere Field Light Attack Fuselage Configuration

To improve the aerodynamic efficiency, the fuselage design is chosen to be similar as the Beechcraft AT-6 Wolverine. The aim of this design is to keep the shape of the fuselage near the egg shape form, which minimizes the exposed skin area where drag has been decreased. The fuselage is optimized to meet the specifications of the design.

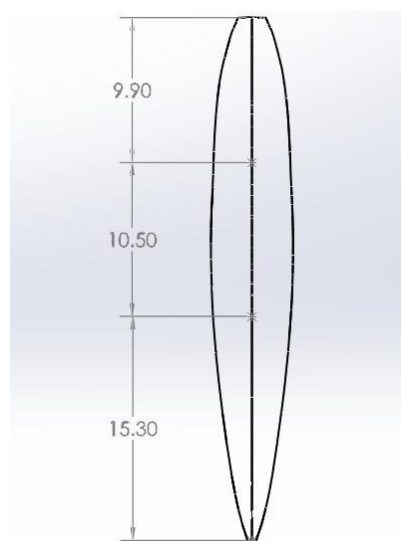


Figure 6.1: Top view of Austere Field Light Attack Aircraft Fuselage Configuration (all dimensions are in feet)



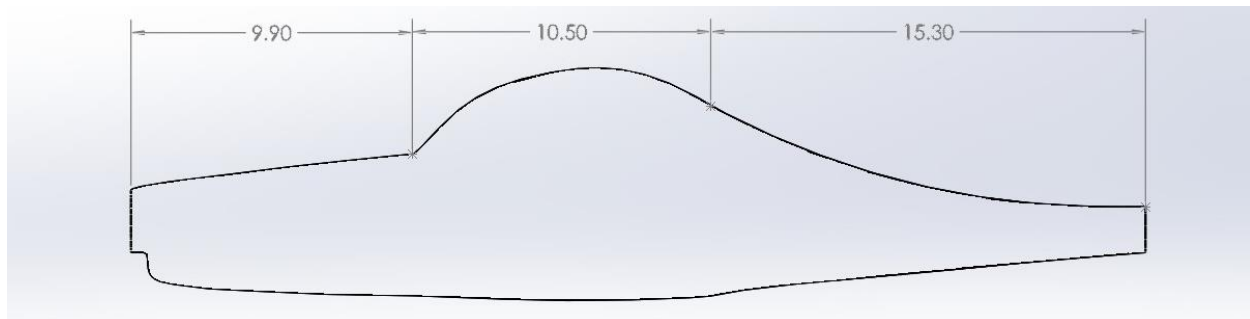


Figure 6.2: Side view of Austere Field Light Attack Aircraft Fuselage Configuration (all dimensions are in feet)

Figure (6.1 & 6.2) shows the dimensions of the designed light attack aircraft which is found using the appropriate calculations and is then verified using SolidWorks as shown in the figures.

6.5. Fuselage material selection

The fuselage monocoque structure is a device structure in which loads, like an eggshell, are supported by the external skin of the object (Monocoque - Wikipedia, 2021).

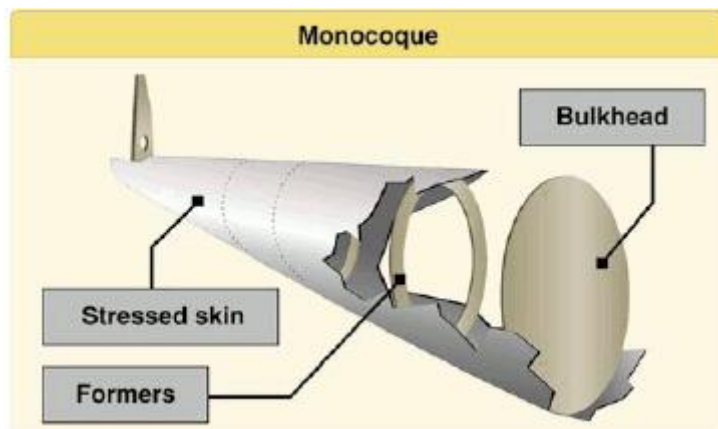


Figure 6.3: Fuselage monocoque structure (What is the difference between a monocoque and semi-monocoque fuselage type? 2021)

As shown in figure (6.3) the monocoque fuselage structure consists of skin, formers (frames), stringers and the bulkhead. The skin is the external surface of an aircraft covering much of its fuselage and wings. Aluminum and aluminum alloys with other elements, zinc, magnesium, and copper, are the most often used materials (Skin (aeronautics) - Wikipedia, 2021).

Fuselage frames move loads into the shell of the fuselage and reinforce the longitudinal string column. The frames usually take the form of open circles, to prevent obstruction of the interior of the fuselage (Fuselage Frame - an overview | ScienceDirect Topics, 2021). Frames are constructed from lightweight aluminum and/or composite materials frequently containing a CREP (Team, 2021).





A longeron is part of an aircraft's construction that adds stiffness and strength to the structure. In longeron development, materials such as wood, carbon fiber and metal could be used. The frame of the aircraft with a bolt is attached directly to the stern. In such planes, the longerons are fixed to shorter longitudinal supports called stiffeners or stringers. Often the longeron and stringer parameters are used interchangeably (Skin stringers-in-an-aircraft, 2021).

Therefore, for the designed aircraft the skin and the frames of the fuselage will be made of an aluminum alloy because it is light weight and has a high strength characteristic. While longerons and the stringers will be made of steel to assure the highest stiffness and strength for the fuselage.





Chapter 7 Propulsion System

7.1. Engine Selection

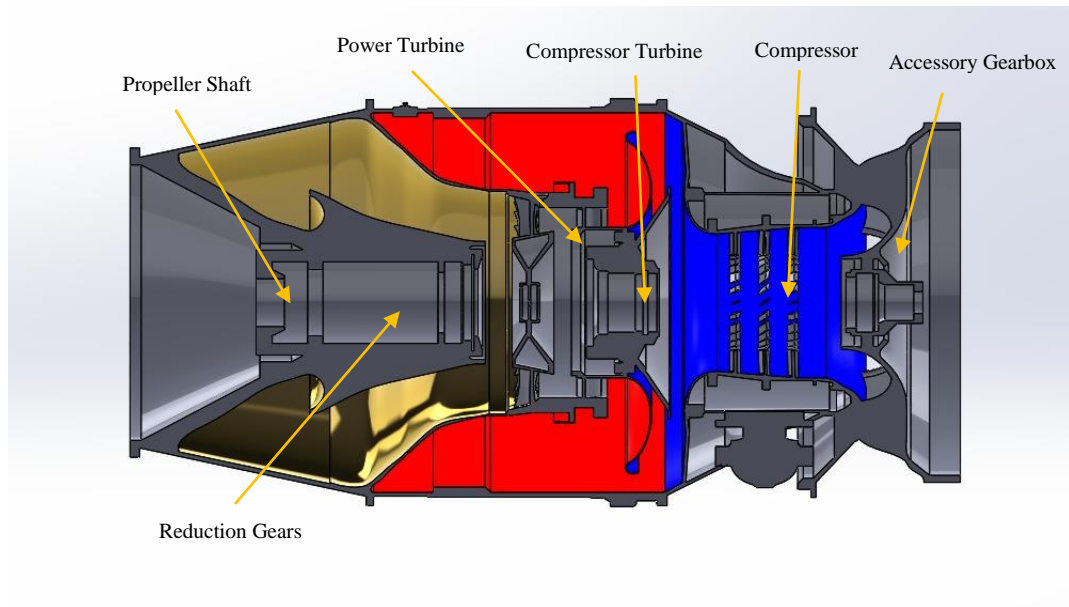


Figure 7.1: PT6A-67F Engine

The best option for the aircraft is the PT6A-67F, the competitor engines in section (7.5), on the other hand, are either used in low performance light attack aircrafts that have been used in investigation purposes or small combat missions, such as the Packard V-1650 Merlin, or are out of service because continued production is slow and due to the complex design of the engine.

Table 7.1: Main characteristics of PT6A-67F engine (TYPE-CERTIFICATE DATA SHEET, 2019)

PT6A-67F Specifications	
Dimensions and Dry Weight	
Overall Length (ft)	6.277
Overall Diameter (ft)	1.529
Dry Spec. Weight (lb)	571.66
Ratings	
Maximum Continuous power (SHP)	1,700
Take-off Power (5 minutes) (SHP)	1,700
Maximum Permissible Air Bleed Extraction	
Maximum External (%)	5.25
Maximum during Start (lb/min)	1.499
Speed Limits	
Gas Generator (N1) (rpm)	39,000
Gas Generator (N1) (rpm) Transient	39,530
Power Turbine Module Output (N2) (rpm)	1,700
Power Turbine Module Output (N2) Transient (rpm)	1,870





Maximum Permissible Torque Limits (ft-lb)	
Take-off (5 min) & Maximum Continuous	5,252.18
Transient (20 sec)	6,092.26
Estimated cost	\$900,000

7.1.1. Compressor Technology

The evolution of the PT6 compressor has succeeded leads towards comprehensive research and concept development, as well as dramatically improved aerodynamic design and analysis capability. Over the years, the original configuration of three axial stages tightly coupled to a centrifugal stage has been improved and expanded to four axial stages. The rotor attachment with six tie-bolts, the load bearing diffuser and cantilevered stators are design designs that have been fine-tuned and carried over to all versions. This technology will provide the aircraft with better performance and smooth gear transition with high efficiency.

7.1.2. Engine Layout

It is feasible to eject the hot components without damaging the rest of the engine or being forced to take the entire engine out of the aircraft. Thus, resulting in minimized costs in repair. The PT6 engine is designed in such a way that the propeller end, gas generator turbine and combustor, contained the hottest sections.

The gas generator is the only component that must be accelerated, making the motor simple to start, especially in cold weather. An inlet screen directs air from the gas generator into the low-pressure axial compressor. For small and medium engine models, there are three stages, and for large engine versions, there are four. The air then passes through a single-stage centrifugal compressor, a folded annular combustion chamber, and a single-stage turbine that spins at about 45,000 rpm to power the compressors. The gas engine, which spins at about 30,000 rpm, sends hot gas into the power turbine.

It has two stages on large engine that is selected for the designed aircraft. This drives a turboprop-specific two-stage planetary output reduction gearbox, which spins the propeller at 1,900 to 2,200 rpm. The exhaust gas then passes through two side-mounted ducts in the power turbine housing. The combustion chamber and turbines are concentric, resulting in a shorter overall length.

This places the control section at the front of the nacelle, where it can directly drive the propeller without the need for a long shaft. In most cases, the engine collects intake air from a vent mounted under it, and the two exhaust outlets are reversed.





7.1.3. Engine Outline

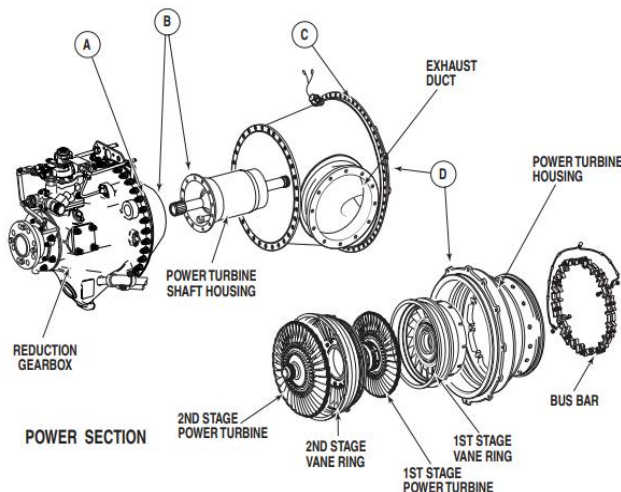


Figure 7.2: Power section (PT6A-67F SERIES TRAINING MANUAL, 2007)

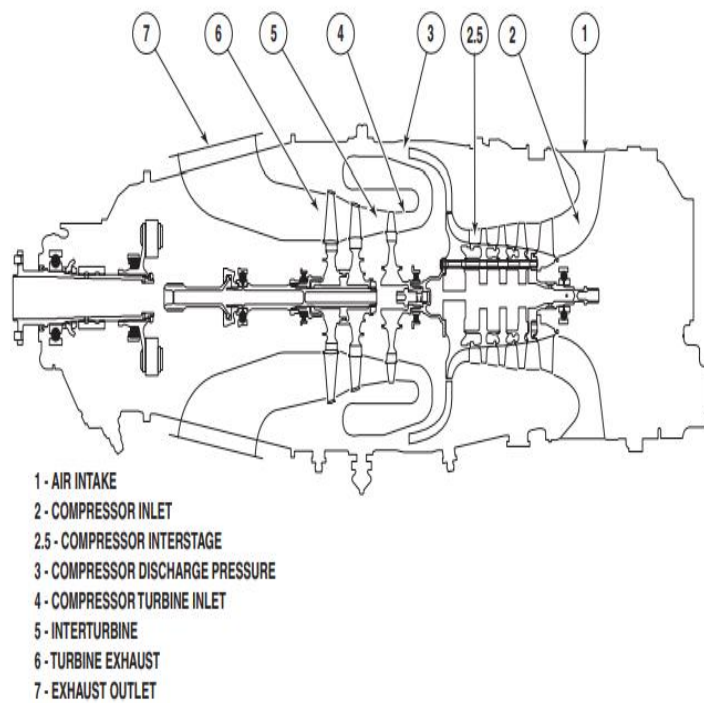


Figure 7.3: Engine stations (PT6A-67F SERIES TRAINING MANUAL, 2007)

The PT6 is a lightweight turbine engine with a two-stage reduction gearbox that drives a propeller. The engine's core is made up of two major revolving assemblies. The compressor and compressor turbine (compressor section) are the first, and the two power turbines and power turbine shaft are the second (power section). The two rotors are not related and spin in opposite directions at different speeds.



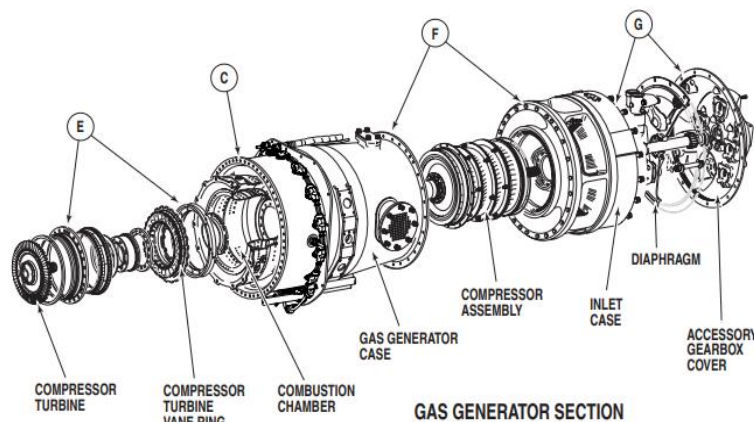


Figure 7.4: Gas generator section (PT6A-67F SERIES TRAINING MANUAL, 2007)

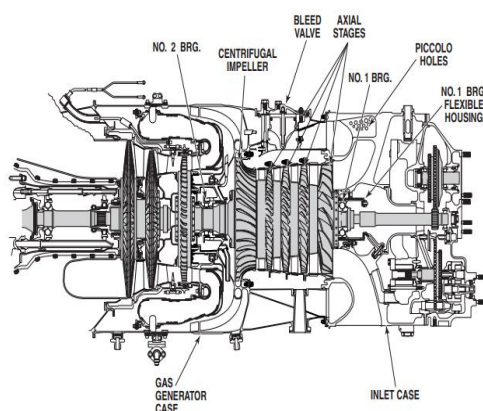


Figure 7.5: Compressor (PT6A-67F SERIES TRAINING MANUAL, 2007)

7.1.4. Engine Performance

Operating limits for each engine class define the upper and lower boundaries, and all engine parameters are detected in the cockpit during normal operation. Excursions outside of these limits will hasten engine wear and lead to part failure. The PT6 is known as the "back-to-front" engine because it is positioned so that the intake end of the engine is at the back of the aircraft.

The control portion is now located at the front of the nacelle, where it can actually drive the propeller without the need of a long shaft. The intake air is normally pumped to the engine through a vent mounted on the underside, and the two exhaust outlets are usually pointed backward. This arrangement makes repair easier by allowing the entire power section, including the propeller, to be removed, revealing the gas-generator section.





7.1.5. Fuel System

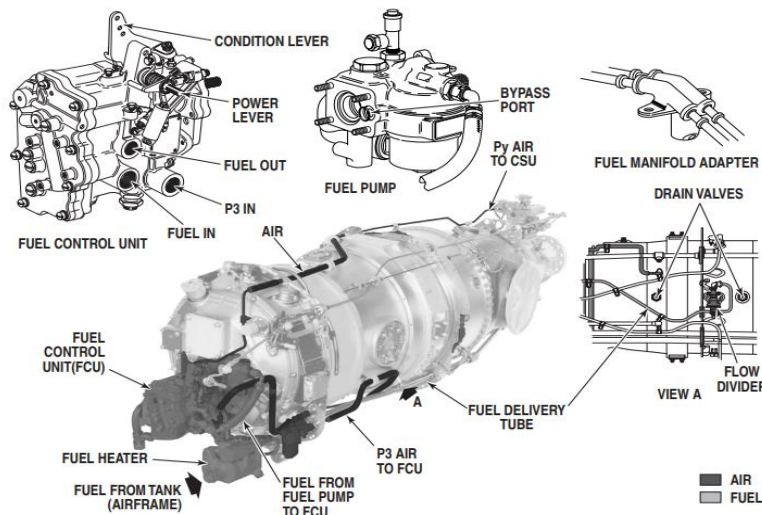


Figure 7.6: Fuel system and its components (PT6A-67F SERIES TRAINING MANUAL, 2007)

Fuel from the aircraft tank is sent by one or more airframe boost pumps to the fuel heater. The fuel pump transfers the fuel to the fuel control unit, which decides the amount of fuel needed by the engine to generate the power required by the power lever and the ambient conditions. Then, the fuel reaches the flow divider where it is directed to the primary and secondary fuel manifolds to supply all the nozzles.

7.1.6. Propeller System

The blades are protected by a hollow spider hub, which is connected to the servo piston by a feathering spring (dome). The feathering spring and centrifugal counterweights on each blade force the propeller blade to feathering stage. The propeller governor's oil pressure causes the propeller to change direction.

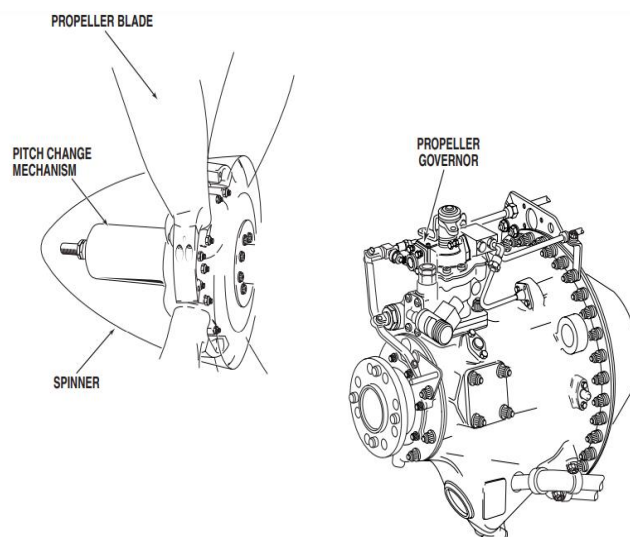


Figure 7.7: Propeller system (PT6A-67F SERIES TRAINING MANUAL, 2007)





7.2. Propulsion System Location

The tractor-style propulsion system is mounted at the front of the austere field light attack aircraft. The reasons for this choice can be reduced to a few concepts that put the pusher at a disadvantage for austere field light attack aircraft.

Since the propeller does not blow air over the engine, the motor of a pusher propeller must be cooled differently than that of a tractor. The use of ducting and ram air, or the incorporation of another cooling system, is then sufficient. Several pusher-type planes had major cooling issues. Another thing is FOD. One of the wheels may be placed behind a pusher prop, which would result in rocks being forced to enter the propeller during takeoff.

When a tractor-type plane takes off, the propeller will spin forward, away from the ground, since it is ahead of the center of mass. A pusher propeller, on the other hand, would usually spin down, increasing the chances of a propeller hit. A pusher propeller acts in a distorted airflow, causing increased vibration and noise. If the propeller is mounted behind a wing, each propeller blade passes through the separate boundary flow twice per turn. These loops generate a lot of noise and reduce the performance of the propeller. The friction makes the propeller blades more prone to metal fatigue.

In addition, the key advantage of a puller-propeller configuration from an aerodynamic perspective is that it adds forward airflow over the wings and tail during the most sensitive phases of flight, when the aircraft as a whole is moving very slowly.

7.3. Propeller Diameter Estimation

Since the PT6A-67F series engine is chosen for the designed light attack aircraft, the engine's maximum power output is 1,700 shaft horsepower, and the number of blades is estimated to be four, the power loading for each blade will be approximated as $4.5 \text{ hp}/\text{ft}^2$ based on appendix (C.2) The diameter of the propeller can now be determined using equation (42).

$$D_p = \sqrt{\frac{4P_{max}}{\pi n_p P_{bl}}} = \sqrt{\frac{4 \times 1700}{\pi \times 4 \times 4.5}} = 10.97 \text{ ft} \quad (42)$$

The diameter of the propeller is calculated as 10.97 ft, which is within the range of current turboprop aircrafts.

7.4. Engine Control System

The pilot will control and monitor the functioning of the aircraft's powerplant using aircraft engine controls.





7.4.1. Gear box

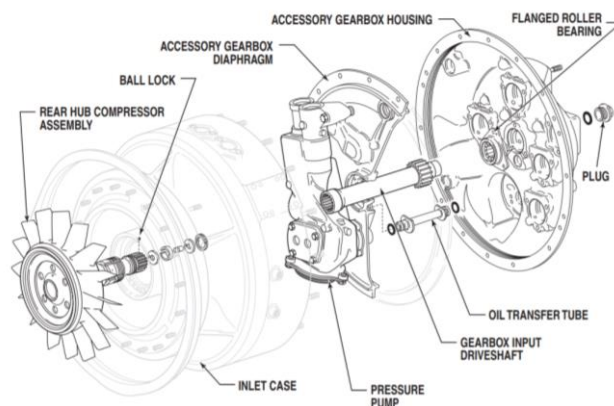


Figure 7.8: Schematic diagram gear box control system (PT6A-67F SERIES TRAINING MANUAL, 2007)

The planetary style reduction gearbox mechanism used in the PT6 engines has two levels of reduction. A sun gear meshes with three planet gears placed in a carrier in the first level. On the exterior, the three planet gears mesh with a ring gear splined into the reduction gearbox framework. In a modular fitting mechanism, the first stage gear carrier controls the second stage sun gear. The first stage reduction mechanism has a provision for measuring torque. The second stage of the reduction mechanism is identical to the first, except instead of three planet gears, it uses five. The propeller shaft is driven by splines from the second stage gear carrier. On the A-66, reverse rotation is accomplished by locking the second stage carrier to the front reduction gear case and rotating the second stage ring gear (PT6A-67F SERIES TRAINING MANUAL, 2007).

7.4.2. Indicating System

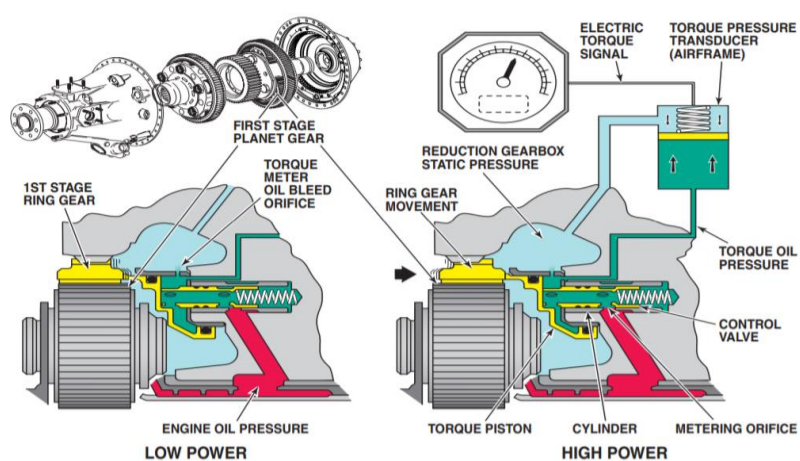


Figure 7.9: Engine Indicating System (PT6A-67F SERIES TRAINING MANUAL, 2007)

The first stage ring gear rotates and moves backward due to the torque applied to the propeller. The helical splines on the ring gear are responsible for this movement. The piston and the control valve are pushed by the ring gear.





The metering orifice is opened as the control valve is moved to the back, allowing more oil pressure to push on the piston against the ring gear mechanical power.

The ring gear can only stop moving until the metered oil pressure in the torque meter chamber precisely balances the ring gear's rearward power. The torque meter piston is affected by static air pressure within the reduction gearbox, resulting in an inaccurate or higher torque reading. As a result, the torque reading is subtracted from the static pressure sent through the sensor. Continuously bleeding oil from the pressure chamber prevents hydrostatic lock (PT6A-67F SERIES TRAINING MANUAL, 2007).

7.5. Trade Analysis

Table (7.2) displays the types of propellers that are suitable in designing an austere light attack aircraft.

Table 7.2: Types of Propellers (Badger, 1993)

Engine type	PT6A-68 series	V-1650	Wright R-3350	PT6A-67F
Overall length	71.3 to 71.65 in	88.7 in	76.26 in	6.277 in
Overall diameter	22.2 to 22.4 in	-	55.78 in	1.529 in
Shaft power	1,250 to 1,600 HP	1,380 to 1,400 HP	2,200 to 3,700 HP	1,700 HP
Unit cost	\$900,000	\$25,000	Depends on design parameter	\$900,000
Dry weight	573.2 to 599 lb	1,645 lb	2,670 lb	571.66 lb

PT6A-68 series: The PT6A-68 series turboprop engine comprises a 2-stage reduction gearbox, five stage gas generator compressors (4 axial, 1 centrifugal), a single annular combustion chamber, a single stage gas generator turbine and a two-stage axial power turbine. The fuel control is by single channel ECU with mechanical backup.

The engine also features a lubricating system capable of aerobatic maneuvers (Badger, 1993).

V-1650: 12-cylinder supercharged liquid-cooled 60° piston aircraft engine. This engine used a single-stage, two-speed supercharger, the gear changing mechanism of which originally came from a French Farman patent license. Two intake and two exhaust valves per cylinder, sodium-cooled exhaust valve stems (Badger, 1993).

Wright R-3350: The Wright R-3350 Duplex-Cyclone is a twin-row, supercharged, air-cooled, radial aircraft engine with 18 cylinders displacing nearly 55 L. Power ranged from 2,200 to over 3,700 hp (1,640 to 2,760 kW), depending on the model. Developed before World War II, A Wright R-3350 radial engine, propeller shaft, reduction gear case, magneto with wiring, two cylinders (rear with connecting rod), impellor casing (and induction pipe outlets) and injection carburetor; separate accessory gearbox at extreme left (Badger, 1993).

PT6A-67F: A two-stage reduction gearbox, five-stage gas generator compressors, a single annular combustion chamber, a single stage gas generator turbine, and a two-stage axial power turbine make up the PT6A-67F series





turboprop engine. A single channel ECU controls the petrol, with a mechanical backup. A lubricating mechanism capable of aerobatic maneuvers is also used in the engine. This version has improved shaft horsepower to 1700 SHP.

The PT6A-67f is the best choice for the Austere field light attack aircraft. It is slightly expensive compared with competitors, but the technology that comes with the PT6A-67F is totally worth the price, and the Pratt & Whitney company provide to the buyers a perfect maintenance plane that will reduce the maintenance cost for the engine and the replaceable parts. Furthermore, the PT6A-67 is only engine with the required technology and the power to meet the design requirements for the Austere field light attack aircraft.

On the other hand, the other hand the other competitors required huge changes in the design requirements like increasing the takeoff or the power loading for the design mission like V-1650, and this will increase the aircraft design cost, because more expensive materials will be used to satisfy the requirements with those engines. On the other side, Pratt & Whitney solutions for their high cost engines usually provide no additional costs for traditional corrosion or non-genuine P&W components, in addition to fair prices and cost assurances. Foreign object destruction (FOD) is not subject to further penalties as long as it does not result in an unplanned evacuation. Also, Shop warranty by Pratt and Whitney (Cost-effective PT6A engines overhaul solutions - Pratt & Whitney, n.d.).





Chapter 8 Landing Gear Configuration

The landing gear is designed to make loading aircraft for surface operations easier. There are a variety of types available depending on the desired operation or output. The landing gear typically consists of three wheels: two main wheels near the aircraft's center of gravity and an auxiliary wheel situated either in the front or back end of the fuselage.

Table 8.1: Landing gear types

Landing Gear					
Aircraft Type	Beechcraft AT-6 Wolverine	Beechcraft T-6C Texan 2	North American P-51 Mustang	Douglas A-1 Skyraider	Embraer EMB 314 Super Tucano
Landing Gear Type	Retractable tricycle	Retractable tricycle	Retractable tricycle	Retractable tricycle	Retractable tricycle

The tricycle landing gear is the most widely used arrangement in today's world for single propeller aircrafts. It comprises two main wheels behind the center of gravity and an additional wheel forward of the center of gravity. Having the center of gravity in front of the main wheel makes the aircraft more stable to the ground while the auxiliary wheel helps to power some steering wheels (Roskam, 1985).

8.1. Landing Gear Sizing

Sizing of the landing gear must be done to ensure the right selection to be suitable for the designed aircraft. sections (8.1.1, 8.1.2, 8.1.3, & 8.1.4) shows the step-by-step method to design the landing gear.

8.1.1. Landing gear arrangement type

For the designed single propeller light attack aircraft, a retractable landing gear is selected having the tricycle landing gear type. The choice is made based on table (8.1) which shows the types of landing gear for the competitors' aircrafts. This type of landing gear also improves potential surface visibility, gives proper landing gear length to prevent tail-running on the landing, and has a tip back angle which avoid tail skid on take-off (Roskam, 1985).

8.1.2. Landing gear strut deposition and tires location

For designing the landing gear strut deposition, the tip-over criteria which includes longitudinal and lateral tip over must be considered.



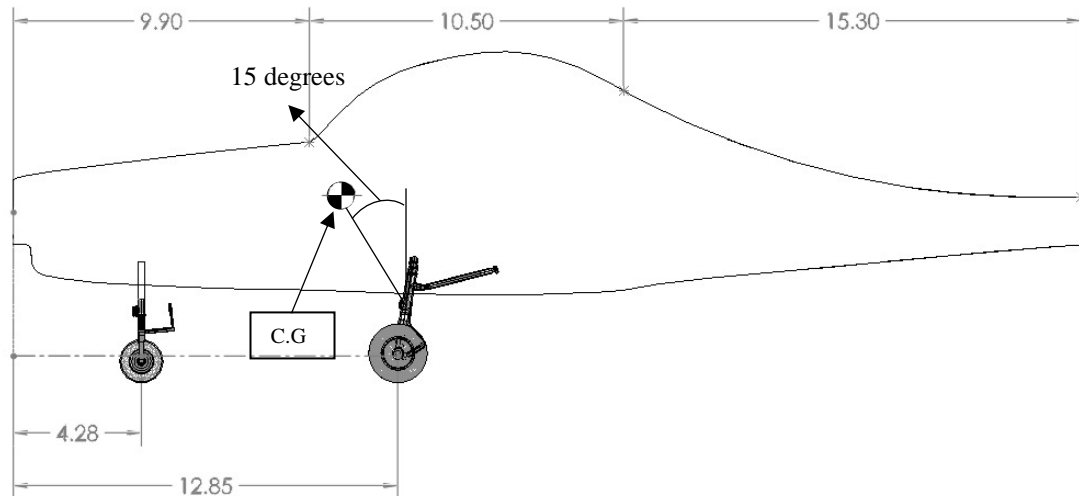


Figure 8.1: Longitudinal tip-over criterion and tire location

For tricycle arrangement, the longitudinal tip-over criterion of the main landing gear must be behind the most aft center of gravity position (15 degrees). Figure (8.1) shows an estimation of the center of gravity for the designed aircraft. Also, figure (8.1) shows an approximation of the locations of nose and main wheels. The nose wheel is around 12% of the total fuselage length while the main wheels are around 36% of the total fuselage length. Therefore, the distances are 4.28 feet for the nose wheel and 12.85 feet for the main wheels (Roskam, 1985).

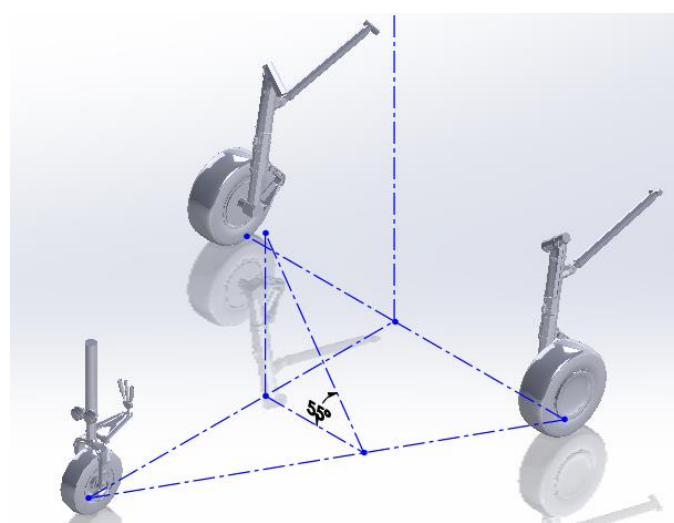


Figure 8.2: Lateral tip-over criterion

For tricycle arrangement, the lateral tip-over is influenced by the turnover angle (ψ), for the designed aircraft this angle must be equal or less than 50 degrees. For the designed light attack aircraft, the main landing gear strut is chosen to be one under each wing, while the nose landing gear strut to be at the forward end of the fuselage (Roskam, 1985).





8.1.3. Maximum static load per strut

The maximum static load per strut will be found for the nose wheel strut using equation (43) as follows:

$$P_n = \frac{W_{TO}l_m}{l_m + l_n} = \frac{11500 \times 2.8}{2.8 + 11.47} = 2256.5 \text{ N} \quad (43)$$

Where:

W_{TO} is the take-off weight, l_m is the distance between the main landing gear and the center of gravity, and l_n is the distance between the nose landing gear and the center of gravity.

The maximum static load per strut is found for the main wheel strut using the following equation (Roskam, 1985):

$$P_m = \frac{W_{TO}l_n}{n_s(l_m + l_n)} = \frac{11500 \times 11.47}{2(2.8 + 11.47)} = 4621.75 \text{ N} \quad (44)$$

Where:

n_s is the number of struts.

8.1.4. Number and size of tires

Using appendix (C.3) and based on the military trainers; having the take-off weight 11,500 pounds which is the closest to the designed aircraft take-off weight, the number of tires for the nose and main wheels are chosen as one tire per strut. The size of the main gear is set to be $23.3 \times 6.5 \text{ in.} \times \text{in.}$ having a $\frac{n_s P_m}{W_{TO}}$ ratio of 0.80 and a tire pressure of 143 PSI. On the other hand, the size of the nose gear is set to be $17 \times 4.4 \text{ in.} \times \text{in.}$ having a ratio of $\frac{P_n}{W_{TO}}$ as 0.19 and a tire pressure of 120 PSI (Roskam, 1985).

8.2. Wheel Arrangement

There are variable types of wheel systems, single, tandem, triple, dual and boogie are available for aircraft. Four types of wheel fittings, cantilever, forked, half-forked and dual. A single wheel setup is selected for both the main and auxiliary landing gears for the designed light attack aircraft. For both main landing gears, the type of wheel fit is selected as cantilever and forked wheel fitting is chosen for the auxiliary landing gear. These decisions are made to have the best possible landing gear for the designed aircraft and based on the five competitor aircrafts (Roskam, 1985).





8.3. Shock Absorbers

The most common form of shock absorbing landing gear is Oleo Strut. It combines a spring effect with a piston and the compressed air, which pushes oil into an opening. The shock is absorbed by a piston during operations and oil is shock absorbed at landing when air absorbs taxi vibrations. To support the wheel arrangement and the full landing gear system, the oleo shock-strut is chosen as the shock absorbing system for the designed light attack aircraft (Landing Gear, n.d.).

8.4. Landing gear material selection

The landing gear must carry the whole aircraft weight, so it must be extremely robust. Therefore, the landing gear is made of a combination of steel and titanium alloys. While the wheels are made of very big rubber to withstand shocks and to slow down the aircraft as it lands (What materials are used to make landing gear? | How Things Fly, 2014).





Chapter 9 Cockpit Configuration

It is essential to take into account many factors while designing a cockpit for austere field light attack aircraft.

- ❖ All control systems must be easily accessible to the pilot.
- ❖ All flight instruments must be visible to the pilot without undue effort.
- ❖ Communications by voice or touch must be without unnecessary effort.
- ❖ Minimum criteria for visibility must be adhered.

For cockpit configuration, there are two important reference points: the seat reference point and the Pilot's eye point. There are many benefits of having a high seatback angle, including reduced drag due to the lower height of the cockpit. Furthermore, it strengthens the pilot's ability to handle strong G-forces (Roskam, 2003).

9.1. Seat selection

An ejection seat is a mechanism used to save the pilot and other crew members in the event of an emergency. The seat is equipped with an explosive charge, which is braced by the crew members. The parachute is deployed in the ejection seat after exiting the aircraft. Martin's baker model (MK-J5D) is selected in designing the cockpit configuration for austere field light attack aircraft. An emergency oxygen supply is triggered as the seat goes up its guide rails, and personal equipment tubing and contact leads are immediately disconnected, as well as leg restraints.

The seat's descent course is stabilized by firing a steel rod known as the drogue gun, which removes two small parachutes. Above 10,000 feet, a barostatic device stops the main parachute from opening, a time delay system works in combination with another mechanism to save the main parachute from opening too quickly. The seat then separates from the occupant for a typical parachute descent; if the automatic mechanism fails, a manual separation handle and ripcord are installed (Martin-Baker Mk.5 - Wikipedia, 2020).

The optimal cockpit length is estimated to be 10 ft where the aircraft system is situated, and two crew members are seated. The interior design of the cockpit should correctly position the seat so that the steering paddle can be approached, and the pilot will not suffer any injuries during ejection because of a canopy bow collision, also, it should have a suitable distance between the aircraft and the pilot so that the panel can easily be reached. It must also include the differences in pilot arm span and combo leg lengths.





In addition, overhead clearance is an important consideration for the design of cockpits that has tall pilots, as the pilot may be hurt while ejection if the pilot's head is higher than canopy breakers. The factors that affect the dimensions of the cockpit were evaluated to cover 18 and 42 in length for each crew member. The avionics system and crew member seat were considered. The distance from the floor of the cockpits to the eye of the pilots is computed as 37 in. The angle of the seatback is chosen to be 18° , the paddle to the bottom end of the seat is 45 inches in length, 2 inches front or rear may be changed. The distance from the wheel to the bottom of the sitting area is 25 inches, enabling the pilot to control the aircraft easily and accurately. The seat of the second pilot, on the other hand, is of the same size and configuration.

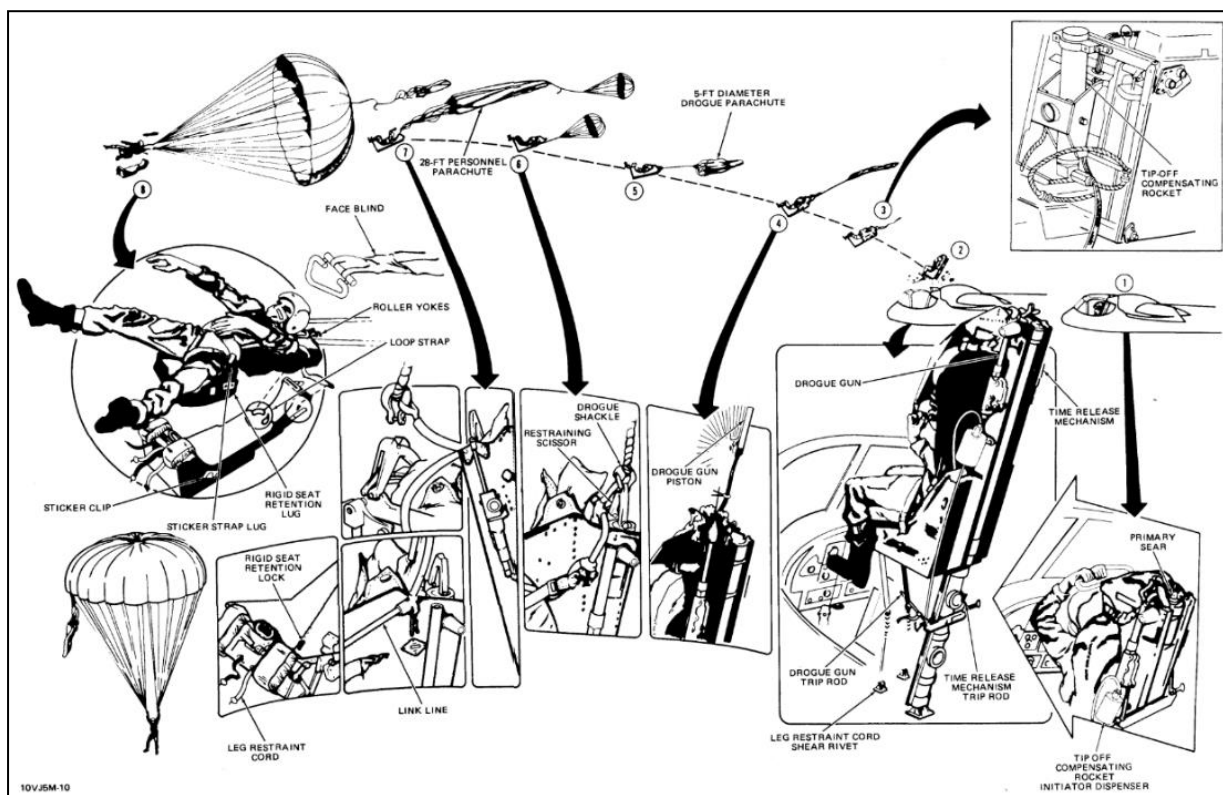


Figure 9.1: Ejection seat mechanism (EJECTION SEAT, MODEL MK-J5D, 2020)

The ground safety lock is made up of safety pins and bucket pins for placement. The safety pins protect against the unintentional discharge of the ejection seat. Figure (9.2) depicts a ground safety lock position view.



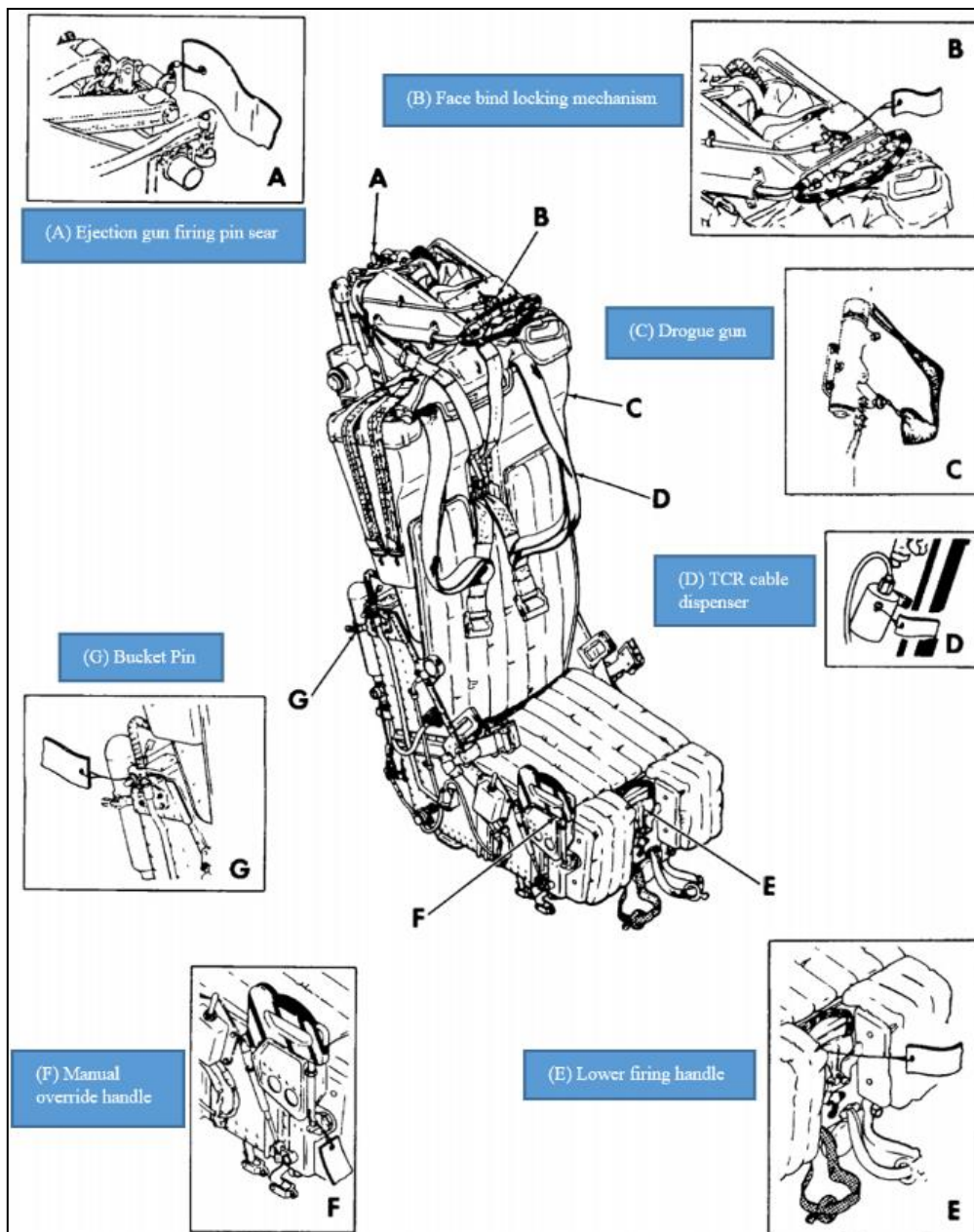


Figure 9.2: MK-J5D ground safety lock location view (EJECTION SEAT, MODEL MK-J5D, 2020)

The specifications of MK-J5D are illustrated in table (9.1).

Table 9.1: MK-J5D seat specifications (EJECTION SEAT, MODEL MK-J5D, 2020)

Operating Ceiling	50,000+ ft (15,250m)
Minimum height/Speed	Zero/zero in near level attitude
Crew boarding mass range	69.2 – 112.2 kg
Maximum Speed for ejection	630 KIAS
Parachute type	GQ Type 1000 Mk 2
Parachute deployment	Drogue assisted





9.2. Avionics System

The Cockpit 4000 Next Gen is a highly designed avionics system that features a glass cockpit resembling today's front-line fighters. Advanced core avionics promotes better information management and aids for netcentric warfare operations (Cockpit 4000 NexGen, 2021).

Main flight monitor, automatic monitoring of communications/navigation, steering point navigation, strategic situation display, engine signal and caution advisory, inventory management, no-drop bombing scoring system, and simulation system for virtual multi-mode radar and radar warning receiver (Cockpit 4000 NexGen, 2021).

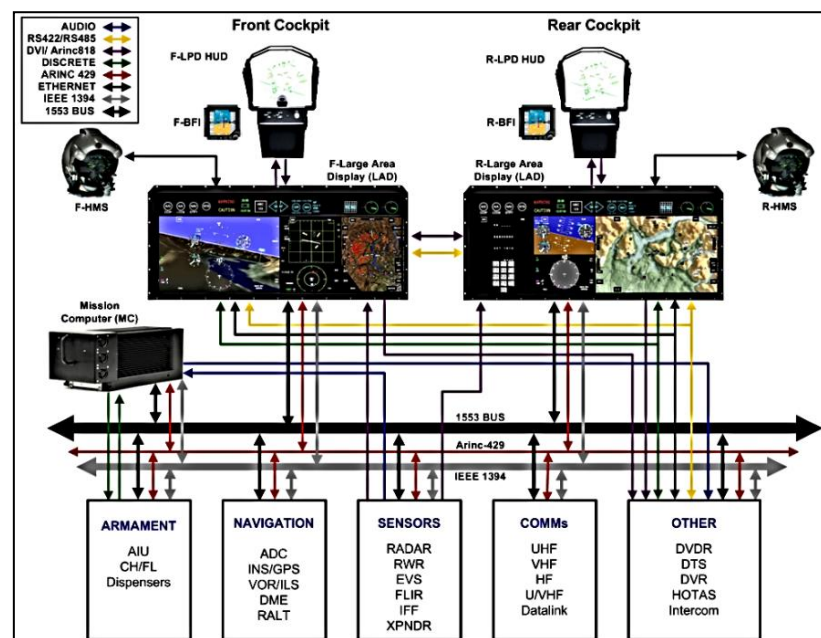


Figure 9.3: Cockpit 4000 Nex Gen Systems (Cockpit 4000 NexGen, 2021)

Cockpit 4000 Nex Gen as illustrated in figure (9.3) suits the requirements of austere field light attack aircraft because it has new advanced technology, efficient in combat phase and inexpensive in terms of cost.

Table 9.2: Specifications of cockpit 4000 Nex Gen (Cockpit 4000 NexGen, 2021)

Specifications of Cockpit 4000 Nex Gen
Centralized cockpit management reduces pilot workload, increases mission efficiency and flight safety
Master Moding control concept to improve pilot task performance by instantly reconfiguring the avionics suite to a particular state of readiness.
Three master modes: Navigation (NAV), Air-to-Air (A/A) and Air-to-Ground (A/G)
Large format Digital Map
Large Area Display (LAD) with touchscreen technology
Helmet Mounted Display Integration
Synthetic Vision System capability





9.2.1. Head-up display (HUD)

The HUD is important for both navigation and mission performance efficiency and safety. It provides the pilot with critical flight and weapon data, allowing for safe and secure aircraft control while attempting to maneuver. The HUD has a wide 26 ° total field of view (TFOV) and a high symbol visibility of more than 3,000 ft for operating in direct sunlight. Furthermore, the HUD is completely compatible with night vision goggles. It has 20" x 8" smart display with touchscreen (Cockpit 4000 NexGen, 2021).



Figure 9.4: Cockpit 4000 Nex Gen Display Screen and Digital Sparrowhawk Head up Display (Cockpit 4000 NexGen, 2021)





Chapter 10 Weapons Carriage

The weapons are an important component of the light attack aircraft's overall weight. The weapons should be placed close to the aircraft's center of gravity. If not, aircraft pitch up or down when the arms are released.

10.1. Weapons and Missiles Selected for Austere Field Light Attack Aircraft

A variation of missiles, bombs and weapons has been selected to ensure that the total payload for a single propeller light attack is equal to the total payload chosen for the 3000 pounds of evaluation portion. Mark 81 bomb, Mark 82 bomb, GBU-59 Enhanced Paveway II GPS/Laser-Guided bomb, T64 H.V.A.R rockets, and AN/M3 cannon are the selected weapons for the designed aircraft.

10.1.1. Missiles Selected for Austere Field Light Attack Aircraft

Mark 81 bomb



Figure 10.1: Mk-81 250LB GP Bomb

The lowest drag of the Mark 80 series is the Mark 81 general purpose bomb. Weight 250 pounds (119 kg), 74 cm (1.88 meters) in circumference, and 9 cm diameter (23 centimeters). It is mounted on the wing of the light-attack propeller and started with an ejection-launch procedure (Mark 81 bomb, 2020).

Mark 82 bomb



Figure 10.2: Mk-82 500LB GP Bomb





The 82-bomb is a low drag unguided bomb that is part of the Mark 80 series. 500 pounds (227 kg), 87.4 inches in length (2.22m) and 10.75 inches in diameter (273 millimeters). It is one of the smallest aircraft currently in use and one of the most recognized airborne weapons in the world. Explosive filling is usually tritonal but is often used for additional formulations. On each wing of the single propeller light attack aircraft, a Mark 82 bomb is installed and started using the ejection-launch procedure (Mark 82 bomb, 2020).

GBU-59 Enhanced Paveway II GPS/Laser-Guided Bomb

Paveway is a chain of laser-guided bombs often used as acronym for vector devices for precision avionics, purely for plane speed and electronics for path management. The GBU-49 consists of a GBU-12 modified version of the Raytheon 500 pounds (227 kg). On each wing of the single propeller light attack aircraft a GBU-49 bomb is mounted and started using the appellation-launch method. (Paveway, 2020).

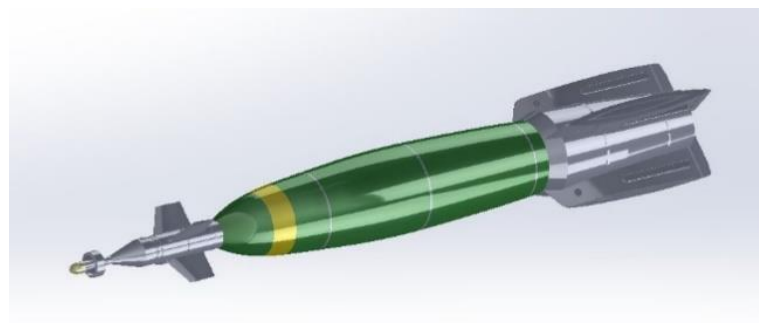


Figure 10.3: GBU-12 Paveway II

PAVE is an expression for precise avionics parametric modeling equipment which regulate the direction and speed of the aircraft. Texas Instruments developed this kind of missile starting in 1964, which is a kind of paving device. GBU-58 Paveway II – Mk 81 250 lb (113,4 kg) bomb is a type of GPS generally used bombs to lead to the target by using the laser. (Paveway, 2020)

T64 H.V.A.R rockets (P-51D-25)

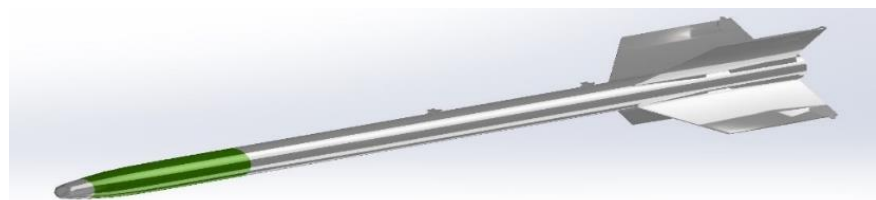


Figure 10.4: T64 H.V.A.R rocket





The high-speed H.V.A.R stands for the Holy Moses also called missile of the plane that its weight is 45 lb. This unguided US missile has been designed to attack the ground targets of the aircraft. These missile types were widely used in WWII and the Korean War. These missiles are suitable for single and double motors (High Velocity Aircraft Rocket, 2020). The 5. inch FFAR (Forward Firing Aircraft Rocket) is an upgrade to the same size as the warhead.

The vision oscillated with the new HVAR missile from 216 m/s is sufficiently increased to 420 m/s and could thus be used to penetrate 4 feet of the concrete block and successfully destroy pill boxes, munition dumps, tanks, and rail locomotives, thereby reducing impacts and reducing the number of bolted ships. One on each wing of the single propeller light attack aircraft, a T64 H.V.A.R missile is installed (HVAR, 2020).

10.1.2. Guns Selected for Austere Field Light Attack Aircraft

AN/M3 cannon

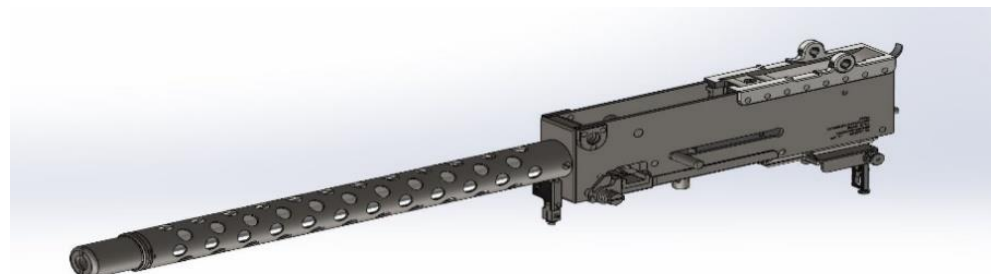


Figure 10.5: AN/M3 cannon

AN/M3 that's (The Army-Navy Model 3). This 20 mm autocannon that is weighted 93 and 110 lb is used by the US Air Force Army (USAF) and by the US Navy both. The cannon weapon itself, but is based on the British Hispano Mk.V., is a revision of the Swiss Hispano-Suiza H.S.404. In comparison with its prior competitor, the AN/M2, the AN/M3 is stronger and used. The AN/M3 used lubricated rifles, less vulnerable to jamming and percussion primed weapons (M3 (20 mm), 2020).





Chapter 11 Stability and Control Analysis

11.1. Weight Estimation

Table (11.1) shows the weight data for different type of components, it can be depicted that structural weight is 23.4% of the total gross weight. Whereas power plant and fixed equipment consist of 5.65% and 37.1% of the total gross weight. While crew and fuel weight comprise 33.85% of total gross weight.

Table 11.1: Weight Data for Austere Field Light Attack Aircraft

Austere Field Light Attack Aircraft	
Number of Engines	1
Weight Item (lb)	
Wing Group	759
Vertical Tail	200
Horizontal Tail	99
Fuselage Group	1,410.2
Main Landing Gear	358.8
Nose Landing Gear	89.7
Structure Total	2,916.7
Propulsion System + Engine controls	650
Power Plant Total	650
Avionics + Instruments	140
Surface Controls	287.5
Hydraulic and Pneumatic System	110
Electrical and Electronics System	243
Armament	3,000
Air-conditioning and de-icing System	96
Oxygen System	20
Furnishings	270
Auxiliary Power Unit	70.5
Paint	28
Fixed Equipment Total	4,265
Fuel + Trapped Fuel Weight	3,268.3
Crew	400
Total Gross Weight	11,500





11.2. Center of Gravity

Table 11.2: Weight and Center of Gravity Location for Major Components of the Austere Field Light Attack Aircraft

Components	Weight (lb)	Location from nose (ft)
Fuselage	1,410.2	17.4
Wing Including Control Surfaces	759	16.8
Horizontal Tail	200	37.67
Vertical Tail	99	36.64
Nose Landing Gear	89.7	6.23
Main Landing Gear (2)	358.8	15.81
Engines + with Engine control	650	5.2
Fuel + Wtfo	3,268.3	16.2
Crew	400	18.2
weapon	3,000	15.2
Hydraulics & Penumatics	100	7.5
Avionics	60	16.3
Other Fixed Equipments	1,105	13.5
Total weight	11,500	Total X_{cg} = 15.7 ft

In table (11.2) center of gravity locations and weight were listed for the main components of the Austere field light attack aircraft. From the results, it can be observed that the center of gravity for the total aircraft is at 15.7 ft from the nose, and the main landing gear location is at 15.81 ft. The location of center of gravity forward of the main landing gear makes the aircraft statically stable.

11.3. Longitudinal Stability and Control

Austere field light attack aircraft develops its longitudinal static stability when the airplane is stable in a pitching plane under steady flying circumstances. There are four criterions to achieve longitudinal balance and stability such as the $C_{M,0} > 0$, $\frac{\partial C_{M,cg}}{\partial \alpha_a} < 0$. Furthermore, the trim angle of attack should fall in within the range of flight. Moreover, the neutral point should be located behind the center of gravity of the whole aircraft. Thus, resulting in a positive static margin which is an essential factor to determine how much the aircraft is stable. These conditions are illustrated in figure (11.1).



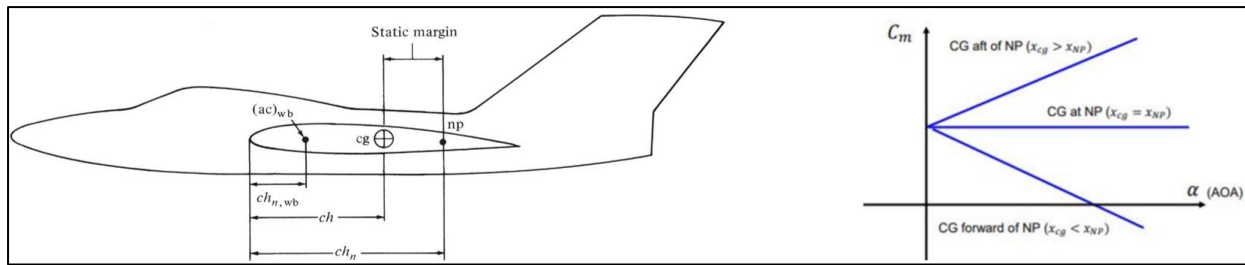


Figure 11.1: Effect of x_{cg} and x_{np} position on the longitudinal static stability (Nelson, 2010)

Equations (45 & 46) are used to calculate the total aircraft aerodynamic center and pitching moment coefficient about the center of gravity.

$$(C_{M,CG})_A = C_{M,ac\,wb} + a_{wb} \alpha_{wb} \left[h - h_{ac\,wb} - V_H \frac{a_t}{a} \left(1 - \frac{\partial \varepsilon}{\partial \alpha} \right) \right] + V_H a_t (i_t + \varepsilon_0) \quad (45)$$

$$\bar{X}_{ac_A} = \frac{\bar{X}_{ac_{wf}} + \frac{C_{L_{\alpha_h}} (1 - \frac{d\varepsilon_h}{d\alpha}) \frac{S_h}{S} \bar{X}_{ac_h}}{C_{L_{\alpha_{wf}}}}}{1 + \frac{C_{L_{\alpha_h}} (1 - \frac{d\varepsilon_h}{d\alpha}) \frac{S_h}{S}}{C_{L_{\alpha_{wf}}}}} \quad (46)$$

Equation (47) is used to evaluate the static margin of the austere field light attack aircraft.

$$Static\ Margin = \frac{x_{NP} - x_{cg}}{\bar{c}} \quad (47)$$

11.3.1. Contribution of aircraft components on Static Stability

The austere field light attack aircraft is deconstructed into specific components such as the wing, fuselage, vertical and horizontal tail and finally propulsion system to examine each component influence on the total aircraft's pitching moment and stability characteristics. Equation (48) is used to evaluate zero-lift moment coefficient for fuselage (Nelson, 2010).

$$c_{m_{0f}} = \frac{k_2 - k_1}{36.5S\bar{c}} \int_0^{l_f} w_f^2 (\alpha_{ow} + i_f) dx = \frac{k_2 - k_1}{36.5S\bar{c}} \sum_{x=0}^{x=l_f} w_f^2 (\alpha_{ow} + i_f) \Delta x \quad (48)$$

The tail involvement can be set to ensure that the overall aircraft moment coefficient is positive. The PT6A-67F engine has a significant influence on its static stability and longitudinal trim. The propellant momentum creates a pitching moment that the flying controls would experience due to movement of the thrust line away from the center of gravity.




Table 11.3: Longitudinal Stability Parameters for Wing Section

Wing
Cruise Mach Number, $M = 0.42$
Maximum Mach Number, $M = 0.45$
Airfoil Lift Curve Slope, $c_{l_\alpha} = 0.1313$
Airfoil Zero-Lift Pitching Moment, $c_{m_0} = -0.027$
Area, $S = 225 \text{ ft}^2$
Aerodynamic center, $X_{ac} = 16.3 \text{ ft}$
Mean Aerodynamic Chord, $\bar{c} = 5.82 \text{ ft}$
Span, $b = 39.69 \text{ ft}$
Zero-Lift Pitching Moment, $C_{m_{ow}} = -0.0229$
Pitching Moment Curve Slope, $\left(\frac{dC_m}{dC_L}\right)_w = -0.104$
Lift Curve Slope, $C_{L_{aw}} = 0.1212$

Table (11.3) shows the parameters of aerodynamic forces and moments for the wing portion, the selected wing airfoils are NASA MS (1)-0317 and NASA MS (1)- 0313 for root and tip respectively. The cruising Mach number is assumed to be 0.42, and the airfoil lift curve slope is calculated using equation (49), yielding a value of 0.1313. The wing airfoils zero-lift pitching moment is found as -0.027.

$$(at M = 0)c_{l_\alpha} = \frac{(at M = 0)c_{l_\alpha}}{\sqrt{1 - M^2}} \quad (49)$$

Equation (50) is used to calculate the wing zero-lift pitching moment as -0.0229, the quarter chord sweep angle for the wing is zero and the aspect ratio is 7.

$$C_{m_{ow}} = \left\{ \frac{\left(A \cos^2 \Lambda_c \right)}{\left(A + 2 \cos \Lambda_c \right)} \right\} \left(\frac{c_{m_{or}} + c_{m_{ot}}}{2} \right) + \left(\frac{\Delta c_{m_o}}{\varepsilon_t} \right) \varepsilon_t \quad (50)$$

For subsonic Mach numbers as 0.42, equation (51) is used to evaluate the wing moment curve slope, the aerodynamic position, and the reference point are obtained from created 3D model of the Austere field light attack aircraft and referred to figure (12.11). The root chord is 7.32 feet long, whereas the mean aerodynamic chord is 5.82 ft. The wing's pitching moment curve slope is determined to be -0.104.

$$\left(\frac{dC_m}{dC_L} \right)_w = \left(\frac{n_{ref} - n_{ac}}{c_r} \right) \left(\frac{c_r}{\bar{c}} \right) \quad (51)$$

The slope of the wing lift curve is determined by the aspect ratio and Mach number, the half chord sweep angle is 0 degrees. Equations (52 & 53) are used to compute k and β , which are dependent on the airfoil lift curve and Mach number. Using equation (54), the wing lift curve is calculated as 0.1212.





$$\beta = \sqrt{1 - M^2} \quad (52)$$

$$k = \frac{(at\ M)c_{l_\alpha}}{2\pi} \quad (53)$$

$$C_{L_{\alpha_w}} = \frac{2\pi A}{2 + \sqrt{\frac{A^2\beta^2}{k^2} \left(1 + \frac{\tan^2 \Lambda_c}{\beta^2}\right) + 4}} \quad (54)$$

The wing zero-lift pitching moment is smaller than the value found for the airfoil from the airfoil characteristics, according to the wing section specifications. The wing is not longitudinally stable by itself because the zero-lift pitching moment is negative. Furthermore, the wing's lift curve slope is substantially smaller than that of the airfoil.

Table 11.4: Longitudinal Stability Parameters for Horizontal Tail and Fuselage Section

Fuselage
Length, $l_f = 35.7$ ft
Maximum Diameter, $D_{max} = 5.1$ ft
Zero-Lift Pitching Moment, $C_{m_{of}} = -0.0218$
Aerodynamic center shift due to fuselage, $\Delta x_{acf} = -0.1381$
Tail
Incidence Angle, $i_t = 0^\circ$
Downwash at 0° Angle, $\varepsilon_o = 0^\circ$
Tail Volume Ratio, $V_H = 0.8351$
Area, $S_t = 54.9$ ft ²
Tail Mean Aerodynamic Cord, $\bar{c} = 4.115$ ft
Aerodynamic Center, $X_{ach} = 36.65$ ft
Lift Curve Slope, $C_{L_{\alpha_h}} = 0.114$

The fuselage contributes to generating lift and pitching moment, so its effect should be considered for total aircraft calculations. Fuselage zero-lift pitching moment is calculated as -0.0218 using equation (48), the equation divides the fuselage into 13 sections and calculates each sections effect to obtain the total moment coefficient.

The aerodynamic center shift due to fuselage is calculated from equation (55), the parameter $\frac{dM}{d\alpha}$ is evaluated from the summation equation (56), which also separates fuselage to 13 parts. However, the aerodynamic shift due to fuselage is -0.1381 ft. From the results, it can be observed that the fuselage moves the aerodynamic center forward. The fuselage zero-lift pitching moment is negative so it's unstable.





$$\Delta x_{acf} = -\frac{\left(\frac{dM}{d\alpha}\right)}{qS\bar{c}C_{L_{\alpha_w}}} \quad (55)$$

$$\left(\frac{dM}{d\alpha}\right) = \left(\frac{q}{36.5}\right) \left(\frac{C_{L_{\alpha_w}}}{0.08}\right) \sum_{i=1}^{i=13} \left\{ (w_{f_i}^2) \left(\frac{d\varepsilon}{d\alpha}\right)_i \Delta x_i \right\} \quad (56)$$

The horizontal tail section has no specific equations, so proper substitutions are made in wing equations to obtain the parameters. The horizontal tail for Austere field light attack aircraft is set at zero degree incidence angle, the downwash angle is also assumed to be 0 degree. The tail volume ratio is calculated using equation (57), and its value is 0.8351, the tail area is 54.9 ft², the wing mean aerodynamic chord is found as 5.82 ft.

$$V_H = \frac{S_t l_t}{S\bar{c}} \quad (57)$$

The tail lift curve slope is calculated as 0.114, the aspect ratio is evaluated as 3.85, and the same cruising Mach number is 0.42. The aerodynamic center of the tail is located at 36.65 ft.

Table 11.5: Longitudinal Stability Parameters for Wing-Fuselage Section and the Total Aircraft

Wing-Fuselage
Wing-fuselage pitching moment, $C_{m_{wf}} = -0.0465$
Wing-fuselage lift curve slope, $C_{L_{\alpha wf}} = 0.121$
Wing-fuselage Aerodynamic Center, $X_{acwf} = 16.162$ ft
Aircraft
Center of Gravity, $X_{cg} = 15.7$ ft
Aerodynamic Center, $X_{ac} = 18.614$ ft
Zero-Lift Pitching Moment Coefficient, $C_{m_0} = 0.01841$
Moment Curve Slope, $\frac{dC_m}{dC_L} = -2.914$
Lift Curve Slope, $C_{L_\alpha} = 0.136$
Moment Coefficient Slope, $\frac{dC_{m,cg}}{d\alpha_a} = -0.0631$
Neutral Point, $X_n = 18.4$ ft
Static Margin = 0.464

The wing-fuselage lift curve slope is 0.121, it is calculated using equation (58), the wing-fuselage interference factor is estimated as 0.99.

$$C_{L_{\alpha wf}} = K_{wf} C_{L_{\alpha_w}} \quad (58)$$

The zero-lift pitching moment for wing-fuselage is calculated using equation (59) as -0.0465, the Mach number effect ratio is obtained from appendix (D.3).





$$C_{m_{o_wf}} = (C_{m_{ow}} + C_{m_{of}}) \frac{(C_{m_o})_M}{(C_{m_o})_{M=0}} \quad (59)$$

The slope of the aircraft lift curve is determined using equation (60) as 0.136, with the canard influence on the lift curve being ignored since the designed light attack aircraft does not feature it. Proper replacements of the horizontal tail parameter are performed for the horizontal tail effect.

$$C_{L_\alpha} = C_{L_{\alpha_{wf}}} + C_{L_{\alpha_h}} \eta_h \left(\frac{S_h}{S} \right) \left(1 - \frac{d_\varepsilon}{d_\alpha} \right) + C_{L_{\alpha_c}} \eta_c \left(\frac{S_c}{S} \right) \left(1 - \frac{d_{\varepsilon_c}}{d_\alpha} \right) \quad (60)$$

Using equation (61), the aircraft's zero-lift pitching moment is calculated to be 0.01841; the canard effect is disregarded. By substituting suitable horizontal tail values in the wing equation, the zero-lift pitching moment coefficient may be calculated.

$$C_{m_o} = C_{m_{owf}} + C_{m_{oc}} + C_{m_{oh}} \quad (61)$$

The distance between the aerodynamic center and the center of gravity, measured from the mean aerodynamic chord leading edge and expressed as a unit of mean aerodynamic chord, is used to calculate the slope of the moment curve. The moment curve slope is -2.914 using equation (62).

$$\frac{dC_m}{dC_L} = \bar{x}_{ref} - \bar{x}_{aca} \quad (62)$$

The moment coefficient slope is determined using equation (63), where a and a_t are the lift curve slopes for the aircraft and horizontal tail, respectively. The value of h represents the position of the center of gravity in units of the mean aerodynamic chord length, and it is 0.146, whereas the aerodynamic center is at 0.647. Whereas, -0.0631 is the moment coefficient against absolute angle of attack graph slope.

$$\frac{dC_{m,cg}}{d\alpha_a} = a \left[h - h_{ac_{wb}} - \frac{V_H a_t}{a} \left(1 - \frac{d_\varepsilon}{d_\alpha} \right) \right] \quad (63)$$

The neutral point is where the slope of the moment coefficient curve is zero, the moment coefficient curve is negative, zero, or positive depending on whether h is less than, equal to, or greater than h_n . The location of the neutral point is calculated to be 0.226.

$$h_n = h_{ac_{wb}} + \frac{V_H a_t}{a} \left(1 - \frac{d_\varepsilon}{d_\alpha} \right) \quad (64)$$





The static margin is calculated by subtracting the center of gravity from the neutral point location. The static margin is 0.464. The static margin is a measure of longitudinal static stability that must be positive for a stable aircraft; the higher the static margin, the more stable the aircraft.

According to the findings, the following conditions are met, the zero-lift pitching moment coefficient is positive, the pitching moment curve slope is negative, the center of gravity is comfortably forward of the neutral point, and the static margin is positive. The Austere field light attack aircraft is statically stable based on these four conditions.

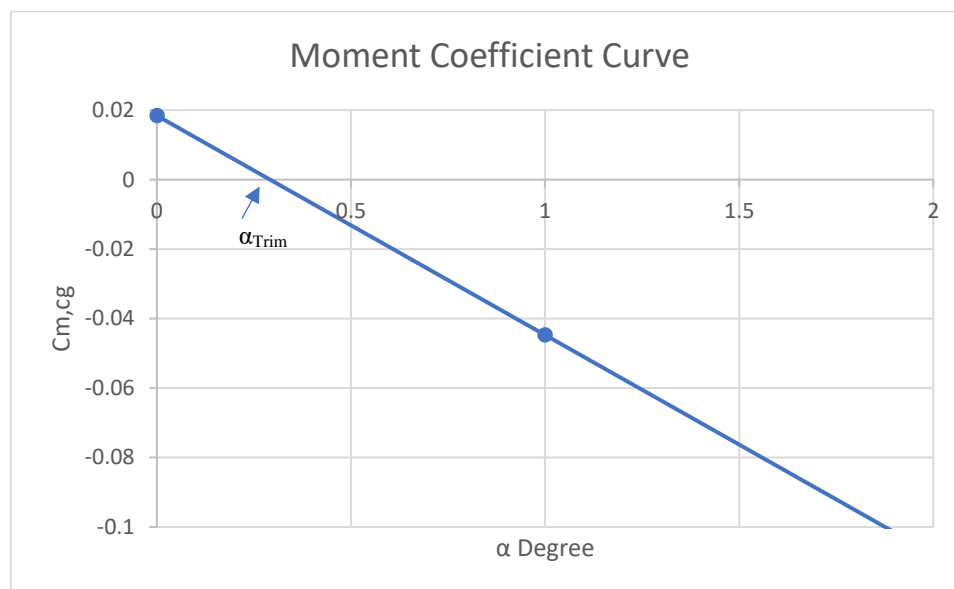


Figure 11.2: Moment Coefficient Versus Angle of Attack Graph for the Designed Light Attack Aircraft

Moment Coefficient curve is plotted in figure (11.2). From the first glance, it can be observed that the slope is negative, which is one of the criteria for longitudinal static stability. The trim angle of attack is found to be as 0.3 degree which is in the range of flight angle of attacks. Furthermore, the zero-lift pitching moment coefficient is calculated as 0.018, and it satisfies the Longitudinal stability condition because it's positive.

11.4. Directional Stability and Control

Static Directional Stability (or Weathercock Stability) is the static stability of the aircraft on its z-axis and thus measures the sliding resistance of the aircraft. The more rigid directional stability the more the aircraft's longitudinal axis would have to adjust to relative winds. For static directional stability, an aircraft disrupted by the balance of flight must restore yawing moment to return the aircraft to its balance. The static directional stability condition is as follows:





$$C_{n\beta} > 0$$

To have a static directional stable aircraft:

$$C_{n\beta} = 0.001 \text{ per degree} \quad (65)$$

And to determine yawing moment due to sideslip derivative, $C_{n\beta} = \frac{dC_n}{d\beta}$:

$$C_{n\beta} = C_{n\beta_w} + C_{n\beta_{fus}} + C_{n\beta_{VT}} \quad (66)$$

Where $C_{n\beta_w}$ is assumed to be equal to 0 because the wing has no effect on the yawing moment. Therefore:

$$C_{n\beta} = C_{n\beta_{fus}} + C_{n\beta_{VT}} \quad (67)$$

$$C_{n\beta} = \left(-57.3 K_N K_{R_l} \left(\frac{S_{f_s}}{S} \right) \left(\frac{l_f}{b} \right) \right) + \left(C_{L_{AVT}} \left(\frac{S_V}{S} \right) \left(\frac{l_v}{b} \right) \right) \quad (68)$$

Where:

S_{f_s} is the side area of fuselage, K_N is an empirical factor, K_{R_l} is a factor dependent on Reynold's Number.

Based on Appendix (D.4 and D.5), K_N is found to be around 0.0025 and, K_{R_l} is found to be around 1.3. $C_{L_{AVT}}$ is found by the following equation:

$$C_{L_{AVT}} = \frac{2\pi AR}{\left(2 + \left(\frac{AR^2 + \beta^2}{k^2 + 4} \right)^{\frac{1}{2}} \right)} \quad (69)$$

Where k and β are found by the following:

$$k = \frac{(C_{l_\alpha})_{at\ M}}{2\pi} = \frac{0.1}{2\pi} = 0.016/rad \quad (70)$$

$$\beta = \sqrt{1 - M^2} = \sqrt{1 - 0.42^2} = 0.9 \quad (71)$$

$(C_{l_\alpha})_{at\ M}$ is found by calculating the slope of the lift coefficient versus alpha graph of the NACA 0015 airfoil which is used for the vertical tail. Therefore:

$$C_{L_{AVT}} = \frac{2\pi \times 1.19}{\left(2 + \left(\frac{1.19^2 + 0.9^2}{0.016^2 + 4} \right)^{\frac{1}{2}} \right)} = 4.67/rad \quad (72)$$





$$C_{n\beta} = \left(-57.3 \times 0.0025 \times 1.3 \times \left(\frac{199.07}{225} \right) \left(\frac{35.7}{39.7} \right) \right) + \left(4.67 \times \left(\frac{25.4}{225} \right) \left(\frac{19.92}{39.7} \right) \right) = 0.11 \quad (73)$$

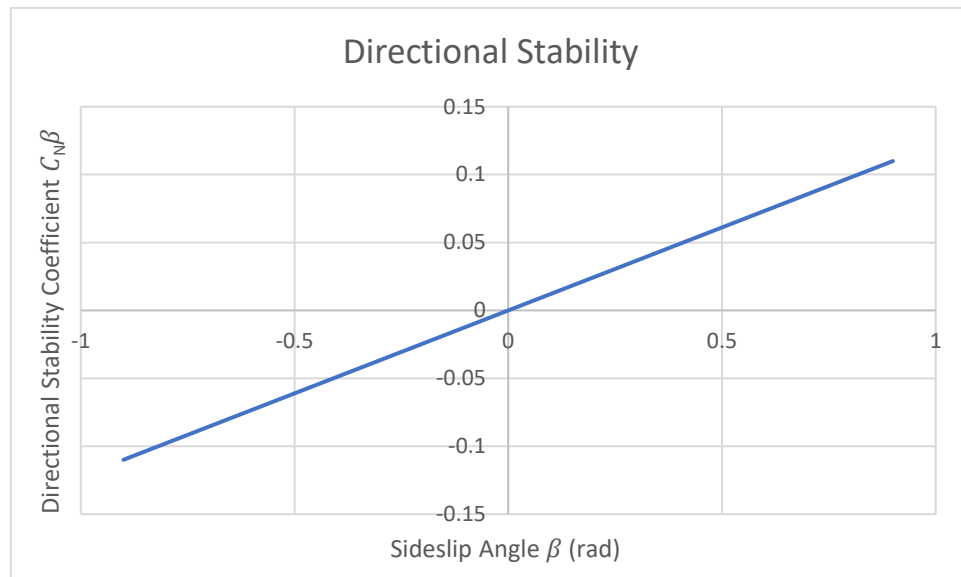


Figure 11.3: Directional Stability

Figure (11.3) shows that the pitching moment coefficient has a positive slope with increasing the side slip angle, this proves that the designed aircraft is statically directionally stable because the result is positive.

11.4.1. Directional Control Requirements



Figure 11.4: Adverse Yaw

If the austere field light attack aircraft is deployed in a synchronized turn, the inner wing will experience less relative wind than the outer wing as shown in figure (11.4), which makes drag smaller in the inner wing than the external wing; this, in turn, creates an adverse yaw (yaw moment opposing the turn). The steering wheel must be deflected so that the synchronized turn is reached to counteract the adverse yaw.



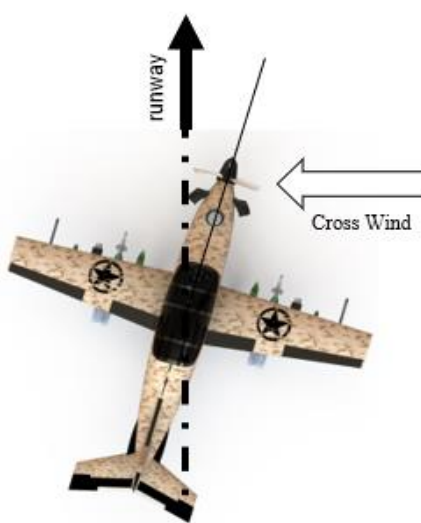


Figure 11.5: Cross-wing landing without rudder deflection

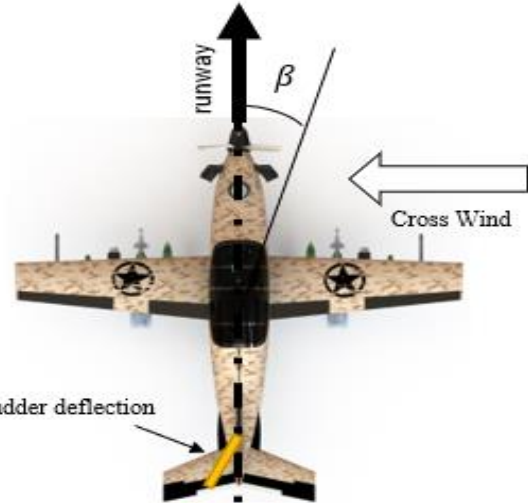


Figure 11.6: Cross-wing landing with rudder deflection

If the austere field light attack aircraft is landing crosswind, the pilot must take the aircraft at an angle of alignment to the route. The rudder must therefore be strong enough to cut the aircraft in the specified crosswind (rudder control power) as shown in figures (11.5 and 11.6).

11.5. Lateral Stability and Control

Lateral stability is the stability of the longitudinal axis of the plane, which stretches nose to tail, is known as lateral stability. This helps balance the side or rolling impact as the wing on the opposite side of the plane is lower than the wing. Four key design factors making an aircraft smooth – dihedral, key impact, weight distribution and sweepback. Later discussions would show that these aspects also contribute to the development of layers or directional stability. For lateral stability, the most common technique is the construction of wings with a dihedral angle of one to three degrees. In other words, the wings on each side of the aircraft creates a small velocity component or dihedral angle with the wings over wing parallel to the lateral axis. The wings are determined by the angle of the wing.

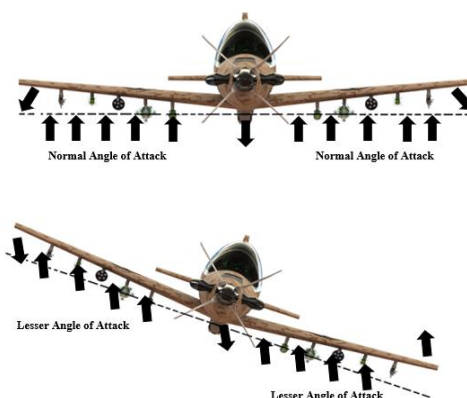


Figure 11.7: Dihedral angle for lateral stability





Naturally, the foundation of rolling stability is the lateral balance of force generated by the wings of the aircraft. Any lifting imbalance will cause the austere light attack aircraft to roll along its longitudinal axis. If one wing of the aircraft rises and the other lowers the momentary breeze, the aircraft will bank. When the aircraft is banked, it continues to fall or go to the lower wing without turning as shown in figure (11.7).

The lift on the bottom wing rises and the elevation on the top wing decreases and helps to return the aircraft to its original side attitude, i.e., the angle of attack and elevation on the two wings are again identical. The dihedral effect is then to create a rolling moment in which the aircraft becomes laterally balanced when a sideslip happens. The restorative force will move the low wing too far, so that the other wing falls now. If so, the mechanism will be recurring, with each side oscillation diminishing until an equilibrium is eventually achieved for the wing level flight (Lateral Stability, n.d.).

11.5.1. Roll Stability

The roll stabilization of the aircraft is provided by the development of a rolling moment if the aircraft is disrupted by the attitude at a wing level. The static roll stability condition is as follows:

$$C_{l\beta} < 0 \quad (74)$$

Rolling moment produced on aircraft when it sideslips depends upon:

1. Wing dihedral angle (Γ)
2. Wing sweep angle (Λ)
3. Wing position relative to the fuselage
4. Vertical tail

The dihedral angle is the upwards angle of the horizontal wings of the austere light attack aircraft. The dihedral effect is the amount of rolling moment produced in relation to the sideslip quantity. It is a crucial factor on the stability of the austere light attack aircraft about the roll axis (Dihedral (aeronautics) - Wikipedia, 2021). A swept wing is a wing which curves back or forth from the root instead of straight sideways. The effects of it are to postpone the shock waves and accompany an aerodynamic drag increase induced by fluid compressibility at sonic speed and performance improvement. For the austere light attack aircraft there is no wing sweep angle (Swept wing - Wikipedia, 2021).

The wing position relative to the fuselage influences the rolling moment and there are many wing positions for the aircraft, but the austere light attack aircraft is set as a low wing to have the best stability possible.





Chapter 12 Model Development

The austere field light attack aircraft was modelled using a CAD software called Solidworks. This modeling application was therefore commonly applied by students, designers, and engineers in various fields of specialization. These means of CAD application tools has effectively enabled to conduct modeling of various light attack aircrafts. After theoretically calculating the dimensions of each component, these dimensions were taken into Solidworks to develop the 3D model of the light attack aircraft.

12.1. Wing

The wing was designed to have a wingspan of 39.7ft with a dihedral angle of 6-degrees. The wing type selected was that of a tapered wing. Furthermore, NASA MS (1)-0317 airfoil with chord length of 7.32ft was applied onto the wing root while the NASA MS (1)- 0313 airfoil with chord length of 4ft was selected for the wing tip as a half body (19.85ft).

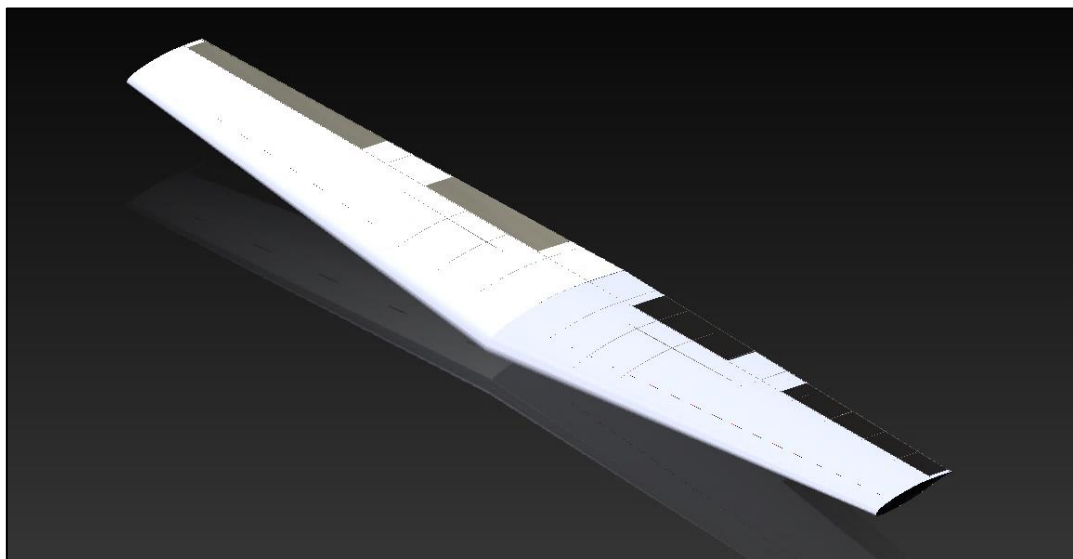


Figure 12.1: Wing Model

Based on the wing sketch in chapter (4), the wing was created using the ‘lofted boss/base’ feature and mirrored to create the complete wing model with the defined wingspan. Following that, the control surfaces were defined using the ‘split line’ feature based on the 2D sketch. Finally, the Spars, ribs and stringers were created and inserted into the aircraft wing which was shown and discussed in chapter (4).

12.2. Empennage

Based on the Empennage configuration in chapter (5), the empennage components (Horizontal and Vertical Tails) were designed to develop the 3D model along with the rudder, elevator and trim tabs.





The vertical tail was designed similar to the wing. The airfoils used at the root and tip were both NACA 0015 with chord lengths of 6.35ft and 3.49ft, respectively. The total span between the 2 airfoils was defined as 5.5ft and the guide curves were applied with a small fillet of 1.3ft radius; as well as, having a 25-degree quarter chord sweep angle.

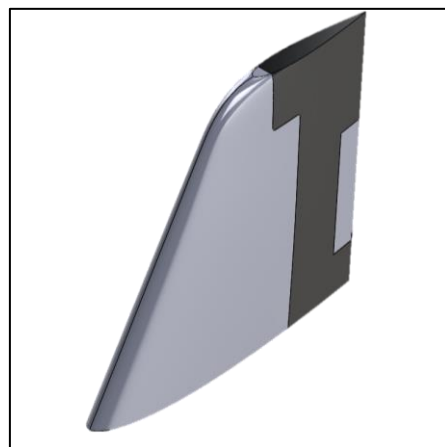


Figure 12.2: Vertical Tail Model

These guide curves help define the path when the airfoils were lofted using ‘lofted boss/base’ feature. The rudder design was inspired from the competitor aircrafts. Following that, the trim tab was applied right after the rudder using the ‘split line’ feature.

The horizontal tail was created using 2 airfoils, NACA 23015 and NACA 63-212 in the root and tip, with a chord length of 4.89ft and 3.23ft, respectively. These airfoils were positioned 6.74ft apart in span. The guide curves were applied, and a small fillet was added at the root; as well as an 18-degree quarter chord sweep angle.



Figure 12.3: Horizontal Tail Model





The horizontal tail was made using ‘lofted boss/base’ feature and the control surfaces were added on using ‘split line’ feature similarly. Finally, the model was mirrored to the required span of 13.48ft. Dorsal and ventral fins were also added on.

12.3. Fuselage

The fuselage was made using the blueprint from the competitor aircrafts but based on the fuselage configuration discussed in chapter (6). The fuselage length was set to 35.7ft with a maximum fuselage diameter of 5.1ft. The fuselage was broken down into three sections: nose, cockpit and cone, with a length of 9.9ft, 10.5ft and 15.3ft, respectively. The top, bottom, left and right-side guide curves were applied based on the blueprints provided in section (2.4). Following that, reference planes were made across the fuselage to create cross section sketches. These sketches were made using a 4-point spline where each point was attached to the respective guide curves using pierce/point relations.

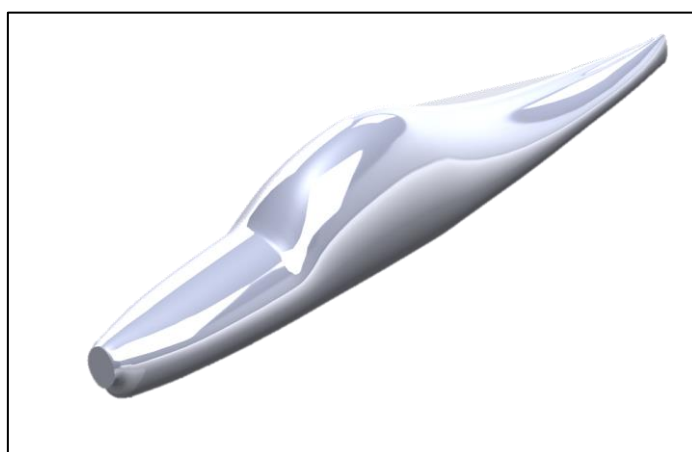


Figure 12.4: Fuselage Model

After all the sections were sketched, the ‘lofted boss/base’ feature was used to develop the 3D model of the fuselage. Furthermore, the ‘split line’ feature was used to define the outline of the cockpit.

12.4. Propulsion System

The propulsion system made using Solidworks include the PT6A engine and propeller system. The engine comprises of the combustion chamber, power shaft, turbine shaft, bearings, mechanical seals, thermocouple, and the casing. These components were designed in different part files.



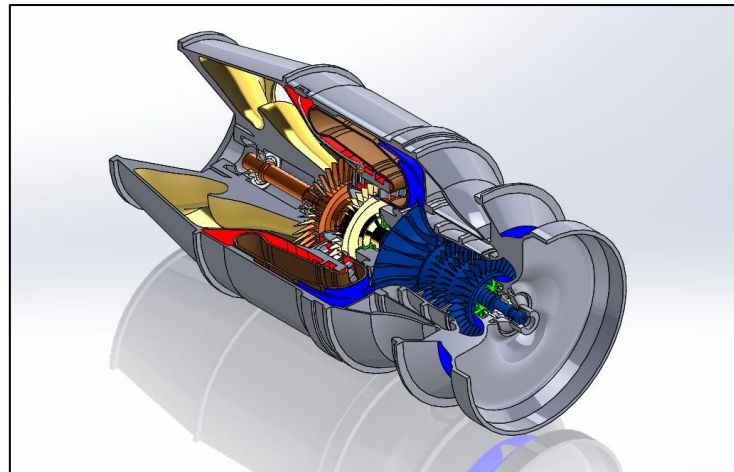


Figure 12.5: Engine Model

Furthermore, the ‘revolve’ feature was primarily used in the development of these components. The compressor and turbine blades were designed using a spline tool for the cross section and applying a twist using ‘rotate entities’ feature. Following that, the blade was lofted using ‘lofted boss/base’ feature and finally by using the ‘circular pattern’ feature, the number of blades was placed around the shaft. The engine model was set to be 4ft long (47.4inches).



Figure 12.6: Propeller System Model

The propeller system consists of 2 parts which were the blades and the nose. To put it simply, the number of blades were set to ‘4’ using the ‘circular patten’ feature. The diameter of the propeller blades was set to 10.97ft. The revolve feature was used to design the nose of the propeller.

12.5. Landing Gear

The landing gear system, which was a retractable tricycle type, consists of 2 parts which were the main landing gear located under the wings, and the nose landing gear located under the nose of the fuselage.



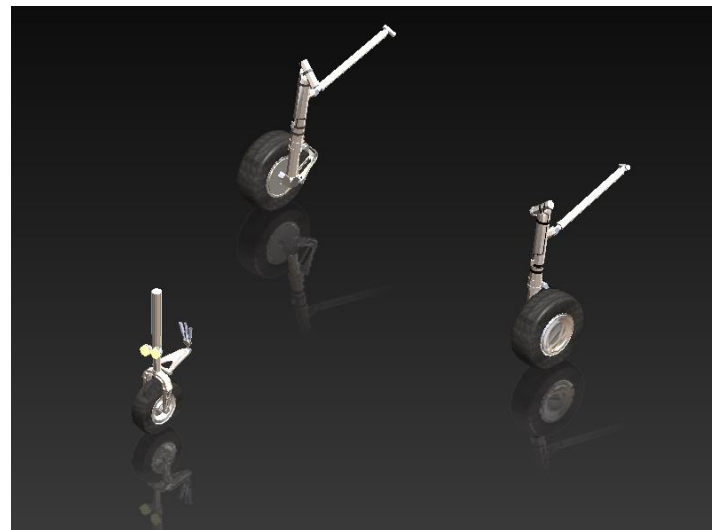


Figure 12.7: Landing Gear Model

The wheels of the nose landing gear was set to be 1.42ft (17 inches) in diameter and 0.37ft (4.4inches) thick; additionally, the main landing gear was set to be 1.94ft (23.3 inches) in diameter and 0.54ft (6.5inches) thick. Following that, the ‘revolve’ feature was used on the respective wheel sketches to form the 3D model. The struts, damper, axle, links and damper hydraulic line were developed using various features like ‘extruded boss/base and ‘lofted boss/base’ with the help of reference planes.

12.6. Cockpit Layout

The cockpit of the aircraft comprises of 2 seats for the pilot and co-pilot. The Seat dimensions are shown in figure (12.8).

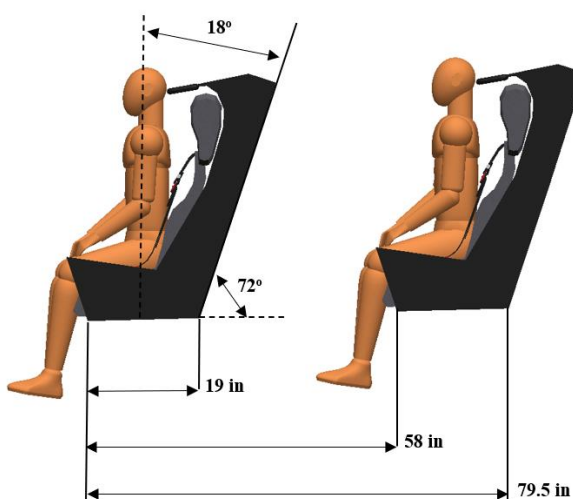


Figure 12.8: Seat Dimension





The simple seat design was made using basic sketches and later extruded using ‘extruded boss/base’ feature. Furthermore, small details like seatbelts and seatbelt shackles were designed by sketches using the spline tool to define the path and lofted to form the 3D model. This can be seen in figure (12.9).



Figure 12.9: Simple Seat Model

The detailed model of the ejection seat was made using a high rendering software called “Autodesk 3DS MAX” which is shown in figure (12.10).

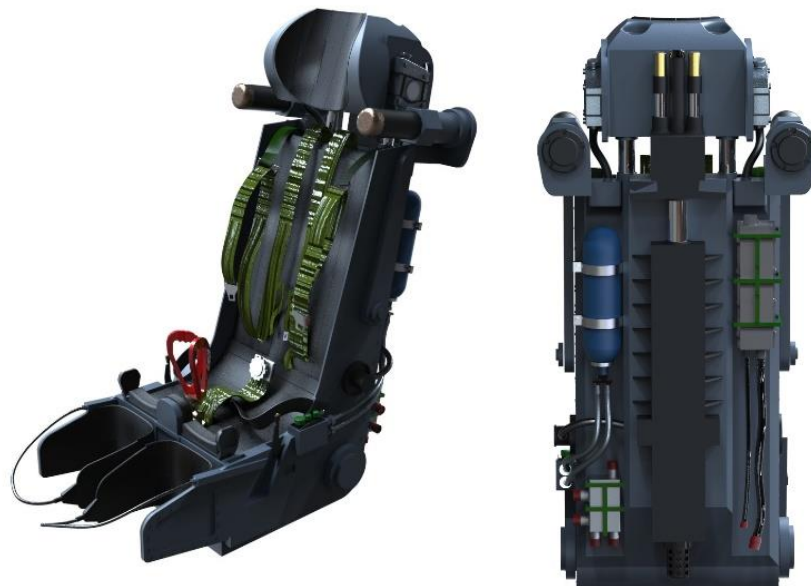


Figure 12.10: Rendered Ejection Seat Model





12.7. Assembly and Final Renderings of Austere Field Light Attack Aircraft

After each component was carefully designed, the aircraft was assembled and rendered. The final renderings are shown below.

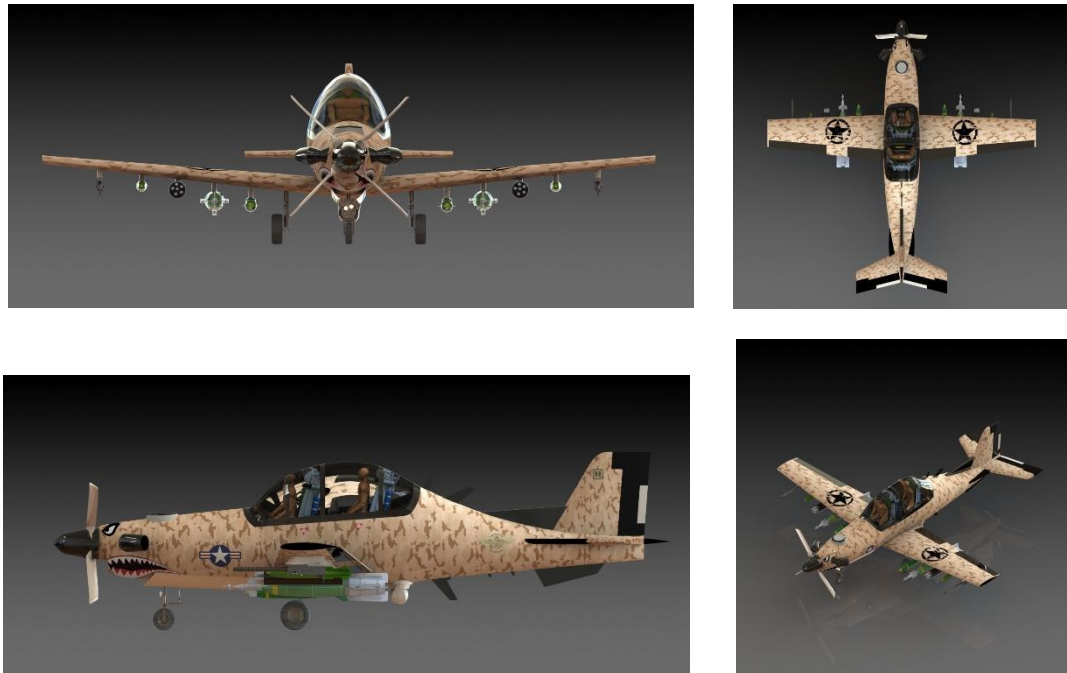


Figure 12.11: Final Renderings

12.8. Auxiliary Systems

Auxiliary systems assist the aircraft in performing its primary task. They are critical and vital for a safe flight, even if failure of one of these systems does not result in the aircraft losing control or crashing immediately (Experimental Aircraft Info, 2021).

Auxiliary systems also have a broad variety of operational and command equipment. This extra equipment links the instruments to the main equipment that isn't being used at the moment, such as the auxiliary power unit, external fuel tank, or flight resupply system (Auxiliary equipment in the virtual aviation and aerospace and space show, 2021).

Furthermore, figure (12.12) shows a high-level schematic of all the major subsystems onboard the Austere field light attack aircraft. This layout was carefully configured to ensure both efficient and safe flying practices.



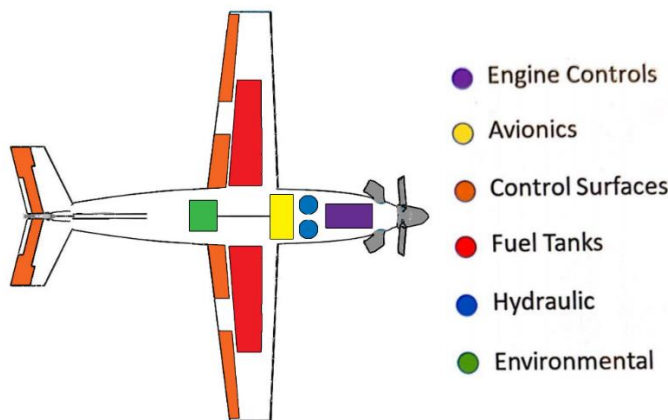


Figure 12.12: Schematic diagram of large systems placement within the aircraft

The hydraulics system in figure (12.12) is situated at the front of the aircraft. It is also shown as two independent hydraulic reservoirs that contain the hydraulic fluid for the system. An engine-driven pump, in addition to each reservoir, gives pressure to the system and permits hydraulic fluid to be transferred to each flight control surface. The engine-driven pumps are powered by shaft work and are installed on an engine-drive gear box. In the event that both engine-driven pumps fail, secondary air-driven pumps are attached to each hydraulic reservoir. The bleed air from the engine powers the air-driven pumps.

Due to the two distinct hydraulic reservoirs and pumps, each flight control surface has two actuators - one from each pump - that may move each control surface when signals from the primary flight control computer are delivered. Because of the redundancy, even if one of the two pumps or one of the numerous hydraulic lines fails, the control surfaces can still be controlled.

12.8.1. Pneumatic and Environmental control system schematic

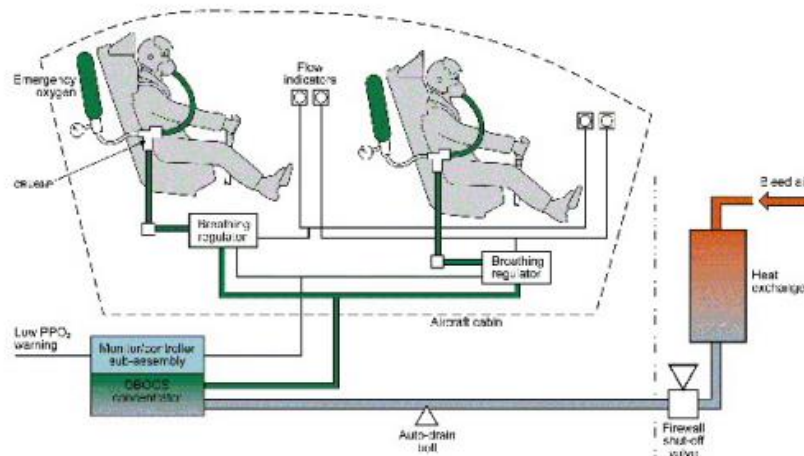


Figure 12.13: Environmental system schematic (Richardson, 2000)



Figure (12.13) presents a summary of the device setup in the Oxygen system schematics. The system's principal components includes the heat exchanger, the primary shut-off valve, the water drain bolt, the oxygen concentrator, the oxygen control unit (OBCU) and the oxygen flow indicator. The heat exchanger functions in order to ensure that the engine compressor bleeds the air to a sufficient oxygen concentration temperature. When not working or the airplane engine is not running, the valve stops the machine, prevents the entry of water and other external items. In case of an engine compartment fire, it also offers a way to switch off the machine.

A condensation water collected on the lower part of a pipe is blown out of the device when the pipe is pressurized in the auto drain bolt. The focuser's job is to supply clean, dry, oxygen-enriched gas to the breathing control unit at a specific concentration on aircraft altitude (Richardson, 2000).

12.8.2. Electrical system

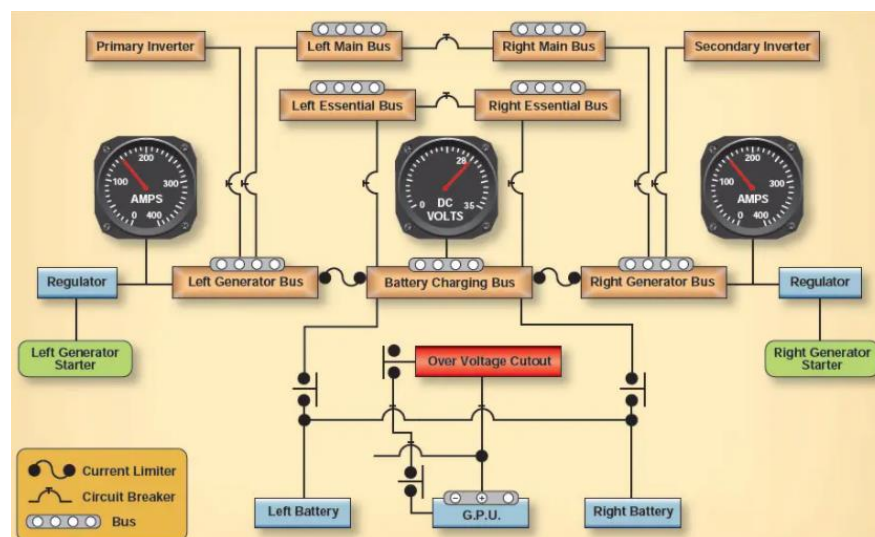


Figure 12.14: Simplified schematic for the electrical system (FlightLiteracy, 2021)

A 28-volt direct current (DC) device that is powered by one or more batteries and a start/generator for the engine is an electrical system. Electrical systems are normally designed to allow any bus to be powered from any source of electricity. For illustration, a typical device might have a right and a left generator bus, which is usually operated by right and left motor generators. If a generator fails, power is lost in its bus, but a bus tie switch can make repairs in that bus. This switch closes the buses and enables the operating generator to provide both buses with power (FlightLiteracy, 2021).



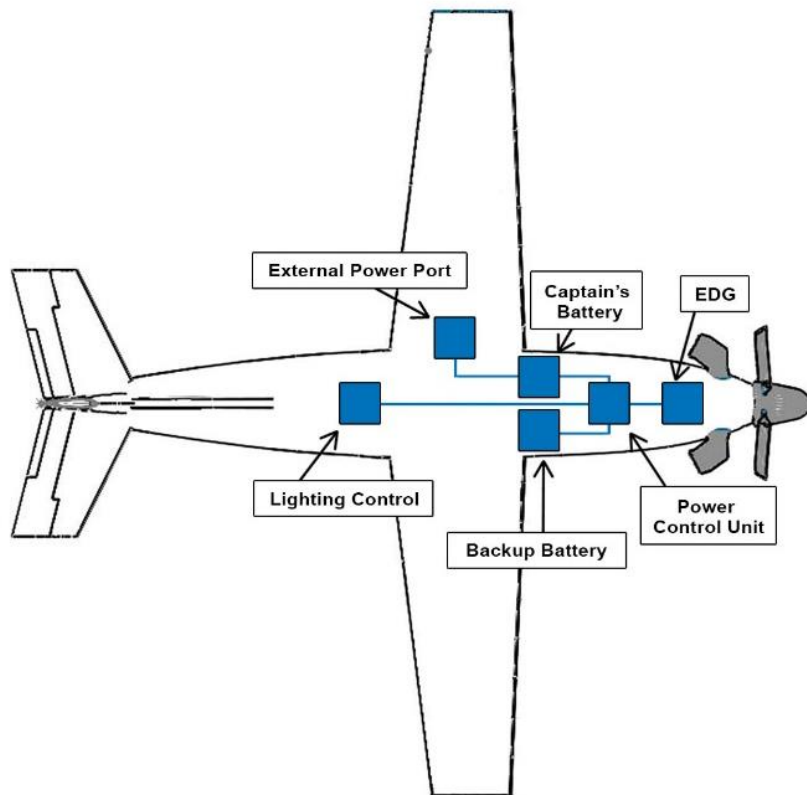
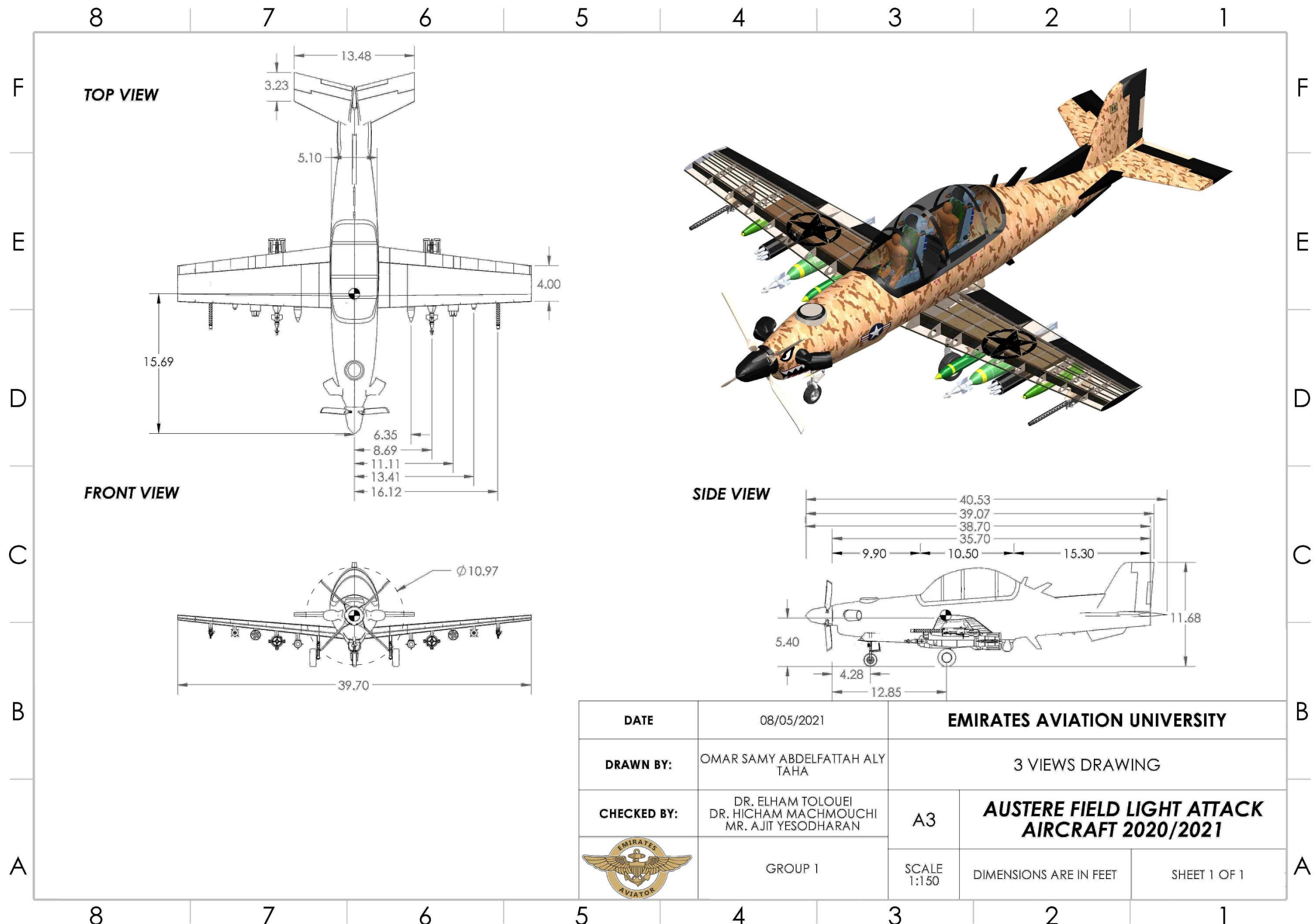


Figure 12.15: Austere Field Light Attack Aircraft Electrical System Path

The Austere Field Light Attack Aircraft's power generating system consists of a single engine driven generator (EDG), which converts mechanical energy to electrical energy via a gearbox linked to the engine. This power is transferred to the power control unit, which converts AC power to DC power for the two batteries on board and frequency- convert it for pilot usage in the cockpit. The captain's battery, which is housed in the cockpit and supplies power to the avionics, is the main battery on board. In the event that the EDG fails, this battery is kept fully charged during the journey.

The EDG also provides power to a second battery in the aircraft's front, which is utilized for backup power. It also features a single external power connection for startup, service, and ground maintenance. Finally, the EDG provides electricity to the aircraft's lighting systems. Navigation lights, emergency lights, and cockpit illumination are all powered by 28 Voltage Direct Current (VDC), which is converted by the power control unit.

Traditional filament lightbulbs, ranging from 3 watts for interior lighting to 600 watts for landing lights, are used to provide illumination. Figure (12.15) shows a high-level schematic of this system. It's worth noting that an auxiliary power unit (APU) isn't required to give the Austere Field Light Attack Aircraft with the necessary electric power, and that it would primarily add unnecessary weight and cost.





Chapter 13 Manufacturing Process of Austere Field Light Attack Aircraft

There are three stages for manufacturing the austere field light attack aircraft, design Stage, production stage, and assembly stage.

13.1. Design Stage

Designing the austere field light attack aircraft is carried out by first doing the necessary calculations for the aircraft specifications. Then comes the aircraft frame design which is done using SolidWorks software in which the whole aircraft components are designed as shown in figures (13.1 and 13.2).



Figure 13.1: Top view of the austere light attack aircraft



Figure 13.2: Front view of the austere light attack aircraft

13.2. Production Stage

Production starts with manufacturing the parts from stocks. Manufacture involves the manufacturing and jigging, sheet metal working, machining, work and service operations of plastic and composites. The major parts of the austere light attack aircraft such as the wings, empennage, fuselage, and the landing gear are made of different materials as mentioned in sections (4.6, 5.5, 6.5, & 8.4). These major parts are produced separately and then assembled all together in the assembly stage (Cameron, n.d.).





13.3. Assembly stage

Assembly starts with the construction of subassemblies of component sections. The main elements include wings, stabilizers, fuselage, the landing gear, doors, and components for the interior. These components are put together by welding and other techniques which must be approved by the safety regulations and standards. The wing mounting is especially intensive and requires the accurate drilling and counter-sunken of a great deal of holes in the skin, through which rivets are guided.

To guarantee a leak-proof fuel compartment, the finished wing is washed and sealed from the inside. The assembly line contains multiple consecutive positions, in which the airframe stays for several days to over a week, with default roles. At each location concurrently, a variety of assembly operations provide the opportunity for cross-exposures of chemical products. After the assembly of the whole aircraft is done, the aircraft is tested to search for any defects that should be analyzed. After finishing the assembly and the final checking the austere light attack aircraft should look like what is shown in figures (13.1 & 13.2) (Aircraft Construction: How are airplanes made? | OxfordSaudia Flight Academy, 2020).





Chapter 14 Cost and Market Analysis

14.1. Cost Analysis

The costs of operation and maintenance are calculated based on assumptions about the Austere Field aircraft. Fuel, crew wages, and repairs are the most significant operation and maintenance costs. Fuel costs for about 15% of operation and maintenance costs for a standard military aircraft, crew wages for about 35%, and maintenance for the majority of the rest 50%. Maintenance employs more than a third of the US Air Force's workforce.

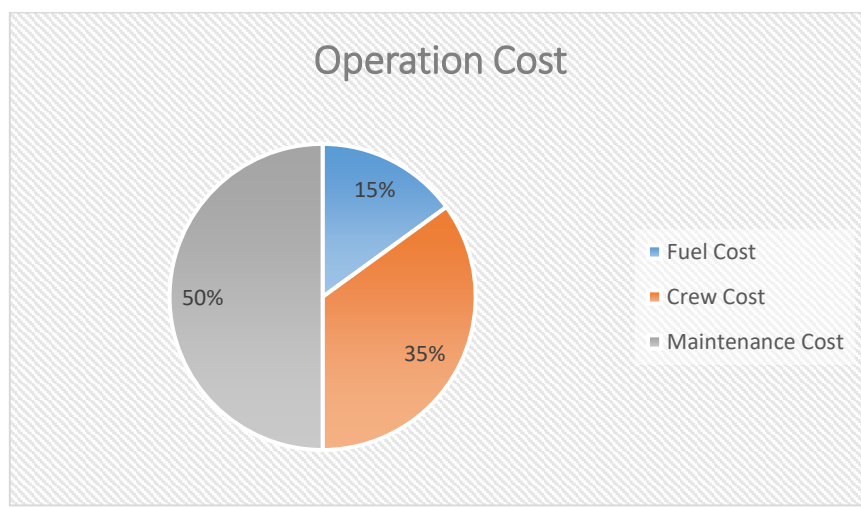


Figure 14.1: Operating Cost Chart

14.2. Yearly Fuel Usage Cost

All aircrafts in general burns all of the available fuel except what is needed for loiter and reaching an alternate airport. Specific equations and assumptions is used to calculate yearly fuel consumption, and the total time and fuel burned are used to calculate the average fuel burned per hour, which must be compared based on historical data in table (2.1 & 2.2) for the Austere Field Light Attack Aircraft. By using table (14.1) which contains the values for different important parameters, the fuel cost per year and the crew cost is going to be calculated (Raymer, 1889).

Table 14.1: Yearly Fuel Usage Cost Assumptions

Givens and Assumptions	
Parameter	Value
Mission Profile Duration	4.5 hours
Average Yearly Flight hours	1,200 hours
Specific Fuel Consumption	0.54 lb/hp/h
Fuel Cost Average Rate Per Gallon	2.5 \$
Cruise velocity	570 ft/s
Take off Weight	11,500 lb





$$\text{Fuel Burned per hour} = 0.54 \times 550 = 297 \frac{\text{lb}}{\text{hr}}$$

Yearly Fuel Burned = $1,200 \times 297 = 356,400 \text{ lb per year} \rightarrow 56,571.37 \text{ gallon per year}$

$$\text{Fuel cost per year} = 56,571.37 \times 2.5 = 141,428.43 \$$$

14.3. Crew Cost

Crew Costs include all costs and expenditures incurred or charged by the Service Provider Group in hiring or engaging such Crew, such as wages, bonuses, monetary value of equity compensation, payroll taxes, employee-related insurance and benefits, and applicable training costs. Crew costs for military aircraft are calculated by calculating how many flight crew members would be required to remain on active duty in order to operate the aircraft (Raymer, 1889).

$$\text{Crew cost for two members} = 35 \times \left(V_c \frac{W_0}{10^5} \right)^{0.3} + 84 = 35 \times \left(337.7 \times \frac{11,500}{10^5} \right)^{0.3} + 84 = 188.916 \$/\text{hr} \quad (75)$$

$$\text{Per Pilot} = 94.458 \$/\text{hr}$$

Table 14.2: Cost per Flight Hour

Aircrafts	Cost per flight hour
Beechcraft AT-6	2,500\$
Beechcraft T-6c Texan 2	2,200\$
North American P-51 mustang	3,500\$
Douglas A-1 Skyraider	1,000\$
Embraer EMB 314 super Tucano	1,000\$
Austere Field Light Attack Aircraft	2,300\$

Table (14.2) shows the cost per flight hour for competitor aircrafts, the cost per flight hour for Austere field light attack aircraft is estimated as 2,300\$ per operating flight hour which is in the range of similar aircrafts.

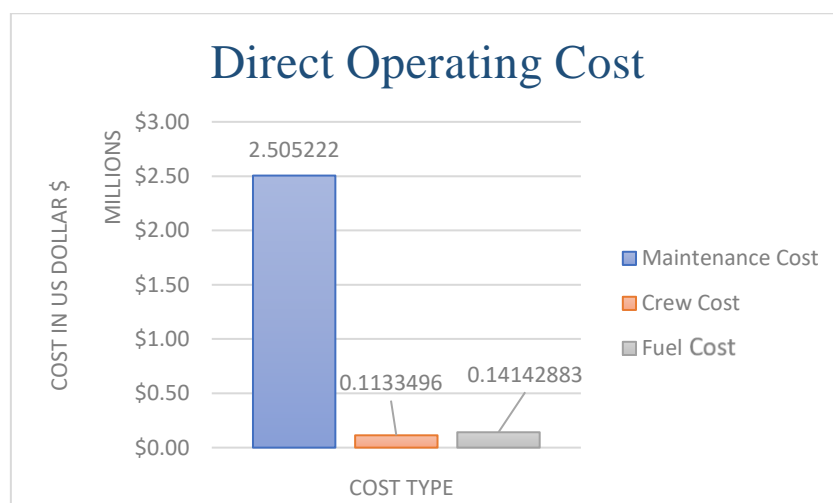


Figure 14.2: Direct Operating Cost for Austere Field Light Attack Aircraft





Yearly direct operating cost is calculated using the estimated value for cost per operating flight hour and the total flight hours every year as AIAA requirements which is 1,200 hours. The distribution for direct operating can be observed in figure (14.2). The maintenance cost is estimated by subtracting fuel cost and crew cost from direct operating cost. However, the obtain result are compatible for light attack aircraft.

14.4. Flyway cost

The aircraft is valued at its marginal cost, which includes only the cost of production and the tools used to produce a single aircraft. It doesn't include sunk costs like research and development, supplementary costs like support facilities, and potential costs like spares and repairs (Wikipedia, 2020).

There are a few other ways to estimate the cost of an aircraft:

1. The estimated net production cost is equal to the amount of the gross flyaway cost and the research and development cost separated by the number of aircraft.
2. Complete cost of the aircraft program over its lifespan, including maintenance, divided by the number of aircraft, which equals overall total cost including maintenance.

In this following chart as it shown the flyway cost for different types of aircrafts.

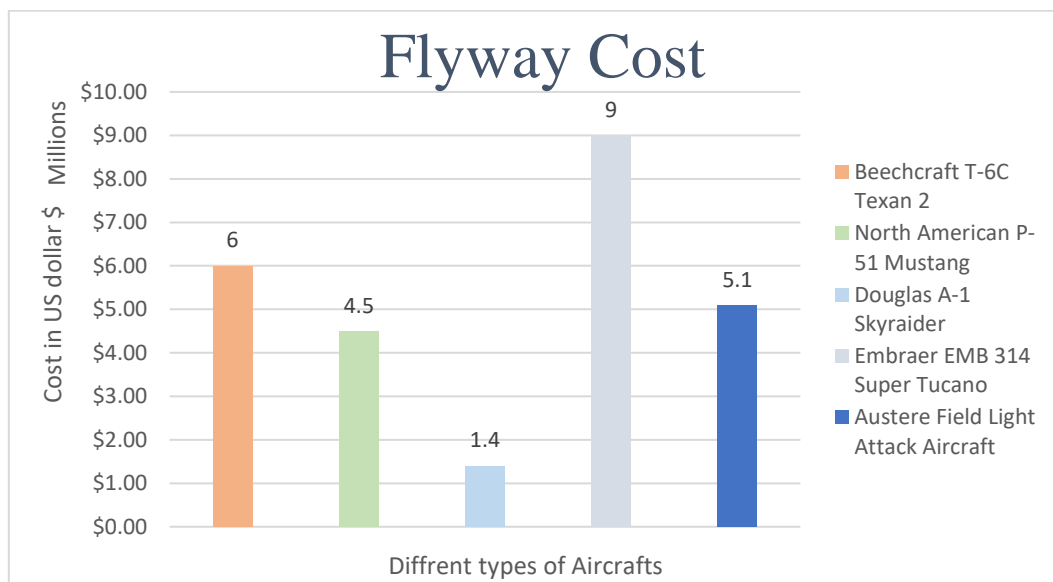


Figure 14.3: Flyway Cost

From figure (14.3) above the Austere Field aircraft flyway cost will be estimated as 5.1 million, which is way less than the Embraer EMB 314 Super Tucano and the Beechcraft T-6C Texan 2 aircrafts.





14.4.1. Development support

Development support shall be described as a repeated manufacturing effort to support engineering in the aircraft program development process. It is the cost of producing labor and material necessary to manufacture mock-ups, prototype parts, static test items and other hardware necessary for the design and development of airframe. In the production contract, the development support costs are related to the weight, speed, and quantities of aircraft of AMPR which resulted in the following equation:

$$D = 0.008325A^{0.873} \times S^{1.89} \times Q_D^{0.346} \quad (76)$$

Where:

The coefficient of correlation= 0.92 - The coefficient of variation = 43% - D: the development support cost,

A: AMPR weight (empty weight) - S: maximum speed, Q_D : the development quantity.

Using Equation (76) the following results are found:

Table 14.3: Development support cost.

Development support	
Beechcraft AT-6 wolverine	\$2,720,030.68
Beechcraft T-6c Texan 2	\$2,458,762.27
North American P-51 mustang	\$4,973,239.71
Douglas A-1 sky raider	\$4,079,250.05
Embraer EMB 314 super Tucano	\$3,288,761.96
Austere Field Light Attack Aircraft	\$3,504,008.93

Table (14.3) represent the development support cost for various light attack aircrafts in dollars. The average cost is found to help in finding the development support cost of the designed light attack aircraft which is reasonable and will make the aircraft more cost efficient.

14.4.2. Military Operating Cost

In the appraisal of FAA expenditure and regulation programs concerning time spent in air transport, aircraft variable operating costs are significant considerations. Aircraft operators are directly and indirectly impacted by the variable aircraft operating costs by higher or lower fares or taxes. The impact of FAA expenditure and regulatory programs, influencing fleet sizes, making aircraft more efficient or make aircraft out of service for longer periods may also be important to determine fixed aircraft costs.

Cost information is known as variable or fixed on air carriers and commercial aircraft. The cost varies proportionally to the use of the aircraft and that includes fuel and oil, repairs, and crew costs. In consultation with





the different armed forces branches, data are established on the operating costs of military aircraft. Data on table (14.4) is for different aircraft types and their cost for different costs category. The operational costs of aircraft include crew members and represent the various sizes of crews for a particular aircraft. (Cost-Estimating Relationships for Aircraft Airframes, 1972).

Table 14.4: Military operating costs per hour (Economic Values for Investment and Regulatory Decisions, 2021.)

Aircrafts Category	Crew	Operations and Maintenance	Asset Utilization	Total Operating Costs (Excluding Crew)	Total Operating Costs (Including Crew)	Total Costs Per Hour (Including Crew)
Turboprop	\$310	\$4,245	\$182	\$4,245	\$4,555	\$4,737
Piston	\$143	\$2,629	\$111	\$2,629	\$2,773	\$2,884
Austere Field Light Attack Aircraft	\$232	\$3,389	\$145	\$3,398	\$3,630	\$3,976

The military operating costs per hour table represent the costs of crew, operations and maintenance, assets utilization, operating costs excluding crew, operating costs including crew and the total per hour for different aircraft categories.

Table 14.5: Military operating costs per hour for various light attack aircrafts

Aircraft Category	Crew	Operations and Maintenance	Asset Utilization	Total Operating Costs (Excluding Crew)	Total Operating Costs (Including Crew)	Total Costs per Hour (Including Crew)
Beechcraft AT-6 wolverine	\$310.00	\$4,245.00	\$182.00	\$4,245.00	\$4,555.00	\$4,737.00
Beechcraft T-6C Texan 2	\$310.00	\$4,245.00	\$182.00	\$4,245.00	\$4,555.00	\$4,737.00
North American P-51 Mustang	\$143.00	\$2,629.00	\$111.00	\$2,629.00	\$2,773.00	\$2,884.00
Douglas a-1 Skyraider	\$143.00	\$2,629.00	\$111.00	\$2,629.00	\$2,773.00	\$2,884.00
Embraer EMB 314 Super Tucano	\$310.00	\$4,245.00	\$182.00	\$4,245.00	\$4,555.00	\$4,737.00
Austere Field Light Attack Aircraft	\$243.20	\$3,598.60	\$153.60	\$3,598.60	\$3,842.20	\$3,995.80

Using table (14.5) the military operating costs for the five competing aircrafts are found based on the engine type of each aircraft. The average cost helps determining the operating cost of the designed aircraft. The operating cost for the designed aircraft is cost efficient and economically viable.





14.4.3. Flight test operations

The cost factor of the flight test operations includes all flight-testing costs of the aircraft itself. It involves planning and data reduction, production assistance, equipment, spares, fuel, and oil, pay for pilots, leasing facilities and insurance. The armed services are not included in their flight test expenses. Table (14.6) shows the total flight test operations that is calculated using equation (77), for the five competitive aircrafts and for the Austere Field Light Attack Aircraft. Preliminary review of these data has shown that costs may not apply to most of the aircraft and that the inclusion of these costs would decrease the efficiency of the resulting estimated relationship. Costs related to flight testing related to altitude, the empty weight and number of test aircraft which resulted in the following equation:

$$F = 0.001244A^{1.16} \times S^{1.371} \times Q_D^{1.281} \quad (77)$$

Where:

Coefficient of correlation= 0.97 - Coefficient of variation= 34% - F: cost of flight operations - A: empty weight,

S: maximum speed - Q_D : number of developments.

Using equation (77) the following results are found:

Table 14.6: Flight test operations cost

Flight Test Operations	
Beechcraft AT-6 Wolverine	\$180,639.99
Beechcraft T-6C Texan 2	\$156,418.26
North American P-51 Mustang	\$320,829.63
Douglas A-1 Sky Raider	\$352,104.45
Embraer EMB 314 Super Tucano	\$227,989.60
Austere Field Light Attack Aircraft	\$247,596.39

Table (14.6) represent the Flight test operations cost for various light attack aircrafts in dollars. The Austere Field flight test operations cost is found to show that this aircraft will cost way less than the Douglas A-1 sky Raider and the North American P-51 Mustang which shows that the flight test operating cost will be good enough compared to the other competitors light attack aircrafts because it is affordable and cost efficient (Cost-Estimating Relationships for Aircraft Airframes, 1972).





14.5. Market Analysis

14.5.1. Regional Analysis

Regional analysis requires an appreciation of the similarities and differences between populations and locations. Functional and formal regions are included under the overall definition of the region. Formal regions display strong homogeneity compared to their distinctive characteristics. These characteristics can include prosperity, dominant land use or religious preferences. Functional areas can be based on distinctive characteristics, but that differ in strength and significance, that occur throughout the region (Dtuon, 2020).

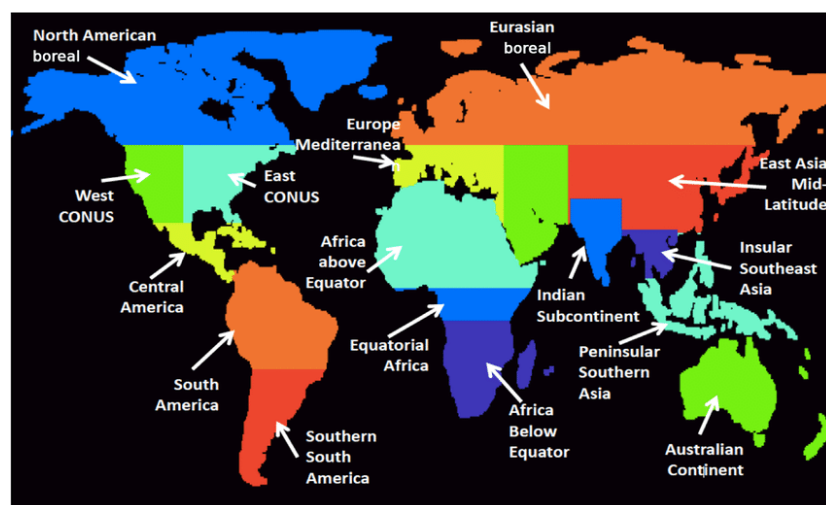


Figure 14.4: 17 parts of the world selected to conduct regional analysis (Anon., 2020)

14.5.2. Market research

Military aviation around the world is on the verge of growth and booming income collection, which goes beyond history every year. The global military aviation industry in North America and Europe is expected to undergo modest declines by 2014 due to proposed budget cuts. Through rising defense outlays from emerging economies such Asia, China, and some Middle East countries, is expected to push the industry forward in reverse.

It is expected that industrial sales will reach US\$ 60 billion, The worldwide military aviation industry includes both military and non-combat aviation producers and suppliers. In terms of both manufacturers and purchasers, the industry is highly concentrated and highly reliant on government spending. This market, dominated by defense costs for multi-year aviation programs partnered in various groupings of countries, is dominated by North America.

In North America and Europe, the global defense budget is around 80 percent. The global economic downturn, economic recession in the US, and the debt crisis across Europe are projected to have negative effects on defense





spending and to result in cuts in the defense budget. As a result, due to financial restrictions on most of the leading defense men, the allocation for military aircraft does not increase substantially during the forecast period (Market Research Reports, 2021).

14.5.3. Market segmentation

Asia pacific is the fastest growing military aviation market. North America has the largest military aviation market out of all continents. The compound annual growth rate is the return rate needed to increase an investment from its start to its final balance, provided that the benefit is reinvested at the end of each year of the lifetime of the investment which is found to be around 3% (Fernando, 2021).

The Austere Field Aircraft will be manufactured by General Dynamics, that is in Reston, Virginia, United States and also by Lockheed Martin, headquartered in Bethesda, Maryland. The General Dynamics and Corporation is an aerospace and military firm based in the United States, which is funded in 1899 (Wikipedia, 2021). The majority of Lockheed Martin's business as a worldwide security, innovation, and aerospace firm is with the United States Department of Defense and federal government agencies in the United States.

Furthermore, Sikorsky supplies military and rotary-wing aircraft to all five branches of the United States armed forces, as well as military services and commercial operators in 40 countries (Lockheedmartin, 2021). The first company will serve the west rejoin of the world and the Lockheed Martin will serve the middle east rejoin, because they already have a partnership with the United Arab Emirates (Lockheednartin, 2021).

14.6. Production Break-Even Point

The break-even point is known as when the total cost and total revenue become even. To calculate the break-even point, first the selling price is calculated in the next few lines by using equation (78).

$$\text{Selling price} = (100 + \text{profit}\%) \text{ cost price}/100 \quad (78)$$

$$\text{Selling price} = (100+9) 8,075,200/100 = \$8,802,000$$

Cost price of the aircraft = \$8,075,200.00, and the Profit% = 9%.

To calculate the break-even point by using equation (79).

$$\text{Break-even point} = \text{Fixed Costs} \div (\text{Sales price per unit} - \text{Variable costs per unit}) \quad (79)$$




Table 14.7: Assumption to calculate the Variable Cost

Fixed cost	50,000,000
Fuel cost per hour	64.58 \$/hr
Per Pilot	94.458 \$/hr
Flyway cost	5.1 million \$
Development support	\$3,504,008.93
Flight test operations	\$247,596.39

$$\text{Variable Costs} = 623 + 64.58 + 94.458 + 5,100,000 + 3,504,008.93 = \$8,604,790.968$$

$$\text{Break-even point} = 50,000,000 \div (8,802,000 - 8,604,790.968) = 253 \text{ units}$$

The cost break-even point occurs at 253 unit when sold for \$8,802,000 per aircraft as shown in figure (14.5).

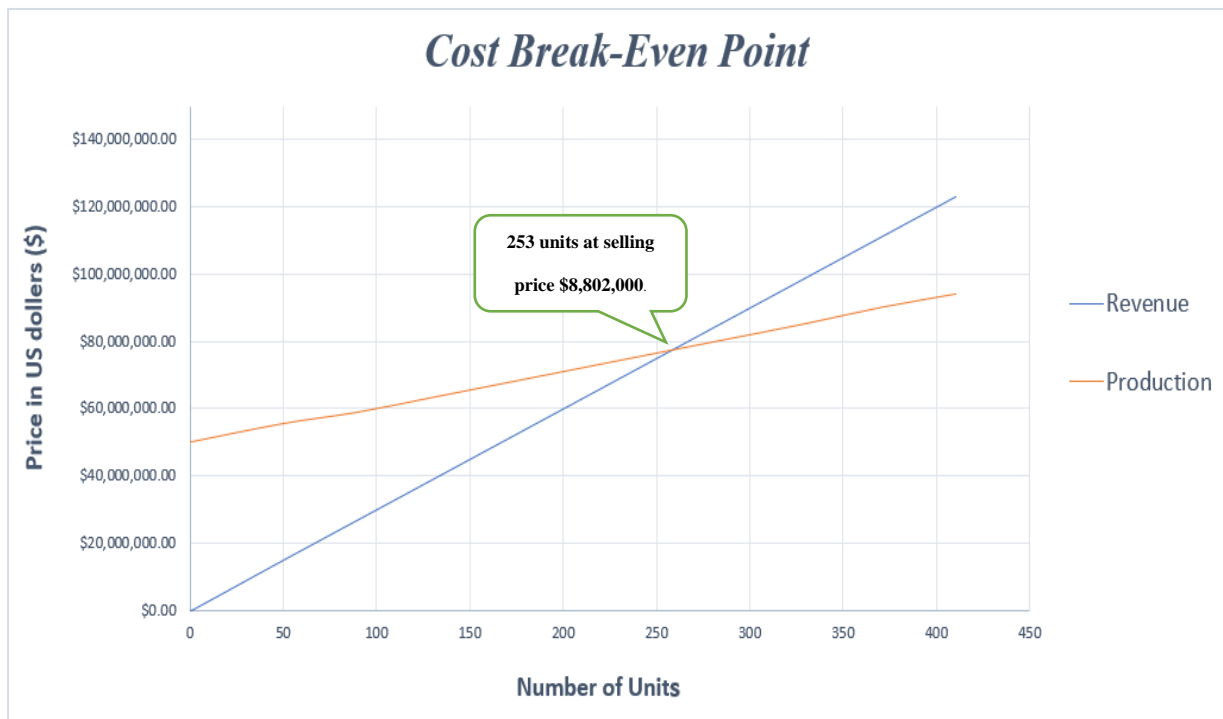

Figure 14.5: Cost Break-Even Point Graph

Figure (14.5) indicates a production plate of 450 units. The intersection of the production and the revenue slopes is the cost break-even point, and it is 253 units when each aircraft is sold \$8,802,000.





Chapter 15 Conclusion

This project was set out to design and compute all the general features and performance parameters of the Austere field light attack aircraft. All the aircraft components were designed using a CAD software called Solidworks. Five different military aircrafts characteristics and performance specifications were found to help in the design of the Austere field light attack aircraft.

The design and ferry mission profiles were sketched based on AIAA requirements. The design mission takeoff weight was evaluated as 11,500 lb and from the ferry mission the takeoff weight is found as 8,000 pounds. The most precise value for zero-lift drag coefficient were selected as 0.030 and 0.031 for both design and ferry mission.

Drag polar showed that when lift coefficient is equal to zero, the zero lift drag coefficient for method one is 0.03, whereas, in method two it is 0.0332. For method one and two, at the maximum lift coefficient, the C_D is at 0.167 and 0.170. The relation between CL^2 against CD showed that the gradient was same for both methods and is 18.692. From matching all sizing requirements, design point P at wing loading of 51 lb/ft² and power loading of 6.8 lbs/hp was selected because it provides optimum performance required. The maximum velocity of the aircraft was found as 480 ft/s while the rate of climb was found to be ≥ 300 ft/min for military climb sizing requirements.

The absolute ceiling was estimated to be 32,000 feet (10 km). The range calculated for the design mission is 1,062 nm at sea level conditions while the maximum range for the ferry mission is 1,164 nm. The total endurance for the design mission was found as 7.2 hours and for ferry mission it was calculated as 10.5 hours. The landing distance for the design mission was found as 1,840.7 ft and 1,835.6 ft for ferry mission.

From the V-N diagram the maximum positive lift capability of this airplane is 6.6 at 280.2 ft/s. The maneuvering speed V_A was calculated as 280.2 ft/s, and the stall speed V_S evaluated as 156.15 ft/s. The dive speed V_D was determined as 525 ft/s. The minimum velocity occurs at a velocity of 280.2 ft/s where the Austere field light attack aircraft is at maneuver stage.

From the carpet plot, the optimum point selected for the designed Austere light attack aircraft at 0.147 hp/lb power to weight ratio, and wing loading of 51 lb/ft² and 11,500 lb takeoff weight, this point provides suitable power loading with low weight and cost.

The designing phase was made to find the wing configuration and parameters. The $Cl_{max,r}$ and $Cl_{max,t}$ obtained from the airfoils selected are 2 and 1.7. The results of the flap geometry for landing and take-off show that the





wing with the high lift device (Flaps) can easily generate the required lift coefficient for landing. The material selected for the wing spar is composite materials, the ribs were selected to be titanium, and the flaps were selected as composite material.

The Austere field light attack aircraft has one vertical stabilizer and one horizontal stabilizer separated into two parts on the tapered tail portion of the fuselage, one on either side of the vertical stabilizer. Furthermore, for vertical tail configuration the symmetrical airfoil was selected as NACA 0015 because it provides improved stability and control. Carbon laminate and carbon sandwiches are the materials used in the empennage section.

The fuselage configuration was selected as a monocoque shell for the structural type of the aircraft. Using the appropriate calculations, the fuselage parameters, fineness ratio, and the fuselage dimensions were calculated and set. For the designed Austere field light attack aircraft, the skin and the frames of the fuselage will be made of an aluminum alloy while longerons and the stringers will be made of steel.

The best propulsion system option for the designed Austere field light attack aircraft was chosen as the PT6A-67F. The engine's maximum power output is 1700 shaft horsepower, and the number of blades was estimated to be four, the power loading for each blade was approximated as $4.5 \text{ hp}/\text{ft}^2$. The diameter of the propeller was calculated as 10.97 ft. Whereas, the retractable landing gear was selected having the tricycle landing gear type. The landing gear distances are 4.28 ft for the nose wheel and 12.85 ft for the main wheels. The main landing gear strut was chosen to be one under each wing, while the nose landing gear strut to be at the forward end of the fuselage.

The number of tires for the nose and main wheels was chosen as one tire per strut. The size of the main gear was set to be $23.3 \times 6.5 \text{ in.} \times \text{in.}$ and a tire pressure of 143 Psi. On the other hand, the size of the nose gear was set to be $17 \times 4.4 \text{ in.} \times \text{in.}$ and a tire pressure of 120 Psi. The oleo shock-strut was chosen as the shock absorbing system for the designed aircraft. The landing gear was selected to be made of a combination of steel and titanium alloys while the wheels are made of rubber. Mark 81 bomb, Mark 82 bomb, GBU-59 Enhanced Paveway II GPS/Laser-Guided bomb, T64 H.V.A.R rockets, and AN/M3 cannon are the selected weapons for the designed aircraft to match the payload weight of the aircraft.

The wing airfoils zero-lift pitching moment was found as -0.027, the wing zero-lift pitching moment was calculated as -0.0229, the wing's pitching moment curve slope was determined to be -0.104, the wing lift curve was calculated as 0.1212. Therefore, the wing was not longitudinally stable by itself because the zero-lift pitching moment is negative. Fuselage zero-lift pitching moment was calculated as -0.0218, the aerodynamic shift due to





fuselage was found as -0.1381 ft. The fuselage zero-lift pitching moment is negative, so it is unstable. The tail volume ratio was calculated, and its value is 0.8351, the tail area is 54.9 ft².

The wing mean aerodynamic chord was found as 5.82 ft. The tail lift curve slope was calculated as 0.114, and the aspect ratio was evaluated as 3.85. The aerodynamic center of the tail was located at 36.65 ft. The wing-fuselage curve slope was calculated as 0.121, the zero-lift pitching moment for wing-fuselage was found as -0.0465. The slope of the aircraft lift curve was determined as 0.136, the aircraft's zero-lift pitching moment was calculated to be 0.01841. The position of the center of gravity in units of the mean aerodynamic chord length was found as 0.146, whereas the aerodynamic center is at 0.647.

The trim angle of attack was found to be as 0.3 degree which is in the range of flight angle of attacks. Furthermore, the zero-lift pitching moment coefficient was calculated as 0.018, and it satisfies the Longitudinal stability condition because it is positive. The center of gravity for the total aircraft is at 15.7 ft from the nose, and the main landing gear location is at 15.81 ft. The location of center of gravity forward of the main landing gear makes the aircraft statically stable. The directional stability coefficient was calculated as 0.11 which has a positive slope with increasing the side slip angle, this proves that the designed aircraft is statically directionally stable because the result is positive.

The manufacturing process of the austere field light attack aircraft discussed the aircraft's production stages which are design, production, and assembly stages. The yearly fuel cost was calculated to be 141,428.43 \$. The cost per flight hour for Austere field light attack aircraft was estimated as 2,300\$ per operating flight hour. Yearly direct operating cost was calculated using the estimated value for cost per operating flight hour and the total flight hours every year as AIAA requirements which is 1,200 hours. The flyway cost was estimated as 5.1 million dollars. The development support cost was found as \$3,504,008.93. The flight test operations cost was found to have a better cost compared to the other competitors aircrafts. And finally, the cost break-even point occurs at 253 unit when sold for \$8,802,000 per aircraft.

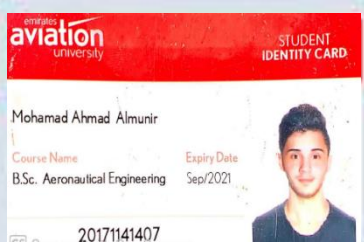
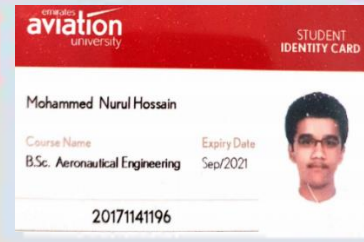
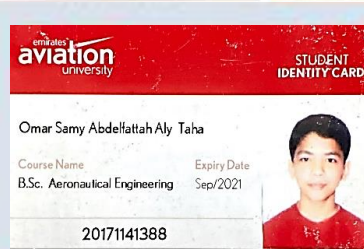
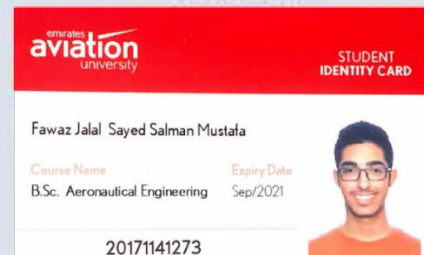




Work Distribution

GROUP MEMBERS

AUSTERE FIELD LIGHT ATTACK AIRCRAFT DESIGN

Team Leader

Name	Percentage (%)
Fawaz Jalal	14.3
Omar El Sardouk	14.3
Omar Samy	14.3
Mohamad Almunir	14.3
Al Shaima Saif	14.3
Abdelmoussaour Boukhatem	14.3
Mohammed Nurul	14.3
Total	100

All members contributed in the following chapters:

- ❖ Abstract
- ❖ Nomenclature and Acronyms
- ❖ Chapter 1: Introduction
- ❖ Chapter 2: Aircraft Features
- ❖ Chapter 3: Design of a Propeller-Driven Austere Field Light Attack Aircraft
- ❖ Chapter 4: Wing Configuration
- ❖ Chapter 5: Empennage Configuration
- ❖ Chapter 6: Fuselage Configuration
- ❖ Chapter 7: Propulsion System
- ❖ Chapter 8: Landing Gear Configuration
- ❖ Chapter 9: Cockpit Configuration
- ❖ Chapter 10: Weapons Carriage
- ❖ Chapter 11: Stability and Control Analysis
- ❖ Chapter 12: Model Development
- ❖ Chapter 13: Manufacturing Process of Austere field light attack aircraft
- ❖ Chapter 14: Cost and Market Analysis
- ❖ Chapter 15: Conclusion
- ❖ Gantt Chart
- ❖ References
- ❖ Appendices
- ❖ Compiling Report
- ❖ Presentation Slides
- ❖ Compiling Presentation





Gantt Chart for Aircraft Design 1

Austere Field Light Attack Aircraft

Aircraft Design 1

Group 1





Gantt Chart for Aircraft Design 2

Austere Field Light Attack Aircraft

Aircraft Design 2

Group 1





References

- [1] 2020. Empennage And Control Surfaces. [image] Available at:<<https://www.sciencedirect.com/topics/engineering/empennages>> [Accessed 23 November 2020].
- [2] 2020. Empennage And Control Surfaces. [image] Available at:<<https://www.sciencedirect.com/topics/engineering/empennages>> [Accessed 23 November 2020].
- [3] 2021. Experimental Aircraft Info. [online] Available at:<<https://www.experimentalaircraft.info/articles/secondarysystems.php#:~:text=Auxiliary%20or%20secondary%20systems%20help,loose%20control%20or%20crash%20immediately>> [Accessed 9 May 2021].
- [4] 2021. PT6A-67F SERIES TRAINING MANUAL. [ebook] Available at:<<https://mikeklochcfi.files.wordpress.com/2018/08/training-pt6a-67F-series.pdf>> [Accessed 3 April 2021].
- [5] Aerocontact.com. 2021. Auxiliary equipment in the virtual aviation and aerospace and space show. [online] Available at: <<https://www.aerocontact.com/en/virtual-aviation-exhibition/products/127-auxiliary-equipment#:~:text=Aircraft%20auxiliary%20systems%20cover%20a,or%20the%20flight%20resupply%20system>> [Accessed 9 May 2021].
- [6] Africair, Inc. 2020. Beechcraft AT-6 Wolverine - Africair, Inc.. [online] Available at:<<https://africair.com/aircraft/beechcraft-at-6-wolverine/>> [Accessed 15 December 2020].
- [7] Airfoiltools.com. 2021. NASA/LANGLEY MS(1)-0313 AIRFOIL (ms313-il). [online] Available at:<<http://airfoiltools.com/airfoil/details?airfoil=ms313-il>> [Accessed 11 March 2021].
- [8] Airfoiltools.com. 2021. NASA/LANGLEY MS(1)-0317 AIRFOIL (ms317-il). [online] Available at:<<http://airfoiltools.com/airfoil/details?airfoil=ms317-il>> [Accessed 11 March 2021].
- [9] Airforce Turbine Service (ATS). 2021. PT6A Engine Sales & Leasing | Airforce Turbine Service (ATS). [online] Available at: <<https://www.pt6a.aero/engine-sales-leasing/>> [Accessed 27 March 2021].
- [10] Anderson, J. D., 1999. Aircraft performance and design. s.l.:s.n
- [11] Army-technology.com. 2021. Beechcraft AT-6 Wolverine – a next-generation light attack aircraft. [online] Available at: <<https://www.army-technology.com/features/beechcraft-at-6-wolverine/#:~:text=The%20AT%2D6%20Wolverine%20aircraft,of%20the%20armed%20forces%20worldwide>> [Accessed 30 April 2021].
- [12] Army-technology.com. 2021. Beechcraft AT-6 Wolverine – a next-generation light attack aircraft. [online] Available at:<<https://www.army-technology.com/features/beechcraft-at-6-wolverine/#:~:text=The%20AT%2D6%20Wolverine%20aircraft,of%20the%20armed%20forces%20worldwide>> [Accessed 30 April 2021].
- [13] armytrainingsupport. (2020, December 2). Retrieved from Mk-82 GP Bomb:
http://armytrainingsupport.com/index.php?main_page=product_info&products_id=22716





- [14] Aviation Environmental Impacts. (2020, December 16). Retrieved from
EASA:<https://www.easa.europa.eu/eaeer/climate-change/aviation-environmental-impacts>
- [15] Aviation Stack Exchange. n.d. What are the differences in aircraft performance between tractor and pusher propeller designs?. [online] Available at: <<https://aviation.stackexchange.com/questions/605/what-are-the-differences-in-aircraft-performance-between-tractor-and-pusher-prop>> [Accessed 28 March 2021].
- [16] AviationChief.Com. 2021. Operating Flight Strength (V-g / V-n Diagrams). [online] Available at:
<<http://www.aviationchief.com/operating-flight-strength-v-g--v-n-diagrams.html>> [Accessed 26 March 2021].
- [17] AviationChief.Com. 2021. Operating Flight Strength (V-g / V-n Diagrams). [online] Available at:
<<http://www.aviationchief.com/operating-flight-strength-v-g--v-n-diagrams.html>> [Accessed 26 March 2021]
- [18] Avstop.com. n.d. Lateral Stability. [online] Available
at:<<http://avstop.com/ac/flighttrainghandbook/lateralstability.html>> [Accessed 5 May 2021].
- [19] Bartlett, A., 2020. Aircraft Tailplane Stalls - Aviation Safety. [online] Aviation Safety. Available at:
<<https://www.aviationsafetymagazine.com/features/aircraft-tailplane-stalls/>> [Accessed 23 November 2020].
- [20] BIBLIOGRAPHY AN/M3. (2014, March 14). Retrieved from war
thunder:<https://forum.warthunder.com/index.php?/topic/115569-anm3-38-m3/>
- [21] BIBLIOGRAPHY Notebook, C., n.d. Landing Gear. [Online] Available
at:<https://www.cfinotebook.net/notebook/operation-of-aircraft-systems/landing-gear> [Accessed 26 3 2021].
- [22] Cameron, B., n.d. Chapter 90 - Aerospace Manufacture and Maintenance. [online] Ilocis.org. Available at:
<<http://www.iloci.org/documents/chpt90e.htm>> [Accessed 3 May 2021].
- [23] Cavagnaro, C., 2019. Performance: The perfect aircraft (for the mission). [online] Aopa.org. Available at:
<<https://www.aopa.org/news-and-media/all-news/2019/september/pilot/performance-the-perfect-aircraft>> [Accessed 26 March 2021].
- [24] Climate change: Should you fly, drive or take the train? (2019, August 23). Retrieved from BBC NEWS:
<https://www.bbc.com/news/science-environment-49349566>
- [25] Cmcelectronics.ca. 2021. Cockpit 4000 NexGen. [online] Available at:
<<https://cmcelectronics.ca/productsservices/cockpitsystemsintegration/cockpit4000nexgen.aspx>> [Accessed 26 March 2021].
- [26] Cutler, C., 2020. The Four Steps Of Spin Recovery, Explained. [online] Boldmethod.com. Available at:
<<https://www.boldmethod.com/learn-to-fly/maneuvers/the-four-steps-of-spin-recovery-explained-pare-fly-it-safely/>>
[Accessed 23 November 2020].
- [27] E.G. Tulapurkara, 2021. [online] Nptel.ac.in. Available
at:<[https://nptel.ac.in/content/storage2/courses/101106035/035_Chapter%206_L26_\(04-10- 2013\).pdf](https://nptel.ac.in/content/storage2/courses/101106035/035_Chapter%206_L26_(04-10- 2013).pdf)> [Accessed 11 April 2021].



- [28] Easa.europa.eu. 2019. TYPE-CERTIFICATE DATA SHEET. [online] Available at: <https://www.easa.europa.eu/sites/default/files/dfu/PT6A_67%20Series%20Issue%2005_20191011.pdf> [Accessed 22 March 2021].
- [29] ECA, 2020. Designing Buildings Wiki. [Online] Available at:https://www.designingbuildings.co.uk/wiki/Electrical_system#:~:text=An%20electrical%20system%2C%20within%20the,that%20consume%20the%20electrical%20energy. [Accessed 14 April 2021].
- [30] En.m.wikipedia.org. n.d. Martin-Baker Mk.5 - Wikipedia. [online] Available at:<https://en.m.wikipedia.org/wiki/Martin-Baker_Mk.5> [Accessed 13 April 2021].
- [31] En.wikipedia.org. 2021. Aircraft engine performance - Wikipedia. [online] Available at: <https://en.wikipedia.org/wiki/Aircraft_engine_performance#Altitude> [Accessed 30 April 2021].
- [32] En.wikipedia.org. 2021. Douglas A-1 Skyraider - Wikipedia. [online] Available at:<https://en.wikipedia.org/wiki/Douglas_A-1_Skyraider> [Accessed 11 May 2021].
- [33] En.wikipedia.org. 2021. North American P-51 Mustang - Wikipedia. [online] Available at:<https://en.wikipedia.org/wiki/North_American_P-51_Mustang> [Accessed 30 April 2021].
- [34] En.wikipedia.org. 2021. North American P-51 Mustang - Wikipedia. [online] Available at: <https://en.wikipedia.org/wiki/North_American_P-51_Mustang> [Accessed 30 April 2021].
- [35] En.wikipedia.org. 2021. *Dihedral(aeronautics)-Wikipedia*. [online] Available at:<[https://en.wikipedia.org/wiki/Dihedral_\(aeronautics\)#:~:text=In%20aeronautics%2C%20dihedral%20is%20the,of%20a%20fixed%2Dwing%20aircraft.](https://en.wikipedia.org/wiki/Dihedral_(aeronautics)#:~:text=In%20aeronautics%2C%20dihedral%20is%20the,of%20a%20fixed%2Dwing%20aircraft.)> [Accessed 1 June 2021].
- [36] En.wikipedia.org. 2021. *Swept-wing-Wikipedia*. [online] Available at:<https://en.wikipedia.org/wiki/Swept_wing#:~:text=Typical%20sweep%20angles%20vary%20from,and%20other%20high%2Dspeed%20designs.> [Accessed 1 June 2021].
- [37] Fas.org. n.d. Ejection Seats. [online] Available at: <<https://fas.org/man/dod-101/sys/ac/equip/eject.htm>> [Accessed 13 April 2021].
- [38] Fi-aeroweb.com. 2021. T-6 Texan II | Info, Forecast, Budget/Costs. [online] Available at: <<http://www.fiaeroweb.com/Defense/T-6-Texan.html>> [Accessed 11 May 2021].
- [39] FlightLiteracy, 2021. Turboprop Airplane Electrical Systems. [Online] Available at:<https://www.flighthliteracy.com/turboprop-airplane-electrical-systems/> [Accessed 14 april 2021].
- [40] Fuselage. (2020, December 2). Retrieved from wikipedia: <https://en.wikipedia.org/wiki/Fuselage>
- [41] Güzelbey, İ., Eraslan, Y. and Doğru, M., 2019. Effects of Taper Ratio on Aircraft Wing Aerodynamic Parameters: A Comparative Study. European Mechanical Science, 3(1), pp.18–23.
- [42] High Velocity Aircraft Rocket. (2020, December 2). Retrieved from wikipedia: https://en.wikipedia.org/wiki/High_Velocity_Aircraft_Rocket
- [43] HVAR. (2020, December 2). Retrieved from war thunder wiki: <https://wiki.warthunder.com/HVAR>





- [44] Information on the environmental impact of aviation. (2020, December 16). Retrieved from Civil Aviation Authority: <https://www.caa.co.uk/consumers/environment/information-on-the-environmental-impact-of-aviation/>
- [45] Kasper, J., 2020. Pratt & Whitney Canada PT6A Turboprop Engine | PowerWeb. [online] Fi-powerweb.com. Available at: <<http://www.fi-powerweb.com/Engine/PW-CANADA-PT6A.html>> [Accessed 23 March 2021].
- [46] Lockheedmartin, 2021. Products. [Online] Available at: <https://www.lockheedmartin.com/en-us/products.html> [Accessed 2 June 2021].
- [47] Lockheedmartin, 2021. Lockheed Martin in United Arab Emirates. [Online] Available at: <https://www.lockheedmartin.com/en-ae/> [Accessed 2 June 2021].
- [48] M3 (20 mm). (2020, December 2). Retrieved from war thunder wiki: [https://wiki.warthunder.com/M3_\(20_mm\)](https://wiki.warthunder.com/M3_(20_mm))
- [49] Mark 81 bomb. (2020, December 2). Retrieved from Wikipedia: https://en.wikipedia.org/wiki/Mark_81_bomb
- [50] Mark 82 bomb. (2020, December 2). Retrieved from wikipedia: https://en.wikipedia.org/wiki/Mark_82_bomb
- [51] Mikeklochcfi.files.wordpress.com. 2007. [online] Available at:<<https://mikeklochcfi.files.wordpress.com/2018/08/training-pt6a-60-series.pdf>> [Accessed 13 April 2021].
- [52] Military Wiki. 2021. Embraer EMB-314 Super Tucano. [online] Available at:<https://military.wikia.org/wiki/Embraer_EMB-314_Super_Tucano> [Accessed 30 April 2021].
- [53] Military Wiki. 2021. Embraer EMB-314 Super Tucano. [online] Available at:<https://military.wikia.org/wiki/Embraer_EMB-314_Super_Tucano> [Accessed 30 April 2021].
- [54] Nelson, R., 2010. Flight Stability And Automatic Control. Chennai: McGraw-Hill Education (India) Private Limited, pp.21-136
- [55] Overall, M., 2021. Book: EMB-314 Super Tucano - Brazil's Turboprop Success Story Continues. [online] LAAHS. Available at: <<https://www.laahs.com/emb-314-super-tucano/>> [Accessed 11 May 2021].
- [56] OxfordSaudia. 2020. *Aircraft Construction: How are airplanes made? / OxfordSaudia Flight Academy*. [online] Available at: <<https://www.oxfordsaudia.com/en/blog/aircraft-construction-how-are-airplanes-made/>> [Accessed 12 May 2021].
- [57] Parameters: A Comparative Study. European Mechanical Science, 3(1), pp.18-23.
- [58] Paveway. (2020, December 2). Retrieved from wikipedia: <https://en.wikipedia.org/wiki/Paveway#Variants>
- [59] Perry, D., 2021. RIAT: Wolverine hopes for US Air Force certification boost. [online] Flight Global. Available at: <<https://www.flightglobal.com/fixed-wing/riat-wolverine-hopes-for-us-air-force-certification-boost/133619.article>> [Accessed 11 May 2021].
- [60] PwC. n.d. Cost-effective PT6A engines overhaul solutions - Pratt & Whitney. [online] Available at:<https://www.pwc.ca/smart-pt6a?utm_campaign=pt6a-smart&utm_source=google&utm_medium=cpc&utm_term=%2Bpt6a&gclid=Cj0KCQjw4cOEBhDMARIsAA3XDRi7dVa0XthkrSYXpcHvW9cBpbhpcwUWD9SzElV11LvDpGuZqK-MJIYaAIEqEALw_wcB>[Accessed 4 May 2021].
- [61] Richardson, D., 2000. OBOGS INTEGRATION INTO A TURBO-PROP TRAINER AIRCRAFT. [online] Icas.org. Available at: <http://www.icas.org/ICAS_ARCHIVE/ICAS2000/PAPERS/ICA0614.PDF> [Accessed 13 April 2021].





- [62] Romeorim.com. 2021. [online] Available at: <<https://romeorim.com/what-are-composites/composites-vs-aluminum/>> [Accessed 1 June 2021].
- [63] Roskam, J., 2003. Airplane Design. Ottawa, Kan.: Roskam Aviation and Engineering Corp.
- [64] SAMANCTA. (2020, December 16). Safe working in Airports (Health and safety). Retrieved from EuropeanCommission:https://ec.europa.eu/taxation_customs/dds2/SAMANCTA/EN/Safety/WorkInAirports_EN.htm
- [65] Sandwiches, L., 2021. Laminates & Sandwiches. [online] Oxyblack. Available at: <<https://www.oxyblack.com/index.php/en/composites/laminates-sandwiches>> [Accessed 1 June 2021].
- [66] Schiff, B., 2007. North American Aviation P-51D Mustang. [online] Aopa.org. Available at: <<https://www.aopa.org/news-and-media/all-news/2007/august/pilot/north-american-aviation-p-51d-mustang>> [Accessed 5 March 2021].
- [67] Science Learning Hub. 2011. Wing aspect ratios. [online] Available at: < HYPERLINK "https://www.sciencelearn.org.nz/images/704-wing-aspect-ratios%3E" \t "_blank" \o "https://www.sciencelearn.org.nz/images/704-wing-aspect-ratios"> https://www.sciencelearn.org.nz/images/704-wing-aspect-ratios> [Accessed 5 March 2021].
- [68] semi-monocoque. (2020, December 2). Retrieved from wikipedia: <https://en.wikipedia.org/wiki/Semi-monocoque#:~:text=The%20term%20semi%2Dmonocoque%20refers,car%20bodies%20and%20motorcycle%20frame>.
- [69] Structures, W., 2021. Wings - Aircraft Structures. [online] Aircraftsystemstech.com. Available at: <<https://www.aircraftsystemstech.com/p/wings-wing-configurations-wings-are.html>> [Accessed 1 June 2021].
- [70] ThoughtCo. 2021. World War II: North American P-51 Mustang. [online] Available at:<<https://www.thoughtco.com/p-51-mustang-2361528>> [Accessed 11 May 2021].
- [71] Torenbeek, E., 2013. Advanced Aircraft Design. Wiley.
- [72] Transport and Environment. (2020, December 16). Retrieved from AISBL: <https://www.transportenvironment.org/file/aviation-emissions-eupng-0>
- [73] Wainfan, B., 2020. Control Surface Design: Keeping Them Balanced. [online] AVweb. Available at: <<https://www.avweb.com/flight-safety/control-surface-design-keeping-them-balanced/>> [Accessed 23 November 2020].
- [74] Weapons Integration. (2020, December 2). Retrieved from iomax: <https://iomax.net/archangel/archangel-strike-platform/weapons-integration/>
- [75] Wikipedia, 2021. General Dynamics. [Online] Available at: https://en.wikipedia.org/wiki/General_Dynamics#F-16_success





Appendix A

Appendix A.1: Suggested Fuel-Fractions for Several Mission Phases (Roskam, 2003)

Mission Phase No. (See Fig. 2.1)	1	2	3	4	7	8	
Airplane Type:		Engine Start, Warm-up	Taxi	Take-off	Climb	Descent	Landing Taxi, Shutdown
1. Homebuilt	0.998	0.998	0.998	0.995	0.995	0.995	
2. Single Engine	0.995	0.997	0.998	0.992	0.993	0.993	
3. Twin Engine	0.992	0.996	0.996	0.990	0.992	0.992	
4. Agricultural	0.996	0.995	0.996	0.998	0.999	0.998	
5. Business Jets	0.990	0.995	0.995	0.980	0.990	0.992	
6. Regional TBP's	0.990	0.995	0.995	0.985	0.985	0.995	
7. Transport Jets	0.990	0.990	0.995	0.980	0.990	0.992	
8. Military Trainers	0.990	0.990	0.990	0.980	0.990	0.995	
9. Fighters	0.990	0.990	0.990	0.96-0.90	0.990	0.995	
10. Mil.Patrol, Bomb. Transport	0.990	0.990	0.995	0.980	0.990	0.992	
11. Flying Boats, Amphibious, Float Airplanes	0.992	0.990	0.996	0.985	0.990	0.990	
12. Supersonic Cruise	0.990	0.995	0.995	0.92-0.87	0.985	0.992	

Notes: 1. The numbers in this table are based on experience or on judgment.
 2. There is no substitute for common sense! If and when common sense so dictates, the reader should substitute other values for the fractions suggested in this table.

 Appendix A.2: Suggested Values for L/D, C_j, C_p, η_p and for C_p For Several Mission Phases (Roskam, 2003)

Mission Phase No. (See Fig. 2.1)	Cruise				Loiter			
	L/D	c _j	c _p	η _p	L/D	c _j	c _p	η _p
Airplane Type								
1. Homebuilt	8-10*		0.6-0.8	0.7	10-12		0.5-0.7	0.6
2. Single Engine	8-10		0.5-0.7	0.8	10-12		0.5-0.7	0.7
3. Twin Engine	8-10		0.5-0.7	0.82	9-11		0.5-0.7	0.72
4. Agricultural	5-7		0.5-0.7	0.82	8-10		0.5-0.7	0.72
5. Business Jets	10-12	0.5-0.9			12-14	0.4-0.6		
6. Regional TBP's	11-13		0.4-0.6	0.85	14-16		0.5-0.7	0.77
7. Transport Jets	13-15	0.5-0.9			14-18	0.4-0.6		
8. Military Trainers	8-10	0.5-1.0	0.4-0.6	0.82	10-14	0.4-0.6	0.5-0.7	0.77
9. Fighters	4-7	0.6-1.4	0.5-0.7	0.82	6-9	0.6-0.8	0.5-0.7	0.77
10. Mil.Patrol, Bomb. Transport	13-15	0.5-0.9	0.4-0.7	0.82	14-18	0.4-0.6	0.5-0.7	0.77
11. Flying Boats, Amphibious, Float Airplanes	10-12	0.5-0.9	0.5-0.7	0.82	13-15	0.4-0.6	0.5-0.7	0.77
12. Supersonic Cruise	4-6	0.7-1.5			7-9	0.6-0.8		




Appendix A.3: Regression Line Constants A and B (Roskam, 2003)

Airplane Type	A	B	Airplane Type	A	B
1. Homebuiltts Pers. fun and transportation	0.3411	0.9519	8. Military Trainers Jets	0.6632	0.8640
Scaled Fighters	0.5542	0.8654	Turboprops	-1.4041	1.4660
Composites	0.8222	0.8050	Turboprops without No.2	0.1677	0.9978
2. Single Engine Propeller Driven	-0.1440	1.1162	Piston/Props	0.5627	0.8761
3. Twin Engine Propeller Driven	0.0966	1.0298	9. Fighters Jets (+ ext. load)	0.5091	0.9505
Composites	0.1130	1.0403	Jets (clean)	0.1362	1.0116
4. Agricultural	-0.4398	1.1946	Turboprops (+ ext. load)	0.2705	0.9830
5. Business Jets	0.2678	0.9979	10. Mil. Patrol, Bomb and Transport Jets	-0.2009	1.1037
6. Regional TBP	0.3774	0.9647	Turboprops	-0.4179	1.1446
7. Transport Jets	0.0833	1.0383	11. Flying Boats, Amphibious and Float Airplanes	0.1703	1.0083
			12. Supersonic Cruise	0.4221	0.9876

Appendix A.4: Typical Values for Maximum Lift Coefficient (Roskam, 2003)

Airplane Type	$C_{L_{max}}$	$C_{L_{max,TO}}$	$C_{L_{max,L}}$
1. Homebuiltts	1.2 - 1.8	1.2 - 1.8	1.2 - 2.0*
2. Single Engine Propeller Driven	1.3 - 1.9	1.3 - 1.9	1.6 - 2.3
3. Twin Engine Propeller Driven	1.2 - 1.8	1.4 - 2.0	1.6 - 2.5
4. Agricultural	1.3 - 1.9	1.3 - 1.9	1.3 - 1.9
5. Business Jets	1.4 - 1.8	1.6 - 2.2	1.6 - 2.6
6. Regional TBP	1.5 - 1.9	1.7 - 2.1	1.9 - 3.3
7. Transport Jets	1.2 - 1.8	1.6 - 2.2	1.8 - 2.8
8. Military Trainers	1.2 - 1.8	1.4 - 2.0	1.6 - 2.2
9. Fighters	1.2 - 1.8	1.4 - 2.0	1.6 - 2.6
10. Mil. Patrol, Bomb and Transports	1.2 - 1.8	1.6 - 2.2	1.8 - 3.0
11. Flying Boats, Amphibious and Float Airplanes	1.2 - 1.8	1.6 - 2.2	1.8 - 3.4
12. Supersonic Cruise Airplanes	1.2 - 1.8	1.6 - 2.0	1.8 - 2.2



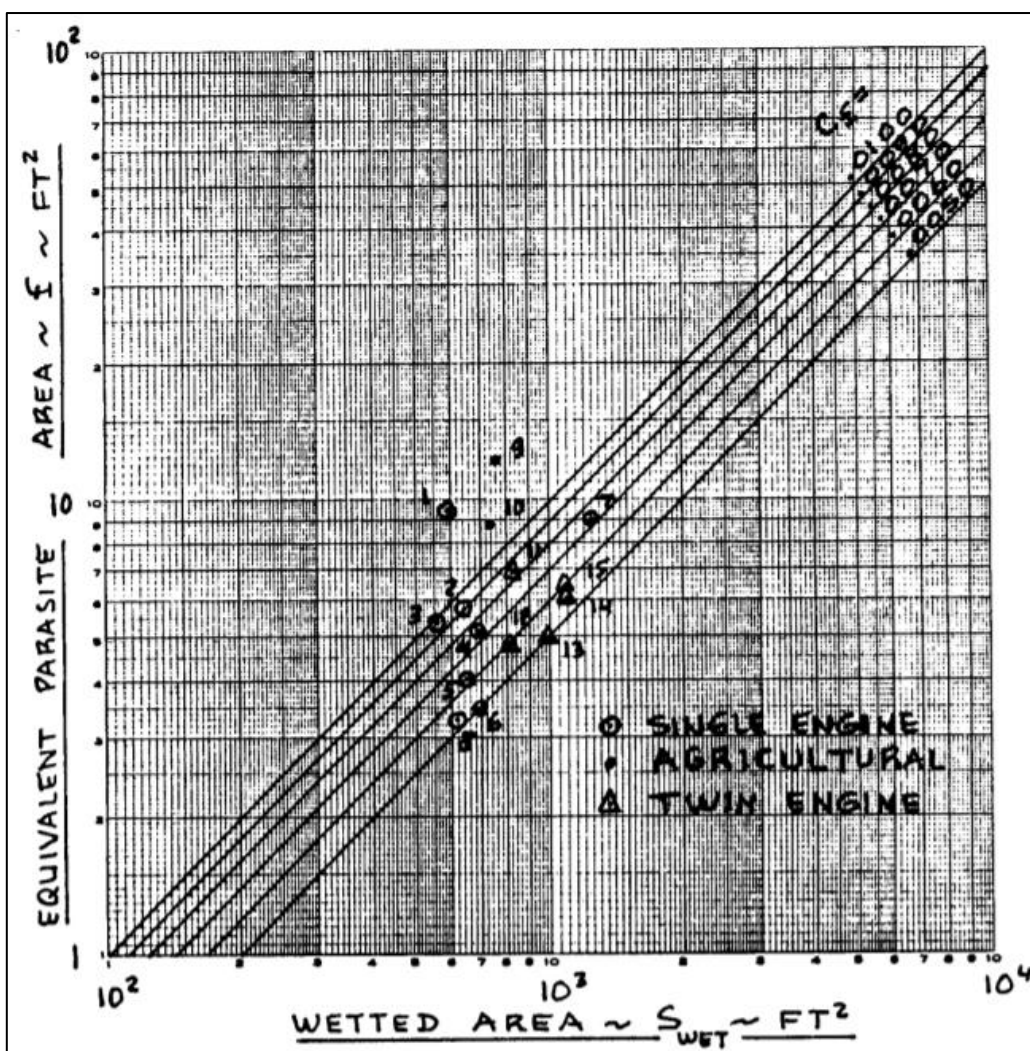


Appendix A.5: Wing Loading from Historical Trends (Roskam, 2003)

Historical trends	Typical takeoff W/S	
	lb/ft ²	{kg/m ² }
Sailplane	6	{30}
Homebuilt	11	{54}
General aviation—single engine	17	{83}
General aviation—twin engine	26	{127}
Twin turboprop	40	{195}
Jet trainer	50	{244}
Jet fighter	70	{342}
Jet transport/bomber	120	{586}

^aIn mks units, multiply metric values times $g = 9.807$ to use in equations.

Appendix A.6: Effect of Equivalent Skin Friction on Parasite and Wetted Areas (Roskam, 2003)




Appendix A.7: Correlation Coefficients for Parasite Area Versus Wetted Area (Roskam, 2003)

Equivalent Skin Friction Coefficient, c_f	a	b
0.0090	-2.0458	1.0000
0.0080	-2.0969	1.0000
0.0070	-2.1549	1.0000
0.0060	-2.2218	1.0000
0.0050	-2.3010	1.0000
0.0040	-2.3979	1.0000
0.0030	-2.5229	1.0000
0.0020	-2.6990	1.0000

Appendix A.8: First Estimates for ΔC_D and 'e' With Flaps and Gear Down (Roskam, 2003)

Configuration	ΔC_{D_0}	e
Clean	0	0.80 - 0.85
Take-off flaps	0.010 - 0.020	0.75 - 0.80
Landing Flaps	0.055 - 0.075	0.70 - 0.75
Landing Gear	0.015 - 0.025	no effect

Appendix A.9: Regression Line Coefficients for Take-off Weight Versus Wetted Area (Roskam, 2003)

Airplane Type	c	d
1. Homebuilt	1.2362	0.4319
2. Single Engine Propeller Driven	1.0892	0.5147
3. Twin Engine Propeller Driven	0.8635	0.5632
4. Agricultural	1.0447	0.5326
5. Business Jets	0.2263	0.6977
6. Regional Turboprops	-0.0866	0.8099
7. Transport Jets	0.0199	0.7531
8. Military Trainers*	0.8565	0.5423
9. Fighters*	-0.1289	0.7506
10. Mil. Patrol, Bomb and Transport	0.1628	0.7316
11. Flying Boats, Amph. and Float	0.6295	0.6708
12. Supersonic Cruise Airplanes	-1.1868	0.9609

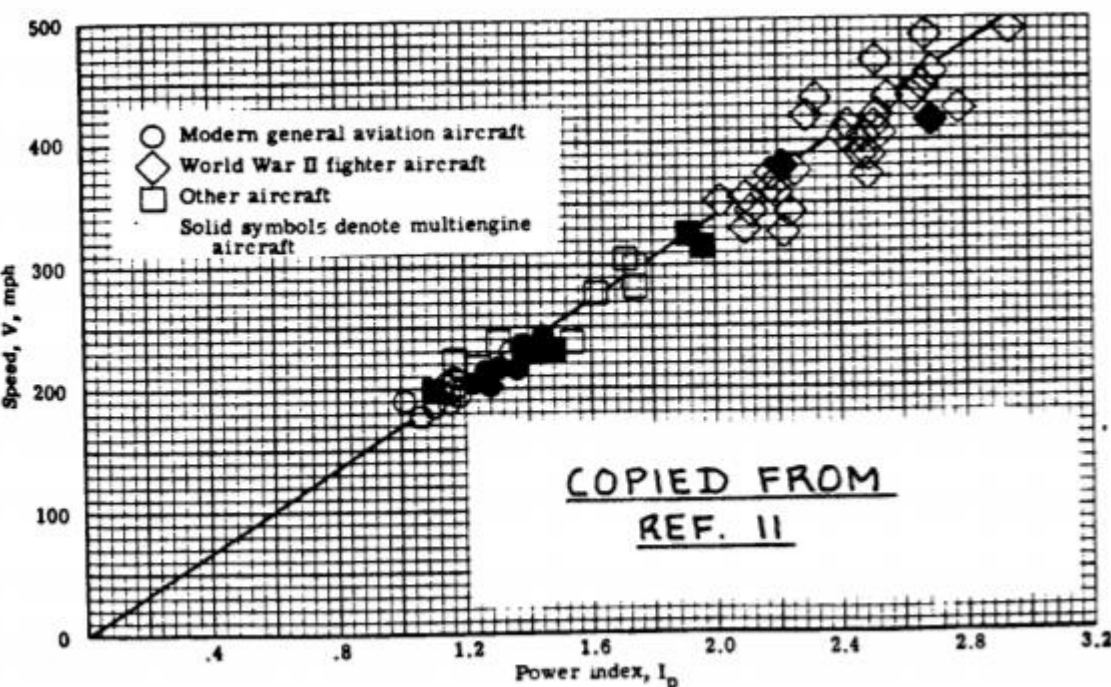




Appendix A.10: Definition of Airplane Ceilings (Roskam, 2003)

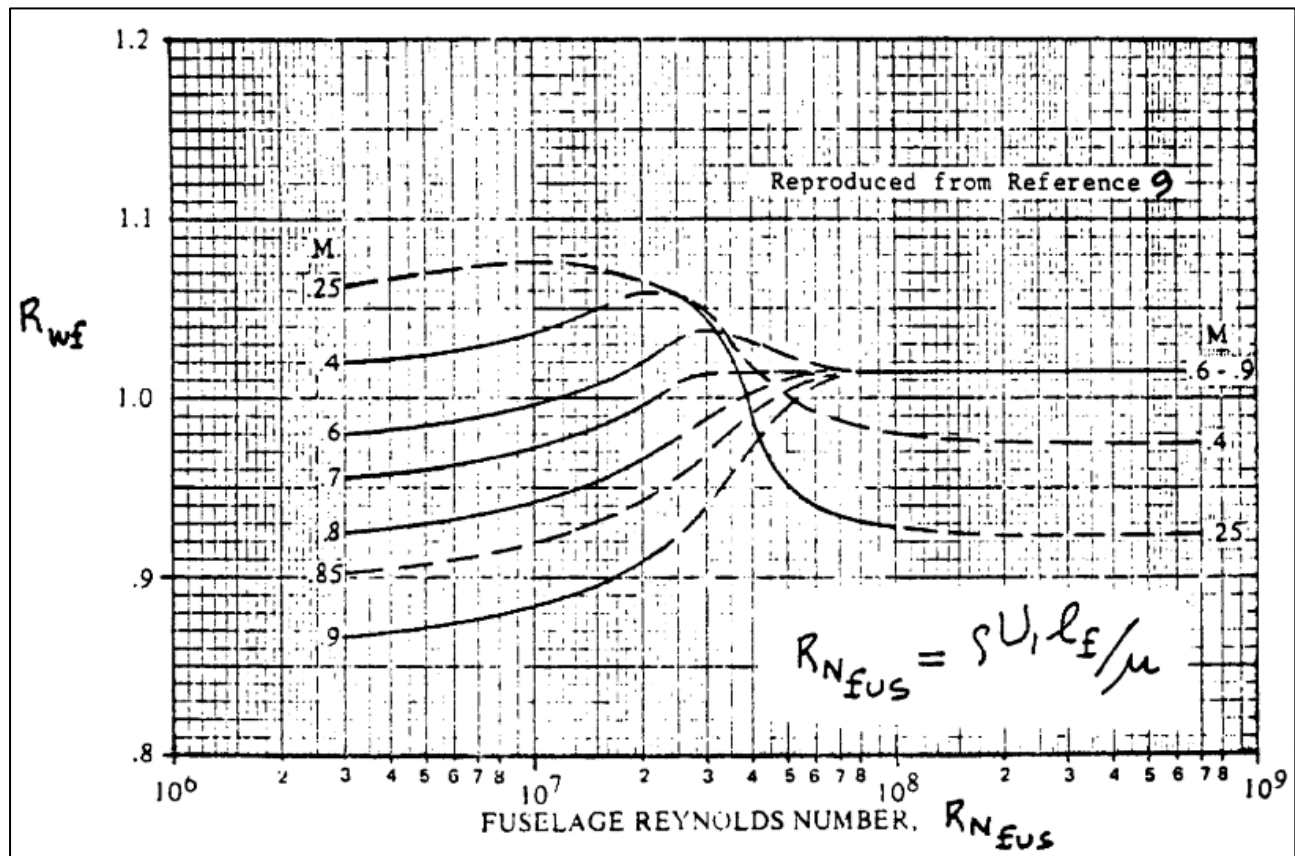
Ceiling Type	Minimum Required Climb Rate
Absolute ceiling	0 fpm
Service ceiling	
Commercial/Piston-propeller	100 fpm
Commercial/jet	500 fpm
Military at maximum power	100 fpm
Combat ceiling	
Military/Subsonic/maximum power	500 fpm at M<1
Military/Supersonic/maximum power	1,000 fpm at M>1
Cruise ceiling	
Military/Subsonic/max. cont. power	300 fpm at M<1
Military/Supersonic/max. cont. power	1,000 fpm at M>1

Appendix A.11: Correlation of Airplane Speed with Power Index for Retractable Gear, Cantilevered Wing (Roskam, 2003)

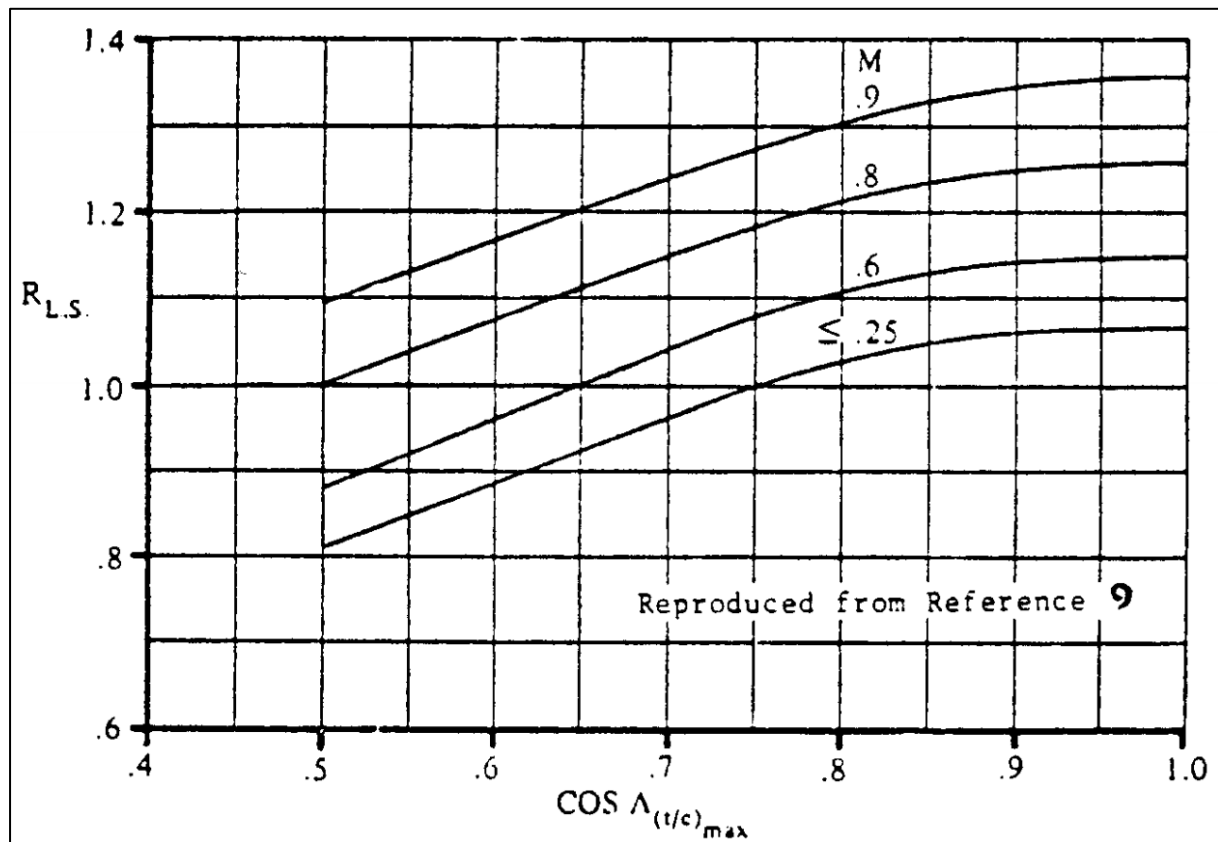


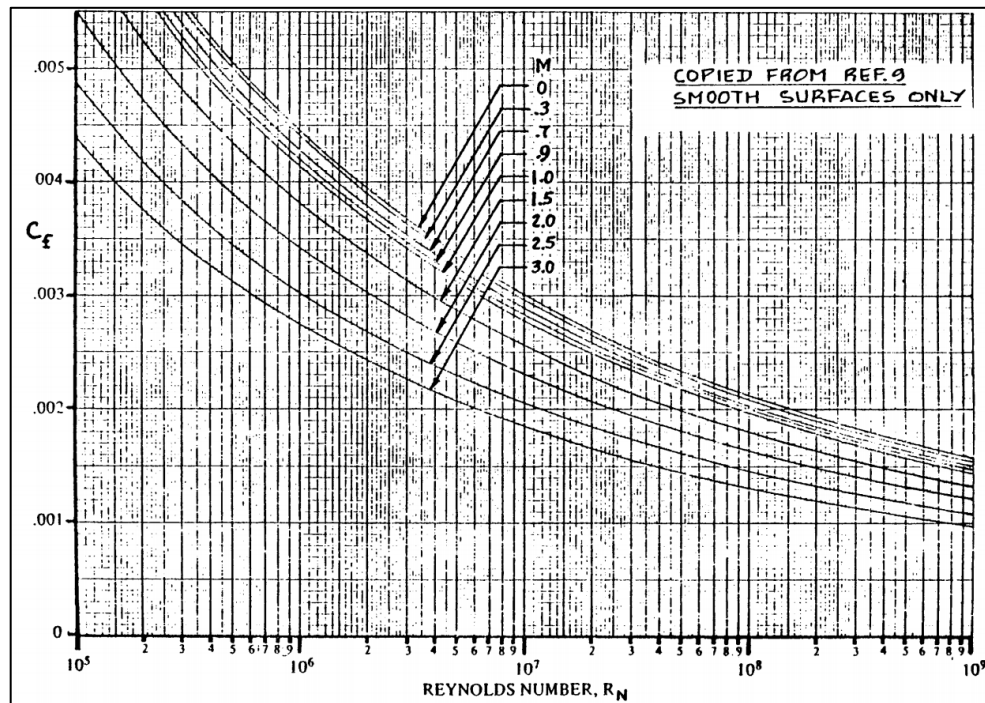
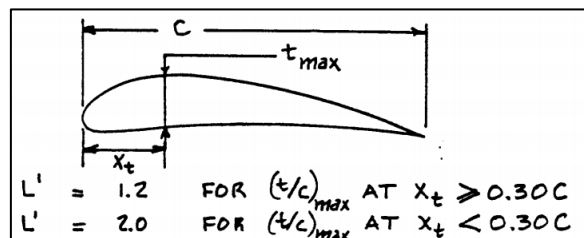
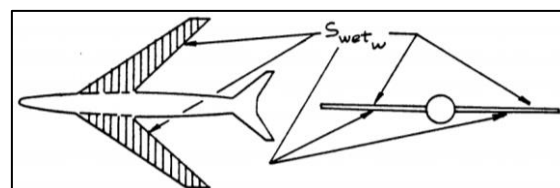
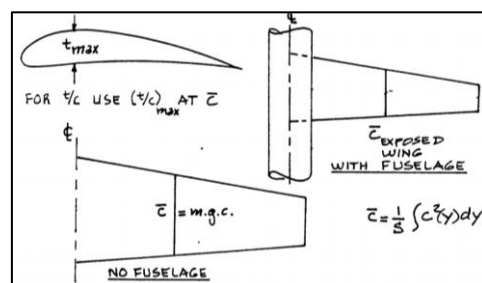


Appendix A.12: Wing Fuselage Interference Factor (Roskam, 2003)



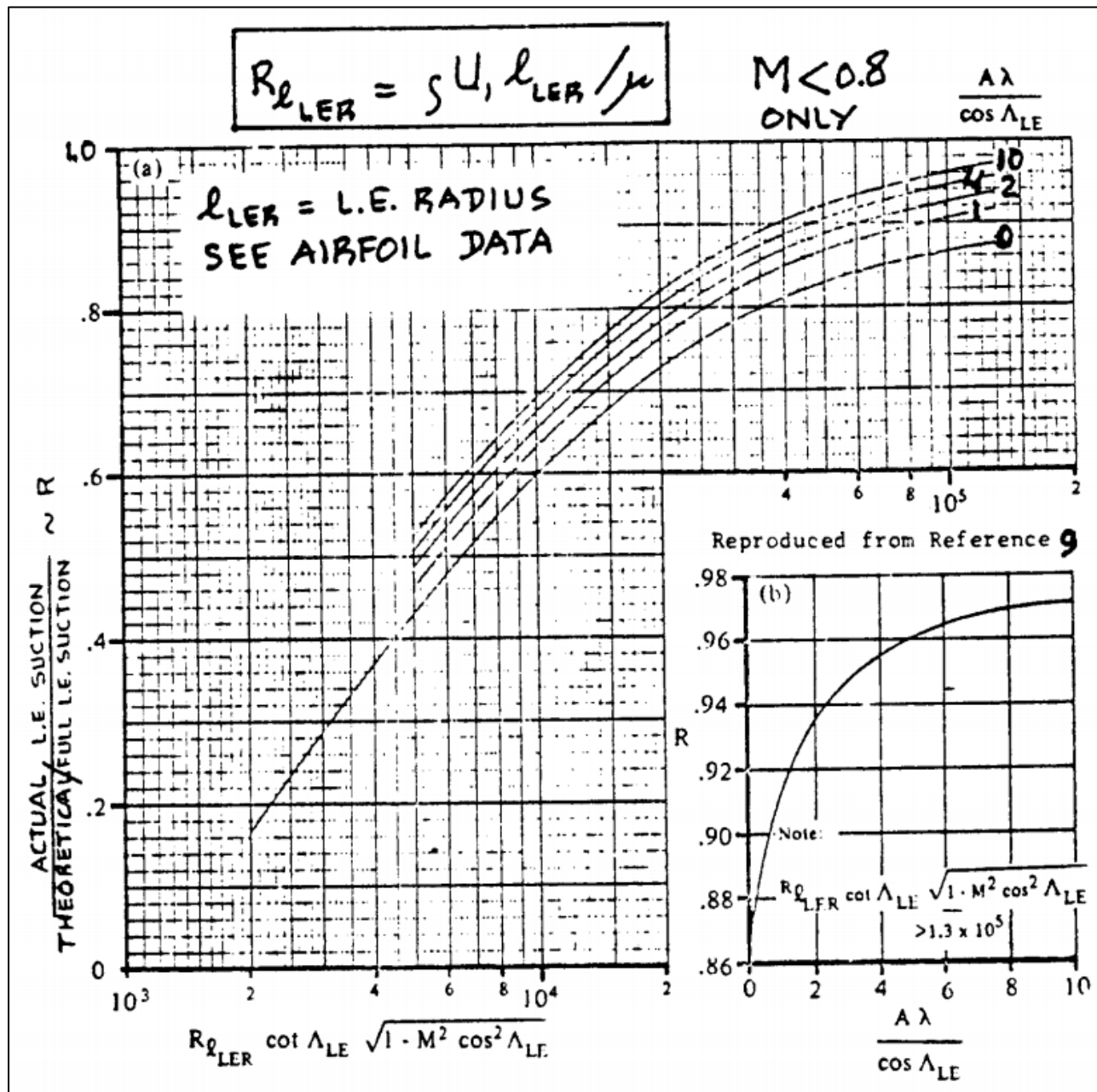
Appendix A.13: Lifting Surface Correction Factor (Roskam, 2003)



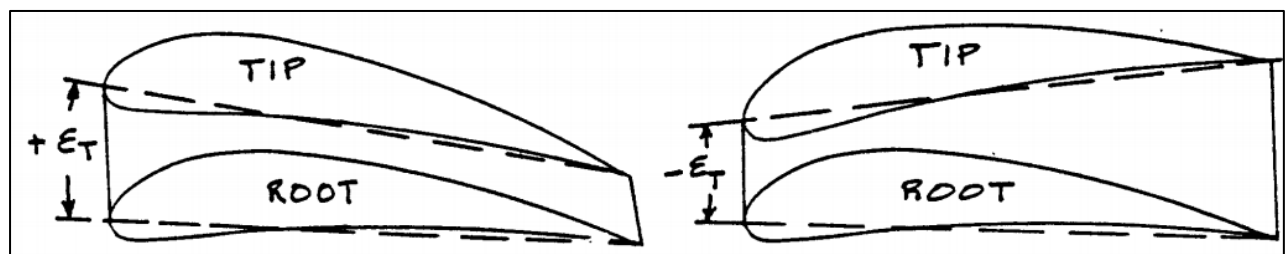

Appendix A.14: Turbulent Mean Skin-Friction Coefficient (Roskam, 2003)

Appendix A.15: Airfoil Thickness Location Parameter (Roskam, 2003)

Appendix A.16: Definition of Wing Wetted Area (Roskam, 2003)

Appendix A.17: Definition of Thickness Ratio for a Wing (Roskam, 2003)


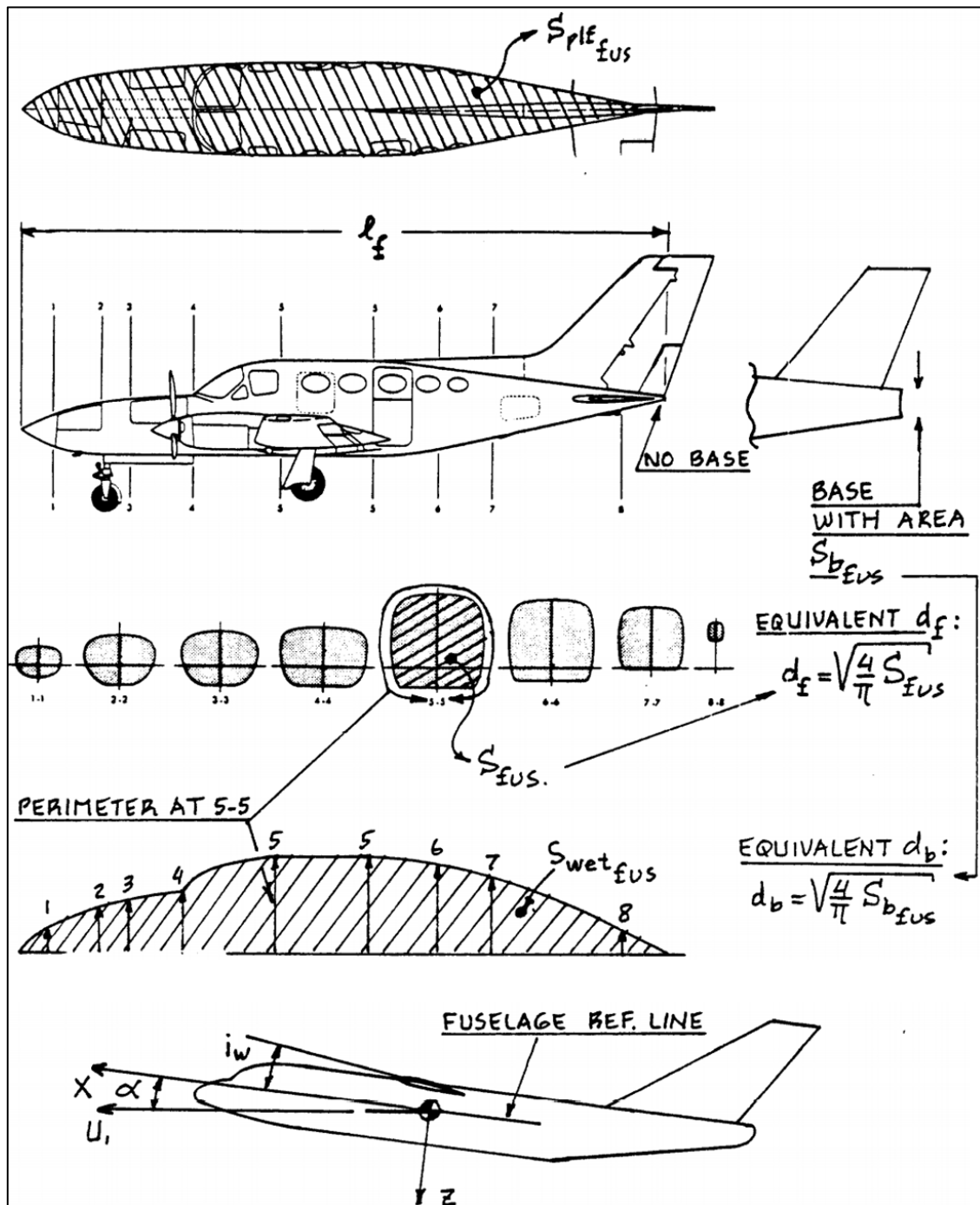


Appendix A.18: Leading Edge Suction Parameter (Roskam, 2003)



Appendix A.19: Definition of Wing Twist Angle (Roskam, 2003)




Appendix A.20: Definition of Fuselage Parameters and Angle of Attack (Roskam, 2003)


Lift-Off Performance

Average Shaft Power produced by the PT6A-67F Series engine is selected as 1700SHP (935,000 lb)

$$T_A = \frac{P_A}{V_{avg}} = \frac{0.8 * (935,000)}{130} = 5,754 \text{ lbs}$$





Using Maximum Takeoff Weight for Lift-Off Distance:

$$\frac{h}{b} = \frac{5.4}{39.7} = 0.136$$

$$\phi = \frac{\left(\frac{16 * 5.4}{39.7}\right)^2}{1 + \left(\frac{16 * 5.4}{39.7}\right)^2} = 0.825$$

Design Mission

$$V_{LO} = 1.2V_{Stall} = 1.2 \sqrt{\frac{2 * (11,500)}{0.002377 * 1.8 * 225}} = 203.2 \text{ ft/s}$$

$$V_{avg} = 0.7V_{LO} = 142.2 \text{ ft/s}$$

$$D = \frac{1}{2} * 0.002377 * 142.2^2 * 225 * \left(0.030 + 0.825 * \frac{1.8^2}{\pi * 0.85 * 7}\right) = 779.2 \text{ lb}$$

$$L = \frac{1}{2} * 0.002377 * 130^2 * 225 * 1.8 = 8,107 \text{ lb}$$

$$S_{LO} = \frac{1.44 * (11,500)^2}{32.2 * 0.00198 * 225 * 1.8 * \{5,754 - [779.2 + 0.02(11,500 - 8,107)]av\}} = 1,503 \text{ ft}$$

Ferry Mission

$$V_{LO} = 1.2V_{Stall} = 1.2 \sqrt{\frac{2 * (8,000)}{0.002377 * 1.8 * 225}} = 169.5 \text{ ft/s}$$

$$V_{avg} = 0.7V_{LO} = 118.6 \text{ ft/s}$$

$$D = \frac{1}{2} * 0.002377 * 118.6^2 * 225 * \left(0.031 + 0.825 * \frac{1.8^2}{\pi * 0.85 * 7}\right) = 545.1 \text{ lb}$$

$$L = \frac{1}{2} * 0.002377 * 108.3^2 * 225 * 1.8 = 5,639.6 \text{ lb}$$

$$S_{LO} = \frac{1.44 * (8,000)^2}{32.2 * 0.00198 * 225 * 1.8 * \{5,754 - [7545.1 + 0.02(8,000 - 5,639.6)]av\}} = 961.4 \text{ ft}$$





Landing Performance

Using Empty Weight for Landing Distance which is determined as 4,831.7 lb:

$$V_T = 1.3 \sqrt{\frac{2 * (4,831.7)}{0.002377 * 2 * 225}} = 135.38 \text{ ft/s}$$

$$V_{avg} = 0.7V_T = 94.7 \text{ ft/s}$$

$$L = \frac{1}{2} * 0.002377 * 86.5^2 * 225 * 2 = 3,995.3 \text{ lb}$$

Design Mission

$$D = \frac{1}{2} * 0.002377 * 94.7^2 * 225 * \left(0.030 + 0.825 * \frac{2^2}{\pi * 0.85 * 7} \right) = 412.5 \text{ lb}$$

$$S_L = \frac{(1.69)(4,831.7)^2}{32.2 * 0.00198 * 225 * 2 * \{0 + [412.5 + 0.4(4,831.7 - 3995.3)]0.7V_T\}}$$

$$S_L = 1840.7 \text{ ft}$$

Ferry Mission

$$D = \frac{1}{2} * 0.002377 * 86.5^2 * 225 * \left(0.031 + 0.825 * \frac{2^2}{\pi * 0.85 * 7} \right) = 414.59 \text{ lb}$$

$$S_L = \frac{(1.69)(4,831.7)^2}{32.2 * 0.00198 * 225 * 2 * \{0 + [414.59 + 0.4(4,831.7 - 3995.3)]0.7V_T\}}$$

$$S_L = 1,835.6 \text{ ft}$$

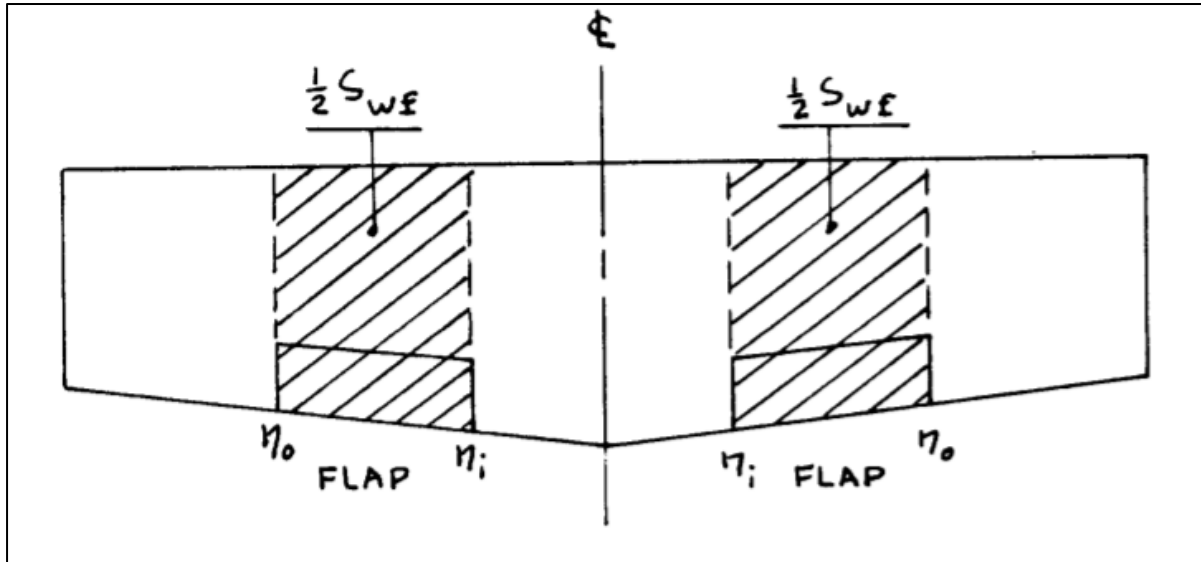




Appendix B

Wing Configuration

Appendix B.1: Definition of Flapped Wing Area (Roskam, 2003)



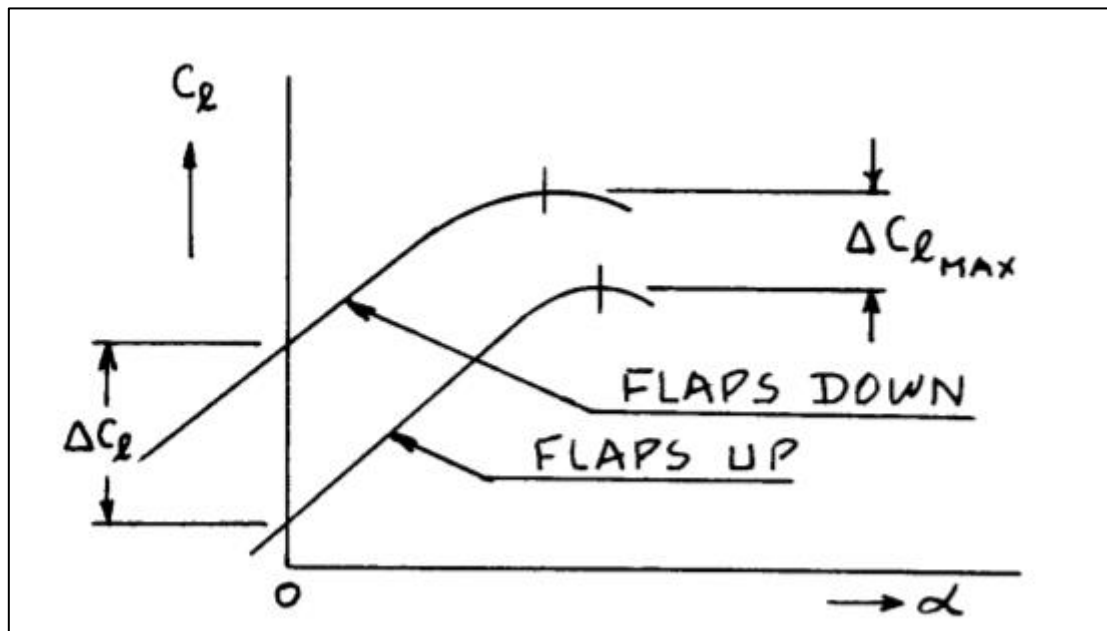
Appendix B.2: Wing Geometric Data for Single Propeller Aircraft (Roskam, 2003)

Type	Dihedral Angle, Γ_w	Incidence Angle, i_w	Aspect Ratio, A	Sweep Angle, $\Lambda_{c/4}$	Taper Ratio, λ_w	Max. Speed, V_{max}	Wing Type
CESSNA							
Skywagon 207	1.7	1.5/-1.5	7.4	0	0.69	182	brcd/high
Cardinal RG	1.5	4.1/0.7	7.3	0	0.73	156	ctl/high
Skylane RG	1.7	0.8/-2.8	7.4	0	0.67	187	brcd/high
PIPER							
Cherokee Lance	7.0	2/-1	6.2	0	1.0	188	ctl/low
Cher. Warrior	7.0	2/-1	7.2	5	0.67	152	ctl/low
Turbo Sarat.SP	6.8	NA	7.3	0	0.68	195	ctl/low
Bellanca							
Skyrocket	2	2	6.7	0	0.57	287	ctl/low
Grumman Am.							
Tiger	5	1.4	7.1	0	1.0	148	ctl/low
Rockwell Commander							
112A	7	2	7.0	-2.5	0.50	180	ctl/low
Trago Mills							
SAH-1	5	3/1	7.5	0	0.54	202	ctl/low
Scottish Aviation							
Bullfinch	6.5	1.2	8.4	0	0.57	150	ctl/low
Robin HR100/4	6.3	4.7	5.4	0	1.0	180	ctl/low
Socata Rallye							
235E	7	4	7.6	0	1.0	148	ctl/low
Fuji PA-200	7	2.5	6.3	0	1.0	123	ctl/low
Gen Avia P15P	6	4	7.7	0	0.49	167	ctl/low
ctl = cantilever		brcd = braced (strutted)					

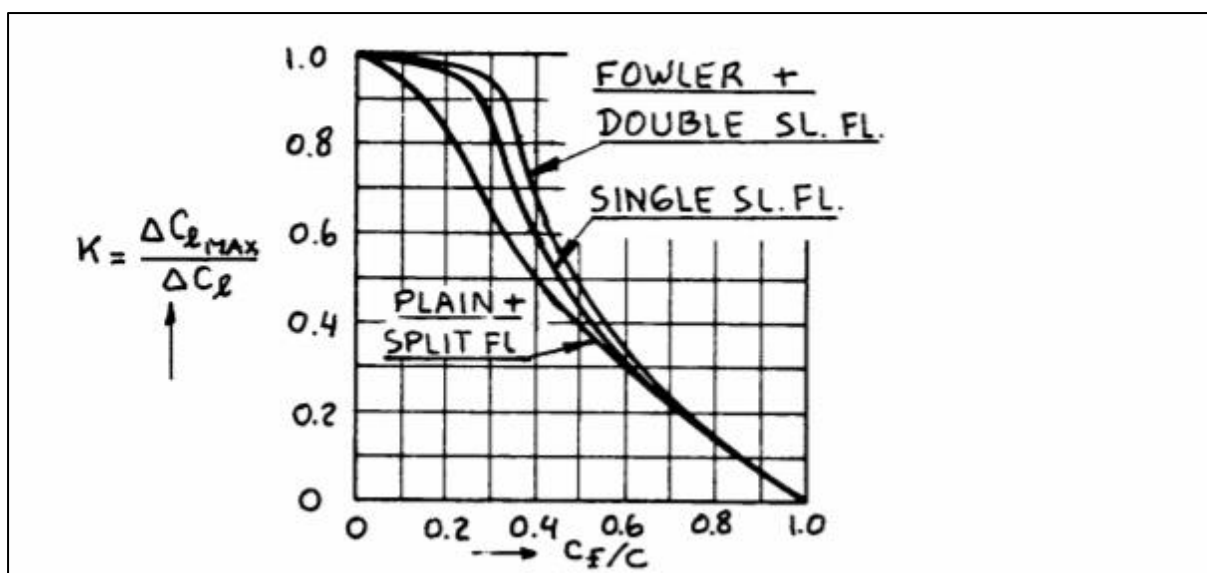




Appendix B.3: Lift coefficient versus angle of attack (Roskam, 2003)

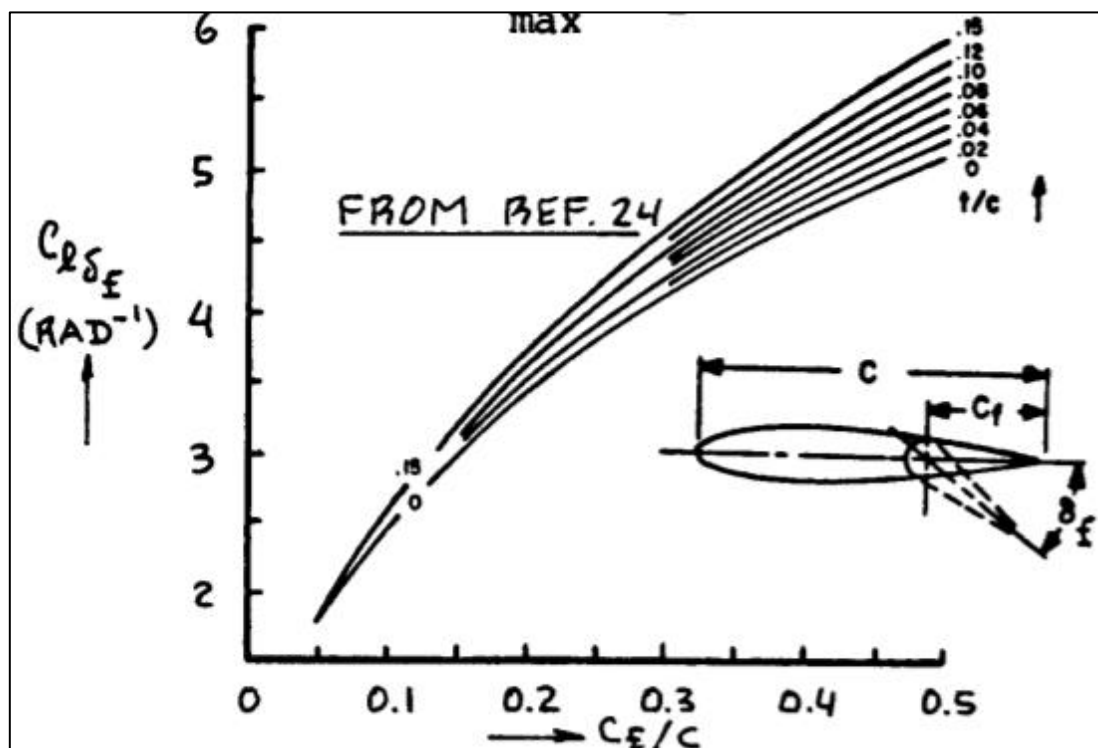


Appendix B.4: Effect of Flap Chord Ration and Flap Type on K (Roskam, 2003)

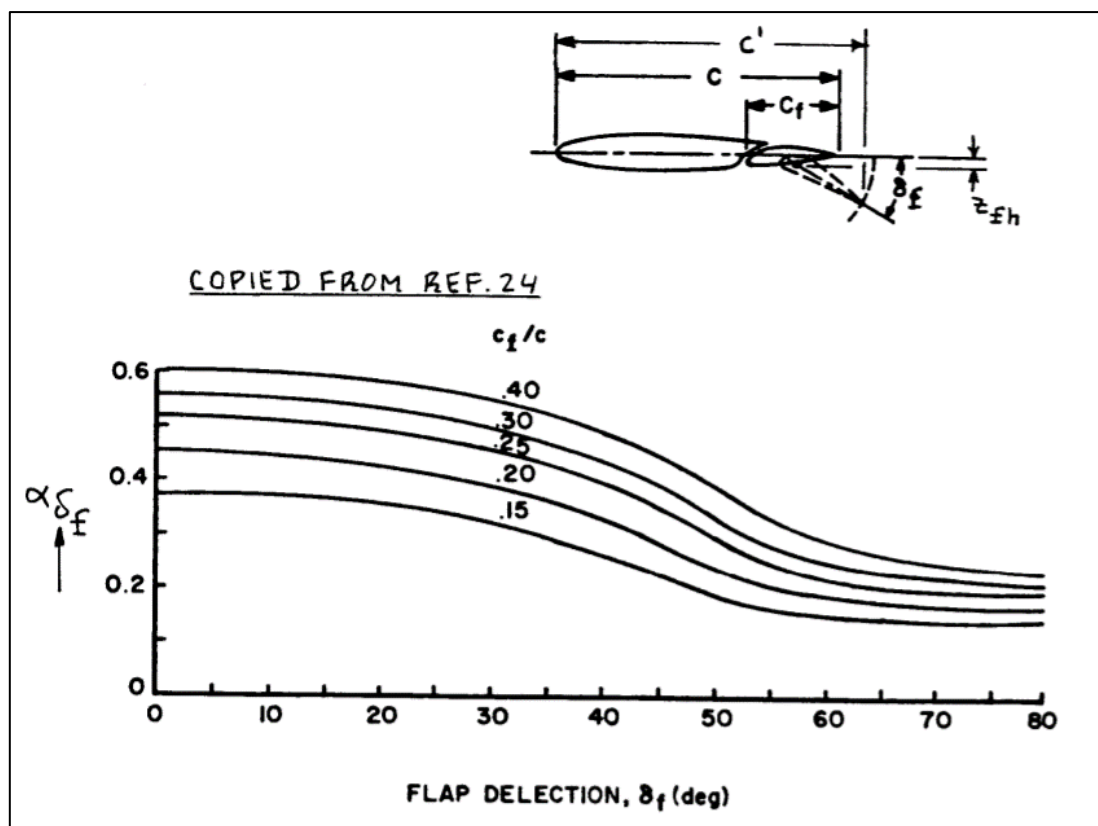




Appendix B.5: Effect of Thickness Ratio and Flap Chord Ratio on C_{l,δ_f} (Roskam, 2003)

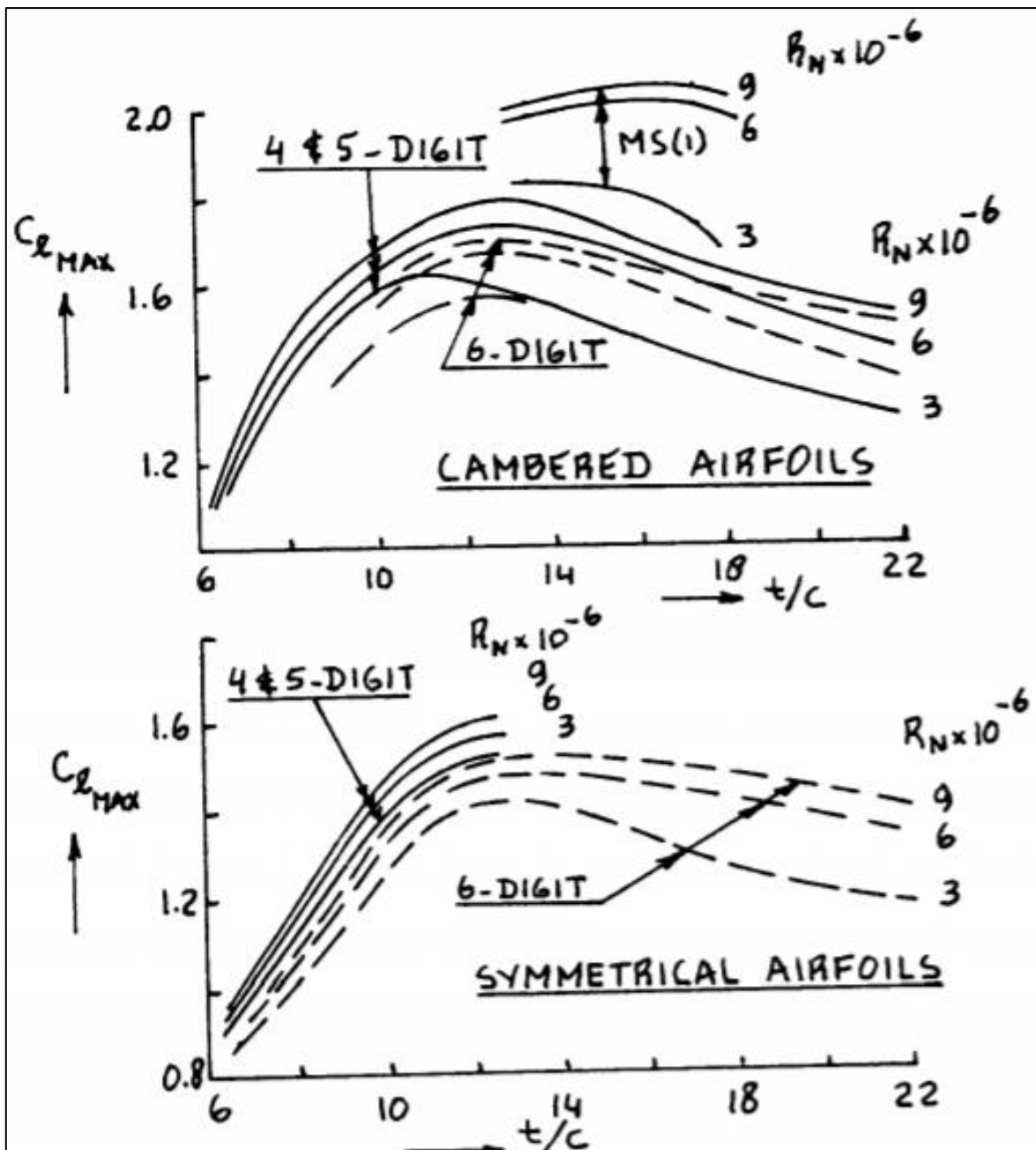


Appendix B.6: Flap Deflection Graph (Roskam, 2003)





Appendix B.7: Effect of Thickness Ratio and Reynold's Number on Section Maximum Lift Coefficient
(Roskam, 2003)




Empennage Configuration
Appendix B.8: Military Trainers: Vertical Tail Volume, Rudder and Aileron Data (Roskam, 2003)

Type	Wing Area	Wing Span	Vert. Tail Area	S_r/S_v	x_v	\bar{V}_v	Rudder Chord	S_a/S	Ail. Span Loc.	Ail. Chord
S	b		S_v				root/tip		in/out	in/out
			ft^2	ft			fr.c _v		fr.b/2	fr.c _w
Turbopropeller Driven										
EMB-312	209	36.5	22.4	0.70	16.6	0.049	.37/1.0*	0.100	.56/.99	.21/.31
Pil. PC-7	179	34.1	20.2	0.47	14.4	0.048	.52/.49	0.082	.56/.97	.23/.27
NDN 1T	126	26.0	13.5	0.52	11.8	0.049	.38/.57	0.110	.50/.87	0.26
T-34C	180	33.3	19.8	0.35	14.4	0.048	.41/.40	0.063	.55/.95	.22/.23
Epsilon	96.9	26.0	11.0	0.39	13.4	0.058	.48/.45	0.090	.58/.91	.30/.29
SP-260M	109	27.4	16.4	0.40	12.5	0.069	.35/.63	0.075	.61/.92	.23/.30
Yak-52	162	30.5	15.9	0.59	13.9	0.045	.46/.51	0.130	.47/.98	.27/.26
Neiva T25	185	36.1	18.5	0.52	15.7	0.043	.53/.52	0.085	.51/.96	.16/.22
Jet Driven										
Aero L39C	202	31.0	37.8	0.28	13.9	0.083	.36/.33	0.066	.62/.93	.36/.34
Microturbo Microjet										
200B	65.9	24.8	14.5	0.39	10.0	0.089	.37/.43	0.073	.64/.96	.29/.32
Dassault-Breguet/Dornier										
Alphajet	188	29.9	32.0	0.21	14.8	0.084	.32/.36	0.059	.68/1.0	.23/.27
Aermacchi										
MB-339A	208	35.6	25.5	0.26	12.6	0.043	.30/.38	0.069	.60/.92	0.25
SM S-211	136	27.7	21.6	0.33	19.5	0.078	.37/.36	0.100	.58/.97	.22/.21
PZL TS-11	188	33.0	24.2	0.31	16.8	0.066	.24/.47	0.085	.55/.95	.23/.27
CASA C101	215	34.8	34.4	0.41	15.8	0.072	.37/.36	0.080	.61/.93	.26/.27
British Aerospace										
Hawk Mk1	180	30.8	27.0	0.23	12.1	0.059	.28/.31	0.063	.65/1.0	.26/.32
* Large hornbalance at tip.										

Appendix B.9: Military Trainers: Horizontal Tail Volume and Elevator Data (Roskam, 2003)

Type	Wing Area	Wing mgc	Wing Airfoil	Bor. Tail Area	S_e/S_h	x_h	\bar{V}_h	Elevator Chord
S	c		root/tip	S_h			root/tip	
			NACA*	ft^2			fr.c _h	
Turbopropeller Driven								
EMB-312	209	5.77	63,A415/63A212	49.2	0.44	16.9	0.69	.42/.44
Pil. PC-7	179	5.23	64,A415/64,A612	36.9	0.49	16.2	0.64	.49/.50
NDN 1T	126	5.4	23012	25.8	0.47	14.0	0.53	0.44
T-34C	180	4.01	23016.5/23012	37.2	0.37	14.8	0.76	.43/.44
Epsilon	96.9	3.97	RA1643/RA1243	21.5	0.48	13.8	0.77	.49/.54
SP-260M	109	4.35	64,212/64,210	26.0	0.40	12.7	0.70	.35/.56
Yak-52	162	5.20	Clark YN	30.8	0.54	13.3	0.49	.54/.60
Neiva T25	185	5.19	63,A315/63,A212	33.0	0.44	15.0	0.52	.46/.40
Jet Driven								
Aero L39C	202	7.04	64A012	54.6	0.23	15.2	0.58	.35/.44
Microturbo Microjet								
200B	65.9	2.79	RA16.3C9	22.9	0.32	8.98	1.12	.37/.34
Dassault-Breguet/Dornier								
Alphajet	188	7.97	N.A.	42.4	1.0	14.1	0.43	stabilator
Aermacchi								
MB-339A	208	6.34	64A114/64A212	46.9	0.23	14.6	0.52	.26/.36
SM S-211	136	5.40	KU .17 sprcrt.	36.4	0.40	15.2	0.75	.41/.40
PZL TS-11	188	5.80	64209/64009	38.1	0.33	16.3	0.57	.31/.32
CASA C101	215	6.32	Norcasa 15	47.8	0.23	15.2	0.54	.33/.46
British Aerospace								
Hawk Mk1	180	6.30	N.A.	46.6	1.0	14.8	0.61	stabilator




Appendix B.10: Planform Design Parameters for Horizontal Tails (Roskam, 2003)

Type	Dihedral Angle, Γ_h deg.	Incidence Angle, i_h deg.	Aspect Ratio, A_h	Sweep Angle, $\Delta c/4_h$ deg.	Taper Ratio, λ_h
Homebuilts	+5 - -10	0 fixed to variable	1.8 - 4.5	0 - 20	0.29 - 1.0
Single Engine Prop. Driven	0	-5 - 0 or variable	4.0 - 6.3	0 - 10	0.45 - 1.0
Twin Engine Prop Driven	0 - +12	0 fixed to variable	3.7 - 7.7	0 - 17	0.48 - 1.0
Agricultural	0 - +3	0	2.7 - 5.4	0 - 10	0.59 - 1.0
Business Jets	-4 - +9	-3.5 fixed	3.2 - 6.3	0 - 35	0.32 - 0.57
Regional Turbo-Props.	0 - +12	0 - 3 fixed to variable	3.4 - 7.7	0 - 35	0.39 - 1.0
Jet Transports	0 - +11	variable	3.4 - 6.1	18 - 37	0.27 - 0.62
Military Trainers	-11 - +6	0 fixed to variable	3.0 - 5.1	0 - 30	0.36 - 1.0
Fighters	-23 - +5	0 fixed to variable	2.3 - 5.8	0 - 55	0.16 - 1.0
Mil. Patrol, Bomb and Transports	-5 - +11	0 fixed to variable	1.3 - 6.9	5 - 35	0.31 - 0.8
Flying Boats, Amph. and Float Airplanes	0 - +25	0 fixed	2.2 - 5.1	0 - 17	0.33 - 1.0
Supersonic Cruise Airplanes	-15 - 0	0 fixed to variable	1.8 - 2.6	32 - 60	0.14 - 0.39

Appendix B.11: Planform Design Parameters for Vertical Tails (Roskam, 2003)

Type	Dihedral Angle, Γ_v deg.	Incidence Angle, i_v deg.	Aspect Ratio, A_v	Sweep Angle, $\Delta c/4_v$ deg.	Taper Ratio, λ_v
Homebuilts	90	0	0.4 - 1.4	0 - 47	0.26 - 0.71
Single Engine Prop. Driven	90	0	0.9 - 2.2	12 - 42	0.32 - 0.58
Twin Engine Prop Driven	90	0	0.7 - 1.8	18 - 45	0.33 - 0.74
Agricultural	90	0	0.6 - 1.4	0 - 32	0.43 - 0.74
Business Jets	90	0	0.8 - 1.6	28 - 55	0.30 - 0.74
Regional Turbo-Props.	90	0	0.8 - 1.7	0 - 45	0.32 - 1.0
Jet Transports	90	0	0.7 - 2.0	33 - 53	0.26 - 0.73
Military Trainers	90	0	1.0 - 2.9	0 - 45	0.32 - 0.74
Fighters	75 - 90	0	0.4 - 2.0	9 - 60	0.19 - 0.57
Mil. Patrol, Bomb and Transports	90	0	0.9 - 1.9	0 - 37	0.28 - 1.0
Flying Boats, Amph. and Float Airplanes	90	0	1.2 - 2.4	0 - 32	0.37 - 1.0
Supersonic Cruise Airplanes	75 - 90	0	0.5 - 1.8	37 - 65	0.20 - 0.43





Appendix B.12: Empennage Configurations Calculations and Assumptions

Horizontal tail

$$C_{r,h} = \frac{2S}{b(1 + \lambda)} = \frac{2 * 54.97}{13.53(1 + 0.66)} = 4.89 \text{ ft}$$

$$C_{t,h} = \lambda \cdot C_r = 3.23 \text{ ft}$$

$$\bar{c} = \frac{2}{3} \cdot C_r \cdot \left(\frac{1 + \lambda + \lambda^2}{1 + \lambda} \right) = 4.115 \text{ ft}$$

$$\bar{Y} = \left(\frac{b}{6} \right) \cdot \frac{1 + 2\lambda}{1 + \lambda} = 3.15 \text{ ft}$$

Vertical Tail

$$C_{r,v} = \frac{2S}{b(1 + \lambda)} = \frac{2 * 25.4}{5.16(1 + 0.55)} = 6.35 \text{ ft}$$

$$C_{t,v} = \lambda \cdot C_r = 3.49 \text{ ft}$$

$$\bar{c} = \frac{2}{3} \cdot C_r \cdot \left(\frac{1 + \lambda + \lambda^2}{1 + \lambda} \right) = 5.05 \text{ ft}$$

$$\bar{Y} = \left(\frac{b}{6} \right) \cdot \frac{1 + 2\lambda}{1 + \lambda} = 1.165 \text{ ft}$$





Appendix C

Fuselage Configuration

Appendix C.1: Currently Used Geometric Fuselage Parameters (Roskam, 2003)

Airplane Type	l_f/d_f	l_{fc}/d_f	θ_{fc} (deg)
Homebuilts	4 - 8	3*	2 - 9
Single Engine	5 - 8	3 - 4	3 - 9
Twins	3.6** - 8	2.6 - 4	6 - 13
Agricultural	5 - 8	3 - 4	1 - 7
Business Jets	7 - 9.5	2.5 - 5	6 - 11
Regionals	5.6 - 10	2 - 4	15 - 19***
Jet Transports	6.8 - 11.5	2.6 - 4	11 - 16
Mil. Trainers	5.4 - 7.5	3*	up to 14
Fighters	7 - 11	3 - 5*	0 - 8
Mil. Transports, Bombers and Patrol Airplanes	6 - 13	2.5 - 6	7 - 25****
Flying Boats	6 - 11	3 - 6	8 - 14
Supersonics	12 - 25	6 - 8	2 - 9

*Tailcone as defined by Figure 4.1 not easily defined
 Cessna 336 (Fig. 3.9c) *Embraer Brasilia (Fig. 3.16d)
 ****Lockheed Hercules (Fig. 3.29d)

Propulsion System Configuration

Appendix C.2: Single Engine Propeller Driven Aircraft (Roskam, 2003)

Airplane Type	Prop. Pitch	Max. Power per Engine, P_{max} '	Prop. Diam., D_p'	Number of Prop. Blades, n_p'	Power Loading per Blade, P_{bl}'
		hp	ft		hp/ft ²
<u>Single Engine FAR23 Certified</u>					
CESSNA					
152	Fixed	108	5.8	2	2.0
Skyhawk	Fixed	160	6.3	2	2.6
Skylane	C.Spd	230	6.8	2	3.2
Skywagon (185)	C.Spd	300	6.7	3	2.8
Caravan I	C.Spd	600	8.3	3	3.7
BEECH					
V35B Bonanza	C.Spd	285	7.0	2	3.7
38P Lightning	C.Spd	550	7.7	3	3.9
PIPER					
PA28 Warrior II	Fixed	160	6.2	2	2.6
Mooney 201	C.Spd	200	6.2	2	3.3
Mooney 301	C.Spd	360	6.5	3	3.6
P _{bl} range: 2.0-3.9					
Note: P _{bl} = 4P _{max} /πn _p D _p ²					





Landing Gear Configuration

Appendix C.3: Typical Landing Gear Wheel Data ($n_s=2$) (Roskam, 2003)

Type	W_{TO} lbs	Main Gear				Nose Gear			
		$D_t \times b_t$	$n_s P_m / W_{TO}$	PSI	n_{mt}	$D_t \times b_t$	P_n / W_{TO}	PSI	n_{nt}
		in.xin.				in.xin.			
Transport Jets	44,000	34x12	0.89	75	2	24x7.7	0.11	68	2
	73,000	40x14	0.92	77	2	29.5x6.75	0.08	68	2
	116,000	40x14	0.94	170	2	24x7.7	0.06	150	2
	220,000	40x14	0.94	180	4	29x7.7	0.06	180	2
	330,000	46x16	0.93	206	4	40x14	0.07	131	2
	572,000	52x20.5	0.93	200	4*	40x15.5	0.07	190	2
	775,000	49x17	0.94	205	4**	46x16	0.06	190	2
Military Trainers	2,500	17x6	0.82	36	1	13.5x5	0.18	28	1
	5,500	20.3x6.5	0.91	60	1	14x5	0.09	40	1
	7,500	20.25x6	0.92	65	1	17.2x5.0	0.08	45	1
	11,000	23.3x6.5	0.90	143	1	17x4.4	0.10	120	1
Fighters	9,000	20x5.25	0.86	135	1	17x3.25	0.14	82	1
	14,000	18.5x7	0.87	110	1	18x6	0.13	37	1
	25,000	24x8	0.91	210	1	18x6.5	0.09	120	1
	35,000	24x8	0.90	85	2	21.5x9.8	0.10	57	1
	60,000	35.3x9.3	0.88	210	1	21.6x7.5	0.12	120	2
	92,000	42x13	0.93	150	1	20x6.5	0.07	120	2

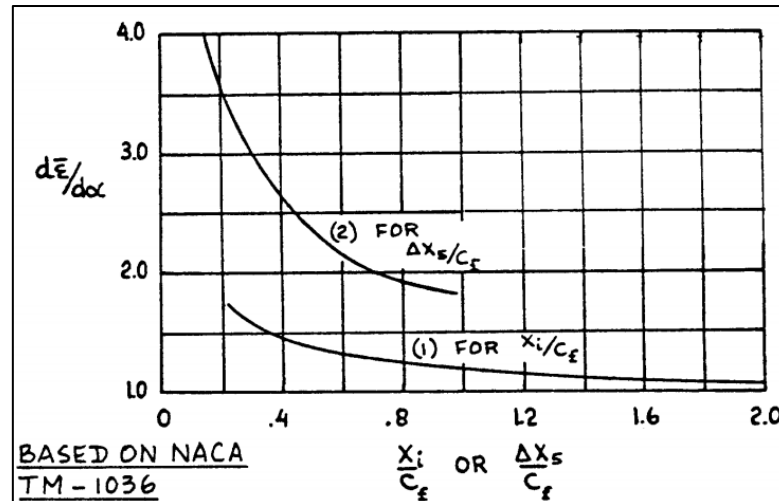




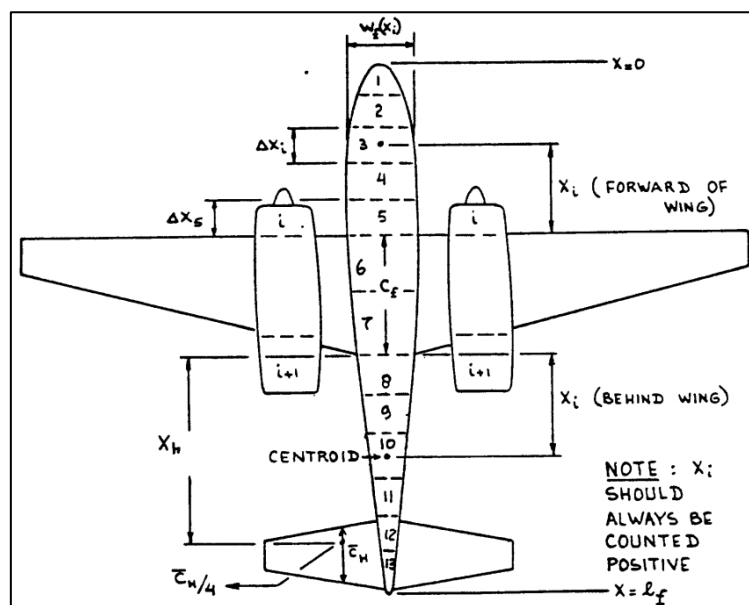
Appendix D

Longitudinal Static Stability

Appendix D.1: Effect of Fuselage or Nacelle segment location on upwash gradient (Roskam, 2003)

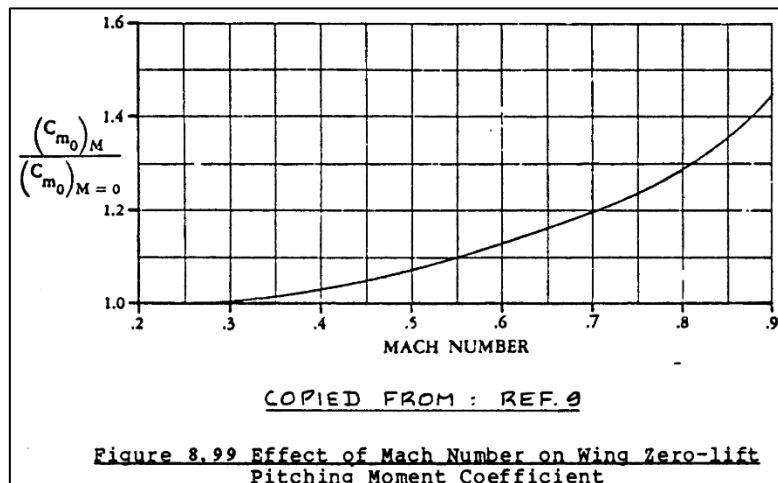


Appendix D.2: Layout for Computing Fuselage and Nacelle Contribution to Airplane Aerodynamic Center Location (Roskam, 2003)



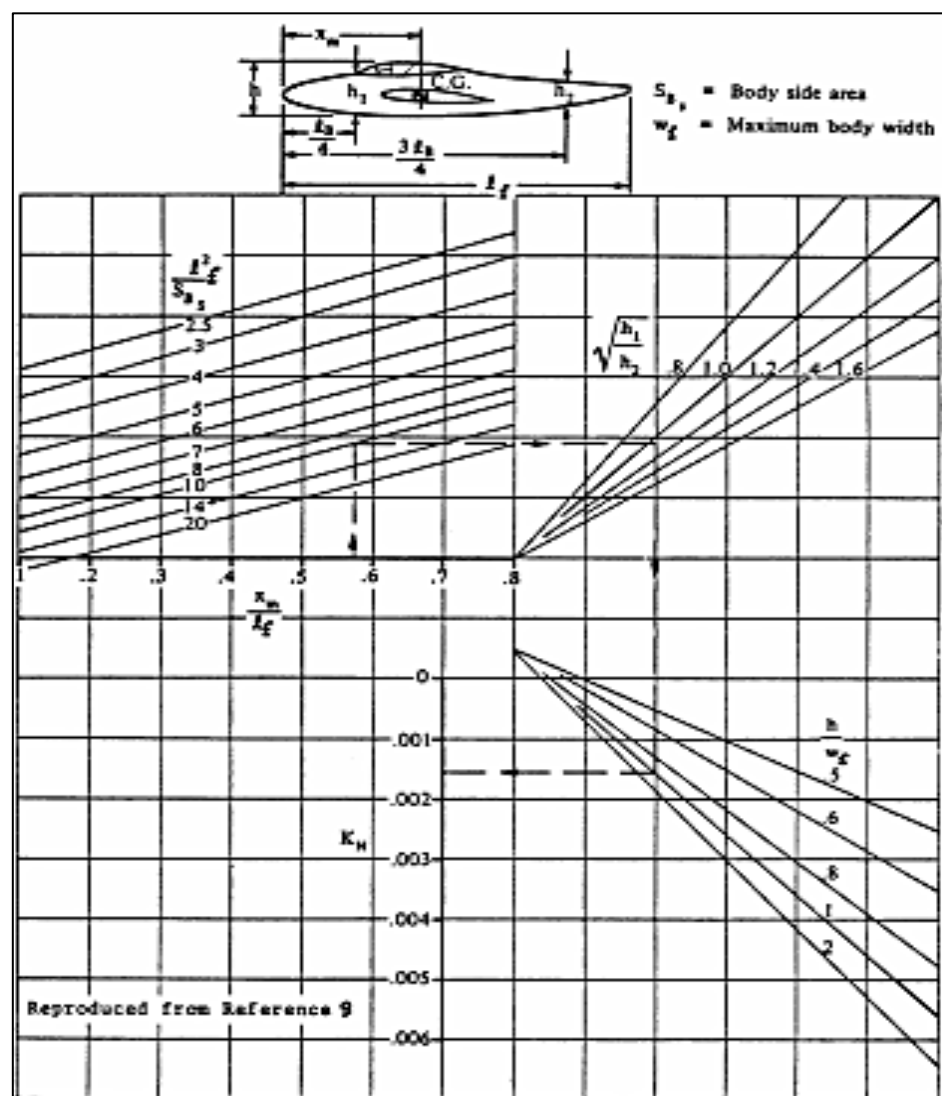


Appendix D.3: Effect of Mach Number on Wing Zero-Lift Pitching Moment Coefficient (Roskam, 2003)



Directional Static Stability

Appendix D.4: Factor Accounting for Wig-Fuselage Interference with Directional Stability (Roskam, 2003)





Appendix D.5: Effect of fuselage Reynold's Number on Wing-Fuselage Directional Stability (Roskam, 2003)

